UNIVERSITÀ
DEGLI STUDI
DI PADOVA

UNIVERSITA' DEGLI STUDI DI PADOVA

DIPARTIMENTO DI INGEGNERIA INDUSTRIALE

CORSO DI LAUREA MAGISTRALE IN CHEMICAL AND PROCESS ENGINEERING

Tesi di Laurea Magistrale in

Chemical and Process Engineering

The effect of silica precursor on sol-gel crosslinking: kinetic modelling and experimental analysis

Relatori: Prof. Martina Roso, Prof. Karen De Clerck, Prof. Dagmar D'hooge

Laureanda: Alice Novello

ANNO ACCADEMICO 2023/2024

Acknowledgments

First and most importantly, I would like to express my deepest gratitude to my supervisors: Prof. Dr. Martina Roso, Prof. Dr. ir. Karen De Clerck and Prof. Dr. ir. Dagmar D'hooge. Your constant support and keen interest in my progress throughout this Master thesis has been invaluable and has constantly motivated me to progress with my research.
I am also very grateful to everyone in the CTSE research group at Ghent University for making me feel so welcome; I look forward to continuing to work with you all.
In particular, I would like to thank ir. Sofie Verschraegen for your continuous guidance and support. I could not have asked for a better mentor. You were always there to offer advice, encouragement and a friendly word.

I wish also to express my sincere gratitude to all my friends. To my Italian friends: from my hometown, school, ballet, university, and those who have been with me since childhood. You are my second family, and I could not have asked for better companions.
To the new friends I made in Ghent, thank you for making me feel at home, even when I was far from it.

Ringrazio soprattutto la mia famiglia per il suo infinito sostegno, sono davvero fortunata ad avere una famiglia così bella.
Desidero ringraziare i miei nonni e le mie zie per avermi sempre accolta nella loro casa dove ho spesso studiato, circondata da un'atmosfera serena e accogliente.

Un grazie di cuore alla mia nonna per essere sempre stata al mio fianco.

Abstract

The synthesis of silica materials, including nanofibers, is frequently achieved through the sol-gel process. This method involves the hydrolysis and condensation reactions of precursor molecules, which result in the formation of a cross-linked network. The reaction kinetics and final material structure are significantly affected by factors such as the reagent concentration, temperature and catalyst. Despite the critical need for efficient material tuning, our understanding of how synthesis parameters impact material structure remains largely reliant on trial-and-error experimental approaches.

In its most researched form, the sol-gel synthesis starts from tetraethylorthosilicate (TEOS), which has four reactive ethoxy groups. The CTSE research group at Ghent University, where this thesis work was conducted, has made significant advances in the understanding of the kinetics of TEOS-based silica sol-gel synthesis through the integration of advanced kinetic modelling and ^{29}Si nuclear magnetic resonance (NMR) techniques.

The first objective of this thesis is to expand the existing knowledge of silica sol-gel systems by investigating the use of a different precursor, methyltriethoxysilane (MTES), which possesses three reactive ethoxy groups. The impact of the number of functional groups on crosslinking reactions remains poorly understood. Gaining insights into this aspect could enhance the use of various precursors in the production of nanofibrous membranes via electrospinning. This thesis work combines kinetic modeling with ^{29}Si NMR analysis to determine the rate coefficients of hydrolysis and condensation reactions during MTES sol-gel synthesis and compare this with TEOS crosslinking.

The second objective of this thesis is to link (organo)silica network characteristics to the flow behaviour of the sol. The flow behaviour, such as the viscosity evolution during the reaction, is a key parameter determining the sol electrospinnability but is highly dependent on the sol synthesis conditions. Combining experimental ^{29}Si NMR analysis and kinetic modeling of the network, allows the extraction of intrinsic network characteristics such as conversion and fraction of functional groups. These intrinsic parameters, when linked with the viscosity data, can help compare different precursors and their electrospinnability. This approach aims to improve the understanding of the rheology of silica and organosilica sols and their processability into nanofibers.

Abstract

La sintesi di materiali a base di silice, comprese le nanofibre, è spesso ottenuta attraverso il processo sol-gel. Questo metodo prevede reazioni di idrolisi e condensazione di molecole precursori, che portano alla formazione di un reticolo. La cinetica di reazione e la struttura finale del materiale sono significativamente influenzate da fattori quali la concentrazione dei reagenti, la temperatura e il catalizzatore. Nonostante la necessità critica di un'efficiente messa a punto del materiale, la nostra comprensione dell'impatto dei parametri di sintesi sulla struttura del materiale rimane in gran parte affidata ad approcci sperimentali.

Nella sua forma più studiata, la sintesi sol-gel parte dal tetraetilortosilicato (TEOS), che ha quattro gruppi etossici reattivi. Il gruppo di ricerca CTSE dell'Università di Ghent, dove è stato svolto questo lavoro di tesi, ha compiuto progressi significativi nella comprensione della cinetica della sintesi sol-gel a base di TEOS attraverso l'integrazione di una modellazione cinetica avanzata e di tecniche di risonanza magnetica nucleare (^{29}Si NMR).

Il primo obiettivo di questa tesi è quello di ampliare le conoscenze esistenti sui sistemi sol-gel di silice studiando l'uso di un diverso precursore, il metiltrietossisilano (MTES), che possiede tre gruppi etossilici reattivi. L'impatto del numero di gruppi funzionali sulle reazioni di reticolazione rimane poco conosciuto. L'approfondimento di questo aspetto potrebbe migliorare l'uso di vari precursori nella produzione di membrane tramite elettrofilatura. Questo lavoro di tesi combina la modellazione cinetica con l'analisi tramite ^{29}Si NMR per determinare le costanti cinetiche delle reazioni di idrolisi e condensazione.

Il secondo obiettivo di questa tesi è quello di collegare le caratteristiche del reticolo di (organo)silica al loro comportamento reologico. La viscosità è infatti un parametro chiave che determina l'elettrofilabilità delle soluzioni, ma dipende fortemente dalle loro condizioni di sintesi. Combinando l'analisi sperimentale ^{29}Si NMR e la modellazione cinetica, è possibile estrarre caratteristiche intrinseche, come la conversione e la frazione di gruppi funzionali. Questi parametri intrinseci, se collegati ai dati sulla viscosità, possono aiutare a confrontare diversi precursori e la loro elettrofilabilità.

Questo approccio mira a migliorare la comprensione della reologia dei solidi basati sulla silice e la loro processabilità in nanofibre.

Table of Contents

Introduction

The aim of this work is to extend the current understanding of silica sol-gel systems by investigating the use of different precursors, such as methyltriethoxysilane (MTES), which has three reactive groups. This investigation is crucial because the effect of the number of reactive groups on the cross-linking reactions is still not fully understood but essential to improve the application of different precursors in nanofibrous membranes produced via electrospinning.
A further objective of this study is to gain a deeper understanding of the flow behaviour of sol-gel systems, which is a crucial factor affecting their electrospinnability. To achieve this, it is necessary to establish a correlation between the characteristics of the (organo)silica network and the sol's flow behaviour, which is significantly influenced by the synthesis conditions. By combining experimental 29Si NMR analysis with kinetic modelling, it is possible to identify intrinsic network parameters such as conversion and functional group fractions. By linking these parameters with viscosity data, it is possible to compare different precursors and their electrospinnability. This approach enhances our understanding of the rheology of silica and organosilica sols and their suitability for nanofiber production.

The importance of this research lies in the versatility and broad application potential of the sol-gel process. This method is known to offer significant control over the properties of the final materials. It involves the hydrolysis and condensation reactions of precursor molecules, which ultimately form a three-dimensional cross-linked network.

Previous research has extensively studied the technique of sol-gel synthesis, particularly using tetraethyl orthosilicate (TEOS) as a precursor. TEOS, characterized by its four reactive ethoxy groups, undergoes complex reactions that can be finely controlled to yield a variety of silica-based materials.

This thesis begins with a literature review to provide a detailed introduction to the topic. This section covers the fundamentals of the sol-gel process, the chemistry of silica materials and the current state of research. It sets the stage for the experimental and theoretical investigations that follow.

The methods chapter outlines the experimental work, detailing the reaction conditions for sol formation under both isothermal and non-isothermal conditions. It describes the tools used for

the 29Si NMR technique, the instrumental setup of the rheometer for rheological measurements, and the code used for kinetic modelling of the sol-gel synthesis.

The subsequent chapters present a detailed analysis of the results obtained from the experimental work. The third chapter focuses on the effects of temperature profile and ethanol evaporation on the reaction, including an in-depth examination of the fitting of reactivity ratios and a comprehensive kinetic comparison of different precursors. This chapter provides valuable insights into how these factors influence the synthesis process and the properties of the final materials.

The fourth chapter examines the rheological implications of varying ratios and precursors, establishing a correlation between viscosity and reaction time. Furthermore, a significant correlation is identified between viscosity and conversion. This analysis provides insights into the flow behaviour of the sols, which is of crucial importance for their processability and suitability for electrospinning.

The final chapter examines the relationship between the electrospinnability of a sol and its characteristics. The objective of this chapter is to identify the key parameters that affect the ability to form nanofibers through electrospinning, by studying data obtained from the kinetic modelling code. A comprehension of this interconnection is crucial for the optimization of the sol-gel process.

In conclusion, this thesis employs a combined approach of kinetic modelling and experimental 29Si NMR analysis to enhance the understanding of silica sol-gel systems, with a particular focus on MTES as a precursor. The objective of this research is to provide valuable insights that could expand the applicability of sol-gel processes in producing advanced silica materials. To this end, the synthesis parameters, rheological behaviour and electrospinnability of these sols have been investigated and linked

Chapter 1

Literature study

A comprehensive literature review is presented in this chapter. This section provides an overview of the basic principles of the sol-gel process, the chemistry of silica materials and the current state of the art in the field.

This literature review begins by exploring the synthesis and kinetics of sol-gel networks, focusing on the mechanisms and models that explain their formation and behaviour. This is particularly significant for (organo)silica-based sol-gels, where the choice of precursor and the nature of hydrolysis and condensation reactions play a crucial role in determining the final properties of the material.

A thorough understanding of the kinetics of sol-gel processes is essential for effectively controlling the structural evolution of silica and organosilica networks. To achieve this, it is necessary to analyse how the reaction evolves over time. Advanced NMR techniques are included in this study because they allow for the analysis of molecular changes during the reaction.

Furthermore, the structural evolution of silica and organosilica networks requires the implementation of kinetic modelling, which is a key focus of this review. The kinetic Monte Carlo model, combined with Gillespie's algorithm, is particularly effective for the comprehensive simulation of complex kinetics and will be thoroughly examined.

Finally, the review analyses the rheological properties of silica and organosilica systems, with a focus on measuring viscosity using rheometry techniques.

1.1 Synthesis of sol gel networks

In response to the demand for materials with complex functionality, new synthetic methods have emerged, including sol-gel chemistry. This method enables the production of intricate inorganic materials, including ternary and quaternary oxides, at reduced processing temperatures and shorter synthesis times. It also provides greater control over particle morphology and size [1], [2].

The origins of sol-gel chemistry date back to the 19th century when it was observed that an alkoxide began to gel when exposed to air. This process, driven by hydrolysis and then condensation, has been extensively studied and can be carefully tuned using techniques such as acid or base catalysis to produce gels of diverse structures [1].

Sol-gel chemistry has found applications in various fields, including materials science and nanotechnology [3]. This process involves the transformation of liquid precursors into a sol. A sol is generally defined as a colloidal suspension which is a dispersion of one phase in another, where the molecules dispersed in a medium must have a dimension between 1 nm and 1 μm in at least one direction. To form the sol metal alkoxide precursors are hydrolysed and then condensed, the term sol can also be applied to the in-situ formation of inorganic polymer particles through covalent bonds such as siloxanes. The sol is then further transformed into a gel, which is defined as a non-fluid 3D network that extends through a fluid phase [3], [4].

The choice of precursor in sol-gel chemistry plays a crucial role in determining the final product's structure and composition. Different precursors can lead to the formation of distinct types of gels with unique properties. For example, metal alkoxides are commonly used as precursors to produce metal oxide gels. By selecting different metal alkoxides, researchers can adapt the properties of the resulting gel, such as its porosity, surface area, and mechanical strength. Moreover, the choice of solvent in sol-gel chemistry also influences the gel formation process. Solvents with different polarities and boiling points can affect the rate of gelation and the final gel's morphology.

Sol-gel chemistry offers a versatile approach for synthesizing a wide range of materials with tailored properties. By carefully selecting precursors and solvents, scientists can design gels with specific characteristics for applications such as membranes, catalysts, coatings, and biomedical materials [3], [5], [6]. However, hydrolysis and condensation chemistry face limitations due to the restricted availability of elements that readily form alkoxides [1]. Variations in the hydrolysis rates of different alkoxides can lead to significant phase separation, presenting challenges in synthesizing ternary or quaternary systems. Despite these limitations, traditional sol-gel chemistry remains a widely used and extensively studied field in materials science.

Beyond precursor preparation, the sol-gel process can be briefly outlined in the following key steps [1]:

(I) Synthesis of the 'sol' by hydrolysis and partial condensation of alkoxides.

(ii) Formation of the gel by polycondensation, leading to the formation of metal-oxo-metal or metal-hydroxy-metal bonds.

(iii) Syneresis or 'ageing', where condensation continues within the gel network, often causing shrinkage and solvent expulsion.

(iv) Drying of the gel, resulting either in a dense 'xerogel' by collapse of the porous network, or an aerogel achieved by supercritical drying.

(v) Removal of surface M-OH groups, if necessary, by calcination at high temperatures up to 800°C.

Alkoxide-based sol-gel chemistry is primarily associated with early transition group metals and early p-block elements. Among these elements, silicon (Si) is one of the most widely used and is driving the development of silica sol-gel chemistry. The focus is now on exploring the details of silica-based sol-gel systems.

1.1.1 Silica based sol-gels

The simplest silica-based compound, tetraethoxysilane (TEOS), with the chemical formula $Si(OC_2H_5)_4$, is widely used as a precursor for sol-gel synthesis in various applications. It was first synthesised in 1845 by Ebelmen, who reacted $SiCl_4$ with ethanol [7]. His subsequent publications documented the hydrolysis of TEOS, leading to the formation of silicate solutions used in the manufacture of fibres and optical elements such as lenses. In the 1850s, Mendeleyev proposed that TEOS could undergo repeated condensation reactions, resulting in high molecular weight polysiloxanes. The discovery of the properties of siloxane polymers aroused considerable interest in the 1930s, when researchers studied the hydrolysis and condensation reactions and laid the foundations for these processes [8]. More recently, the formation of monolithic gels and the conversion of gels to glasses at low temperatures have renewed interest in the subject, prompting further research into the hydrolysis and condensation of silica compounds [9], [10].

Silicate gels are commonly synthesised by hydrolysis of monomeric tetrafunctional alkoxide precursors using either a mineral acid (HCl) or base (NH_3) as a catalyst [8].

At the functional group level, three primary reactions, namely hydrolysis (and reverse hydrolysis), water condensation and alcohol condensation, typically describe the sol-gel process as shown in Figure 1.1.

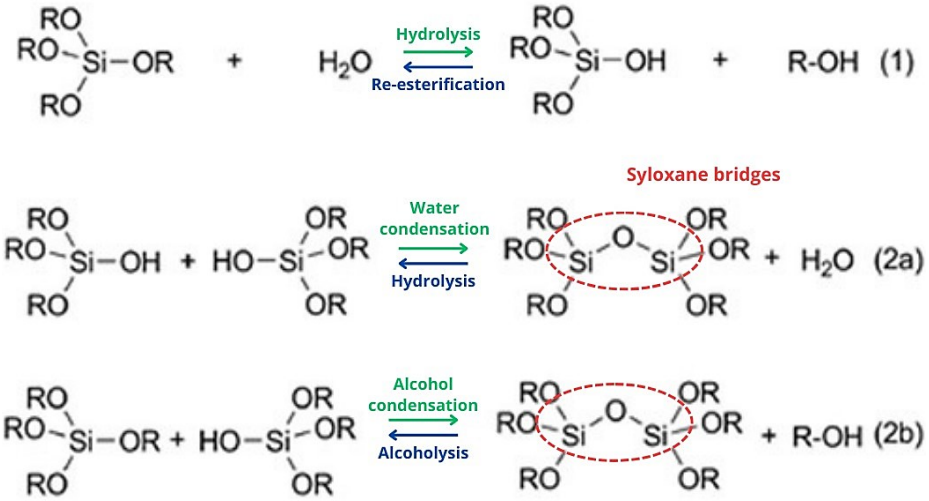

Figure 1.1: Reactions involved in hydrolysis and condensation steps of the sol-gel process: (1) hydrolysis of an alkoxy group to form silanol groups and the corresponding alcohol; (2a) condensation of two silanols; (2b) mixed condensation of a silanol group and an alkoxy group [11], [12]

The sol-gel process involves the hydrolysis of the precursor alkoxide ($Si(OR)_4$), where R is an alkyl group C_xH_{2x+1}, resulting in the replacement of alkoxide groups (OR) by hydroxyl groups (OH). Silanol groups (Si-OH) then undergo subsequent condensation reactions, resulting in the formation of siloxane bonds (Si-O-Si). Depending on the specific reaction, the by-products may be alcohol (in the case of alcohol condensation) or water (in the case of water condensation). An alcohol is commonly used as a solvent to ensure homogeneity, as water and alkoxides are immiscible. It can also act as a direct solvent without the need for additional solvents, as it is produced as a by-product during the reaction. The alcohol can be involved in reverse reactions as shown in the reaction scheme in Figure 1.1.

Different ratios of water to precursor have been investigated [13], [14], and since water is produced as a by-product of the reactions, a ratio of 2 is theoretically sufficient to achieve complete hydrolysis and condensation, resulting in anhydrous silica, as shown in the reaction scheme below.

$$nSi(OR)_4 + 2nH_2O \rightarrow nSiO_2 + 4nROH \tag{1.1}$$

Even if excess water is used, the hydrolysis reaction does not proceed to completion. Instead, a broad spectrum of intermediate species $\left[SiO_x(OH)_y(OR)_z\right]_n$ where $2x + y + z = 4$ is generated. Considering the notation Q^n, where n is the number of cross-linking sites, the result is a complex distribution of Q^0, Q^1, Q^2, Q^3 and Q^4 species. Numerous investigations [1], [8], [15] have shown that variations in synthesis conditions such as water/silica ratio, catalyst type and concentration, solvent, temperature and pressure lead to changes in the structure and

properties of the polysilicate products. For example, acid-catalysed hydrolysis at low water to silica ratios produces weakly branched polymer sols that are spinnable (capable of being drawn into fibres). In contrast, base-catalysed hydrolysis at high water to silica ratios produces highly condensed particulate sols. Intermediate conditions result in structures between these two extremes.

In summary, sol-gel silicates undergo sequential hydrolysis and condensation reactions, as well as reverse reactions such as re-esterification and depolymerisation. The specific order of these reactions is dependent on various chemical and physical factors.

1.1.2 Different precursors

The sol-gel process using tetraethoxysilane (TEOS) typically forms silica networks. However, introducing organic additives or co-precursors during this process results in organosilica materials. Precursors such as MTES, DMDES and TMES present these hybrids combine properties from both organic and inorganic components, making them versatile for various applications.

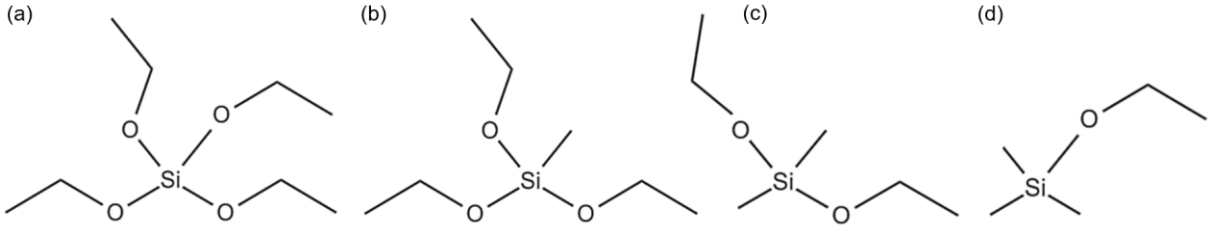

Figure 1.2: (a) tetraethoxysilane (TEOS) which has four reactive groups, (b) methyltriethoxysilane (MTES) with three reactive groups and one methyl, (c) dimethyldiethoxysilane (DMDES) with two methyl groups and two reactive groups, (d) trimethylethoxysilane (TMES) which has three methyl groups and only one reactive group.

Some organosilica networks incorporate organic groups into their bonding, unlike silica, which is linked only by oxygen. The presence of these organic bridges in organosilica enhances their flexibility and porosity, making them suitable for various applications. Therefore, the choice of precursor plays a crucial role in determining the final structure of sol-gel materials [8].

Understanding the suitability of precursors for alkoxide sol-gel chemistry requires consideration of key hydrolysis and condensation reactions. Factors such as the nature of the *R* group, the water to alkoxide ratio and the presence and concentration of catalysts play a crucial role. It's important to note that molecular silicon chemistry is complex and there are several precursors with different structures. Tetraethoxysilane (TEOS) and tetramethoxysilane (TMOS)

are among the most commonly used tetraalkoxysilanes in sol-gel processes. Traditionally, tetraalkoxysilanes are prepared by reacting tetrachlorosilanes with alcohol. When anhydrous ethanol is used, TEOS is produced with hydrogen chloride as a by-product [8].

$$SiCl_4 + EtOH \rightarrow Si(OEt)_4 + 4HCl \quad (2.2)$$

Organotrialkoxysilane $R'Si(OR)_3$ or diorganoalkoxysilane $SiR'_2(OR)_2$ precursors, such as methyltriethoxysilane (MTES) and dimethyldiethoxysilane (DMDES), can be used to reduce the reactivity of the alkoxide precursor since they contain non-hydrolysable organic substituents R' (methyl for MTES and DMDES), which decrease the potential number of sites capable of forming Si-O-Si bonds [8], [15].

These compounds, derived from different precursors or hybrid systems, exhibit different properties and functionalities, thus broadening their potential applications in different fields. In addition, the selection of specific precursors can also be based on considerations related to the solubility or thermal stability of the organofunctional substituents [8].

When considering these monomeric precursors, the steric bulk and electron-donating or electron-withdrawing properties of the alkoxide or organic substituents attached to silicon significantly influence the kinetics of hydrolysis and condensation reactions [8]. As a result, the choice of specific precursors often depends on kinetic factors.

1.1.3 Hydrolysis

Hydrolysis is a chemical process in which an alkoxy group is replaced by a hydroxyl group. This occurs by nucleophilic attack of the oxygen in water on the silicon atom, as shown by the reaction of water with TEOS.

$$Si - OR + H_2O \rightleftarrows SiOH + ROH \quad (3.3)$$

The same behaviour is found in organoalkoxysilanes $R_xSi(OR)_{4-x}$ where $x = 1, 2, 3$.

Hydrolysis can be facilitated by homogenizing agents like alcohols, dioxane, and acetone. However, the addition of solvents may promote esterification or depolymerization reactions.

Hydrolysis is most rapid and complete when a catalyst is used. Both acid and basic catalysts are employed, but various authors report that mineral acids are more effective than equivalent concentrations of base. The rate and extent of the hydrolysis reaction is most influenced by the

strength and concentration of the acid or base catalyst, with temperature and solvent playing a minor role. Interestingly, all strong acids behave in a similar way. In contrast, weak acids require a longer reaction time to achieve the same extent of reaction. Under acid catalysis the reaction follows first order kinetics. However, under basic conditions the kinetics are not always first order, and the hydrolysis rates are more influenced by the nature of the solvent [16].

The rate of hydrolysis is also affected by steric and inductive effects, which influence the stability of the transition state [17]. Steric factors have a significant effect on the hydrolytic stability of organoalkoxysilanes. The more complicated the R group, the more the hydrolysis of alkoxysilanes is slowed down, with branched alkoxy groups causing the greatest reduction in hydrolysis rates.

The electron density increases when alkyl groups replace alkoxy groups on silicon, while hydrolysis or condensation decreases it. This means that alkyl substitution or bridging oxygen substitution can improve the stability of positively and negatively charged transition states. Hydrolysis is influenced by steric and inductive effects that are specific to acidic or basic conditions. Based on these factors, it is generally assumed that hydrolysis proceeds via bimolecular nucleophilic displacement reactions (S_N2-Si reactions) involving pentacoordinate intermediates or transition states [8], [17]. Inductive effects are particularly important when studying the hydrolysis of methylalkoxysilanes $(CH_3)_x(C_2H_5O)_{4-x}$, where (x) varies from 0 to 3 [15], [18].

Research [8], [15], [19] has shown that under acid catalysis (HCl), the hydrolysis rate increases with the degree of substitution (x) of the electron donating groups. Conversely, under basic catalysis, the opposite trend is observed. This reasoning leads to the conclusion that under acid conditions the hydrolysis rate decreases with each subsequent hydrolysis step, whereas under basic conditions the increased electron withdrawing capabilities of OH compared to OR may lead to faster subsequent hydrolysis steps as hydrolysis and condensation progress.

When considering organically modified alkoxysilanes $(R_xSi(OR)_{4-x})$, inductive effects suggest that acidic catalysed conditions are more favourable since the acid catalyst is effective in promoting hydrolysis for both $x = 0$ and $x > 0$ [15].

The water to silica ratio (r) also has a significant effect on the hydrolysis rate. Although higher r values generally promote hydrolysis, if hydrolysis is carried out at a constant solvent to silicate ratio, an increase in r will give a lower silicate concentration. As a result, hydrolysis and condensation rates are reduced, resulting in longer gelation times [20], [21].

The focus is now on acid-catalysed hydrolysis, as it is highly effective for silica sol-gel formation, even when organically modified alkoxysilanes are used as precursors. Acid-catalysed hydrolysis is preferred for electrospinning purposes because it results in a more linear network than base-catalysed sol-gel systems. Under acidic conditions, an alkoxide group is rapidly protonated; this protonation makes the silicon more electrophilic and susceptible to water attack. The preferred transition state for this reaction has significant S_N2-type character; during this process, the water molecule attacks and acquires a partial positive charge. At the same time, the positive charge decreases primarily due to the nature of the transition state and the stabilization of the leaving group. This results in making the alcohol more willing to dissociate from the molecule, facilitating the reaction. Lastly, the transition state undergoes decay by alcohol displacement, accompanied by inversion of the silicon tetrahedron. This phenomenon occurs when the alcohol molecule replaces another group or atom in the transition state, resulting in the rearrangement of the silicon tetrahedron's structure. This inversion can have significant implications for the overall reaction mechanism and the stereochemistry of the resulting product [16].

According to this mechanism, the hydrolysis rate is positively influenced by substituents that reduce steric crowding around silicon. In addition, electron donating substituents (such as alkyl groups) can stabilise developing positive charges, leading to an increase in the hydrolysis rate. However, their effect is somewhat limited because silicon only acquires a small charge in the transition state [8].

In the case of hydrolysis of silicon compounds under basic conditions, water dissociates to form nucleophilic hydroxyl anions in a rapid initial step. Again, the proposed mechanism is similar to an S_N2-Si mechanism where OH- displaces OR- with inversion of the silicon tetrahedron. While both steric and inductive effects influence this process, steric factors play a more significant role as silicon acquires minimal charge during the transition state [16], [17].

In Figure 1.2 below both acid and basic catalysed hydrolysis can be observed.

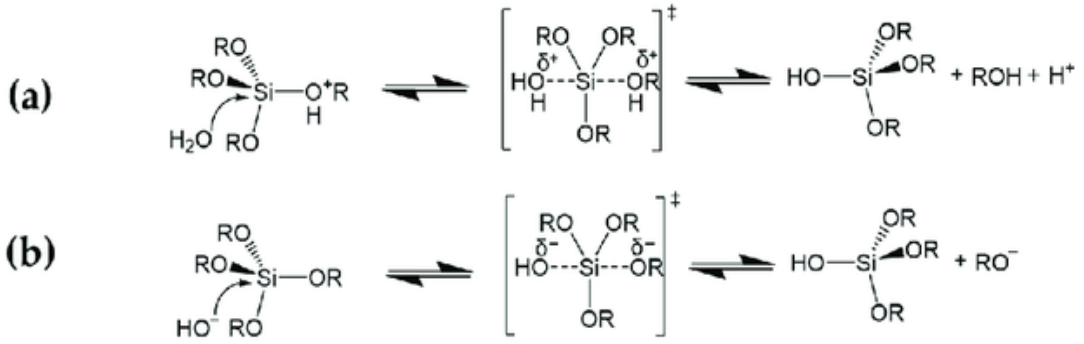

Figure 1.3: (a) acid hydrolysis and (b) basic hydrolysis mechanisms [22]

The hydrolysis reaction can also occur in the reverse direction, in this case it is called reverse hydrolysis or reesterification. In this reaction, an alcohol molecule displaces a hydroxyl group, forming an alkoxide ligand and water as a by-product. This mechanism occurs via bimolecular nucleophilic substitution reactions similarly to the forward reactions. In particular, the re-esterification of polysiloxanes proceeds much further under acidic conditions. This observation led to the conclusion that the base-catalysed mechanism of re-esterification involves configuration inversion, whereas the acid-catalysed mechanism does not. In acid-catalysed reesterification, the first step is likely to be the protonation of a silanol group, whereas in base-catalysed conditions, the first step is the deprotonation of an alcohol to form the nucleophile group (OR).

In conclusion, in sol-gel processing, the hydrolysis of alkoxides with different alkyl groups leads to the production of various silicon alkoxides; this reaction plays a crucial role in the development of materials with desired functionalities. The kinetics of the subsequent hydrolysis reactions is influenced by the steric and inductive properties of the alkoxide being exchanged [23].

1.1.4 Condensation

After hydrolysis, the siloxane bond is formed by either an alcohol-producing condensation or a water-producing condensation. This process requires the availability of monomers in solution equilibrium with oligomeric species or generated by depolymerisation.

In alcohol-water solutions, commonly used in sol-gel processing, the rate of depolymerisation is lower than in aqueous media, especially at low pH. With these synthesis conditions, the

condensation can be considered almost irreversible: once siloxane bonds are formed, they cannot be hydrolysed. The resulting condensed polymer of siloxane chains is similar to the classical polycondensation of polyfunctional organic monomers, resulting in a 3D molecular network that cannot undergo rearrangement into particles [24].

Silanol condensation can occur thermally without a catalyst, but catalysts are often introduced to improve the process, especially with organosilanes where both acid and base catalysts are commonly used. However, understanding the precise effect of the catalyst is difficult due to the increasing acidity of the silanol groups with the extent of hydrolysis and polymerisation, and the influence of reverse reactions, which become more significant with higher water content.

Condensation can occur via two different reactions (producing water or alcohol) and can involve very different species (monomers, oligomers, etc.) with different degrees of hydrolysis. Consequently, precise data on the influence of steric and inductive effects on these reactions are difficult to obtain. However, it is expected that substituents which increase steric crowding in the transition state will have a retarding effect on condensation [8].

The acid-catalysed and base-catalysed condensation mechanisms involve protonated and deprotonated silanols, respectively. Organic substituents have a significant effect on the acidity of the silanols involved in condensation. For example, electron donating alkyl groups decrease silanol acidity, whereas electron withdrawing groups (-OH, -OSi) increase silanol acidity. For organoalkoxysilanes, the reaction mechanism is determined by the degree of substitution on the silicon atom, indicated by the value of x in $(R_xSi(OR)_{4-x})$, as well as the condensation and hydrolysis rates [8].

In acid-catalysed condensation reactions, although inductive effects are also important, research has shown [17] that steric effects play a dominant role. Therefore, in tetrafunctional alkoxide precursors, longer-chain alkyl substituents are likely to have even less significant inductive effects. The mechanism most widely accepted for acid-catalysed condensation involves protonation of the silanol, which makes the silicon more electrophilic and susceptible to nucleophilic attack. Condensation reactions may preferentially occur between neutral silanol species and protonated silanols located in monomers and end groups of chains. This is because the most basic silanol species, found in monomers or weakly branched oligomers, are more likely to be protonated.

Also, during basic catalysed condensation OR and OH groups are replaced with OSi. This increases the acidity of the remaining silanols due to the reduced electron density on Si, and

tends to favour reactions between larger, more highly condensed species (containing acidic silanols) and smaller, less condensed ones [8].

To summarise, when subjected to alkaline conditions, multiple condensation steps lead to the formation of small, highly branched agglomerates that eventually form a colloidal gel [16], [17], [19]. Conversely, under acidic conditions, condensation initiation occurs before hydrolysis is complete, typically on terminal silanols, resulting in chainlike structures.

Figure 1.3 illustrates the mechanism of both acid and base-catalysed condensation reactions.

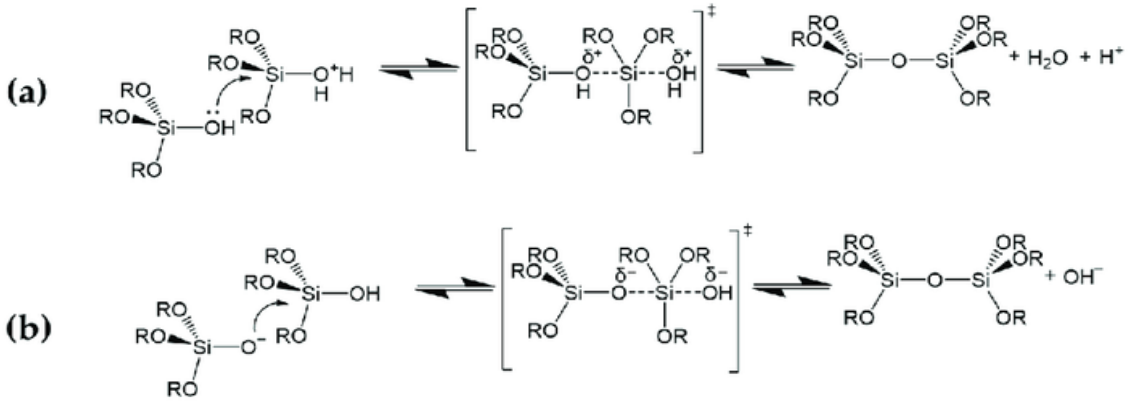

Figure 1.4: (a) acid condensation and (b) basic condensation [22]

To conclude, the structure of silica sol-gels can be influenced by several factors, which affect the rates of hydrolysis and condensation. Significant roles are played by acid and base catalysts, choice of solvents, steric and inductive effects of different silicon alkoxides, alkoxy-to-water ratios, and the presence of chelating agents.

Sol-gel chemistry is further complicated by the intricate molecular diversity of silicon compounds beyond simple tetraalkoxides. Understanding the interrelationship of these factors is crucial for designing the sol-gel process.

1.2 Silica sol-gel kinetics

Although described separately above, hydrolysis and condensation reactions occur simultaneously in a silica sol-gel system and their kinetics are strictly linked. Silicon atoms in stable molecules maintain a coordination number of 4 and can only bond to functional groups such as OR, OH, or OSi. At the nearest functional group level, there are 15 distinguishable local silicon chemical environments [25], [26] that are used to formulate the chemical kinetic rate equations.

At the elementary level, there are three reaction rates: hydrolysis, alcohol condensation, and water condensation. At more advanced levels, however, the number of rate coefficients increases significantly, complicating the study of reaction pathways.

To investigate these reactions, techniques such as nuclear magnetic resonance (NMR), are used to measure the relative amounts of alkoxy functional groups and alcohol molecules as a function of reaction time. Considering two extremes, in the case of rapid hydrolysis, where the rate of hydrolysis is much higher than the sum of the rates of condensation, the concentration of the alkoxy functional groups decreases rapidly to the value corresponding to complete hydrolysis, subsequently the decrease in the concentration of the alkoxy functional groups occurs at a slower rate, which is consistent with the overall rate of the condensation reaction [8].

In contrast, if hydrolysis is much slower than either of the condensation rates, condensation will occur immediately. In this case, the decrease in concentration of the alkoxy functional group is proportional to the rate of hydrolysis.

Several studies [27], [17] have shown that the condensation rate decreases as the extent of condensation and reesterification increases, especially for large values of r (water to silica ratio).

Furthermore, steric effects become increasingly significant as the size of alkoxide substituents increases or when reacting species become more highly condensed. In particular, this phenomenon is observed in organoalkoxysilanes. Kinetic models have been proposed to explain the temporal evolution of functional groups around silicon, with inductive effects thought to play a crucial role; however, for higher alkoxy groups, steric considerations may outweigh any inductive effects [23].

1.2.1 Structural evolution of silica and organosilica networks

Silica and organosilica networks, similar to organic polymer networks, demonstrate their potential based on the degree of cross-linking. In addition to mechanical properties, the hydrophilic behaviour of silica-based systems is of great interest, as the degree of crosslinking significantly influences material strength and stiffness [28].

Hydroxyl groups emerge during the synthesis process as a result of cross-linking reactions. The number of hydroxyl surface groups increases with the occurrence of hydrolysis and reverse condensation reactions, resulting in improved hydrophilic behaviour. It is essential to

comprehend the complex correlation between cross-linking reactions, hydroxyl surface groups, and hydrophilicity to customize the properties of organosilica-based networks. By precisely controlling the degree of cross-linking, researchers can manipulate the properties of the material, expanding its potential applications in various industries [29].

Silicate solution species display a range of structures at different length scales. At the smallest scale, silicon's nearest neighbours consist of alkoxide groups (OR), hydroxyl groups (OH), and bridging oxygen (OSi). At intermediate length scales, oligomeric species (dimers, trimers, tetramers) can be linear, branched, or cyclic. On a larger scale, the structures between monomers and polymers can vary significantly. For example, dense arrangements with well-defined solid-liquid interfaces provide robust materials. On the other hand, uniformly porous networks and tenuous networks form more delicate structures.

The synthesis and crosslinking kinetics of organosilica networks are complex processes that require careful characterization and design. Researchers use non-intrusive in situ techniques, such as nuclear magnetic resonance spectroscopy (NMR), Raman, infrared spectroscopy, photoprobe investigations, and X-ray, neutron, and light scattering to understand the intricate relationships between cross-linking reactions, hydroxyl surface groups, and hydrophilicity. These methods allow for precise control of material properties, revealing how they evolve over time [8].

Infrared and Raman spectroscopy, when used in combination with NMR, are important for identifying specific oligomeric species and tracking the evolution of inorganic frameworks. Through comparison with model compounds of known structures, the Raman and ^{29}Si NMR spectra were used to identify certain Raman bands observed during the initial stages of hydrolysis and condensation reactions of non-OH substituted dimers, trimers, and tetramers (which were isolated through fractional distillation) [30], [31]. Recent advances have been made to improve the sensitivity of these techniques, however, NMR still surpasses them in this aspect [32].

Photoprobe investigations provide valuable insights into the structural changes that occur during the sol-to-gel-to-xerogel transition. By incorporating photophysical or photochemical probe molecules into the medium, we can obtain information about the probe molecule's surroundings on a length scale ranging from one to several nanometres. For example, a photophysical probe molecule such as pyrene shows changes in its emission spectrum in response to variations in its environment. The addition of photoprobes to a reacting sol-gel

system enables the monitoring of structural changes in situ. However, it is essential to ensure that the added probe does not alter the course of the hydrolysis and condensation reactions in its surroundings. Despite their advantages, photoprobe investigations have some drawbacks, such as the challenge of providing atomic-level detail since the penetration depth of visible light is limited, especially in dense or turbid samples [33].

Small angle scattering investigations using neutrons (SANS), X-rays (SAXS), or visible light (QELS) have been exploited for studying the growth and topology of macromolecular networks. These investigations explore the aggregation of colloids, and reveal the structures of porous gels and aerogels [34], [35]. In small-angle scattering, an incident light beam (light, neutrons, or X-rays) interacts with a sample, and the angular dependence of the scattered intensity is measured. However, performing SAXS requires a larger sample size for nanomaterial characterization compared to NMR. Additionally, as particle size increases, the sensitivity of SANS is reduced due to the dilution of surface ligands by bulk nanomaterials [36]. Quantum dot-based visible light techniques, such as QELS, may also suffer from limited penetration depth in biological samples. In contrast, NMR can penetrate the sample more deeply.

Upon analysing the methods used to study the evolution of organosilica sol-gel synthesis, it is evident that NMR is frequently the preferred method. The next section will provide further details on this powerful technique.

1.2.2 NMR investigations

Nuclear magnetic resonance (NMR) is a spectroscopic technique that exploits the intrinsic spin of atomic nuclei for the investigation of material properties. The application of an external magnetic field and weak radio frequency waves facilitates transitions between nuclear energy levels. This technique is primarily employed for the determination of the structure of small molecules. High-Resolution ^{29}Si NMR is a specialized branch of NMR that focuses on silicon-containing compounds at an atomic scale. The technique exploits the spin properties of atomic nuclei, in particular the non-zero spin and magnetic moment of silicon. In ^{29}Si NMR, the silicon-29 nuclei align themselves within an external magnetic field and respond to radio frequency waves. This technique is useful in determining molecular structures, investigating the kinetics of hydrolysis and condensation reactions, understanding polymerisation kinetics in the sol-gel

process, and providing information on the spectral composition of silicate solutions and the impact of solvents on sol-gel polymerization.

NMR provides insight into the behaviour of different precursors such as tetramethoxysilane (TMOS), tetraethoxysilane (TEOS), Methyltriethoxysilane (MTES), dimethyldiethoxysilane (DMDES) and trimethylethoxysilane (TMES), and the progression of their reactions.

The next paragraphs will examine ^{29}Si NMR spectra of different precursors for silica sol gels, the reactions in the following data and plots are consistently acid catalysed.

1.2.2.1 Tetraethoxysilane, TEOS

Silicate units with four reacting functional groups, like TEOS, are indicated by the letter Q in accordance with the Q^n notation. The numerical superscript n ranges from 0 to 4 indicating the number of siloxane bridges or crosslinks for each silicon atom; for a more complete description also a subscript indicating the number of hydrolysed groups can be added. The monomer is represented by the symbol Q^0, in particular the non-hydrolysed monomer is expressed as Q^0_{0OH} and for TEOS it is identified at -82 ppm. End-groups, middle groups, and branching positions are indicated as Q^1, Q^2, Q^3 and Q^4 respectively [37]. Figure 1.4. illustrates the comparison between TMOS and TEOS in methanol and ethanol. In the *^{29}Si* NMR spectra of TMOS systems, major features can be understood in terms of an approximately +2 ppm shift for each -OH that substitutes for -OCH_3, and an approximately -8 ppm shift for each -OSi that substitutes for -OCH_3, relative to the reference peak of TMOS (around -79.0 ppm).

Similar effects of hydrolysis and condensation on silicon resonances are observed in TEOS systems [38].

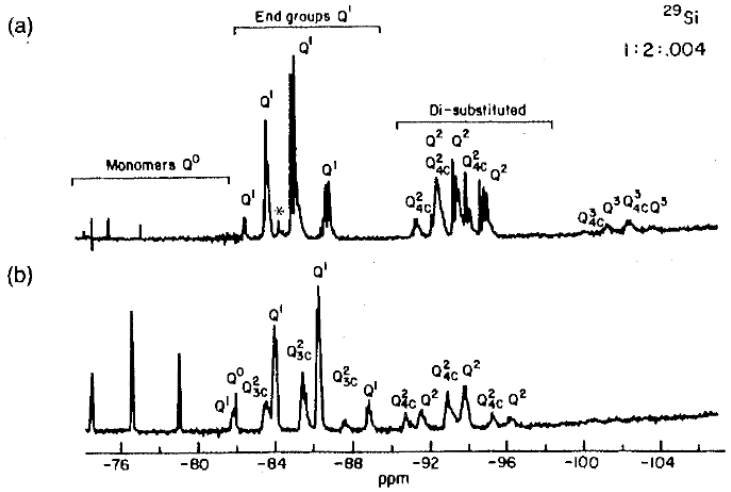

Figure1.5: comparison between ^{29}Si NMR spectra of (a) $TMOS + MeOH$ and (b) $TEOS + EtOH$ at t_0+2 hours with a silicon: water: acid ratio of 1: 2: 0.02 [38]

In the most basic synthesis procedure, polymer network molecules are constructed using TEOS as the inorganic building block. The TEOS molecules undergo partial hydrolysis before participating in intermolecular polycondensation. During this process, water is released, and Silicon-Oxygen-Silicon bridges form, leading to network crosslinking. Both intermolecular and intramolecular condensation reactions are possible, with the latter becoming more important at higher Si-O-Si yields.

In their analysis of the ^{29}Si NMR spectrum for the TEOS precursor, Pouxviel *et al.* [27] carried out a kinetic study of TEOS network synthesis using hydrogen chloride (HCl) as a catalyst at pH 2.5, more precisely the solution studied consisted of 11ml TEOS, 11ml EtOH and 3.6ml of catalyst solution with the ratio H_2O/HCl 1:0.00023. The ^{29}Si NMR technique was used due to its ability to quantitatively describe the Q^n moieties over different chemical shift regions. The results improve the understanding of the initial stages of TEOS network formation by localising the identified Q species within specific chemical shift ranges.

The Q species were identified in the regions of chemical shift summarized in in Table 1.1; all measures are expressed in [ppm].

Table 1.1: ^{29}Si NMR spectra of TEOS

Q^0	Q^1	Q^2	Q^3	Q^4
-72.4, -82.0 [23]	-81.8, -89.0 [23]	-91.3, -96.4 [23]	-100.5, -103.0 [23]	-110.0 [23]
-79.0, -82.0 [39]	-85.0, -89.0 [39]	-91.0, -97.0 [39]	-100.0, -103.0 [39]	-108.0, -110.0 [39]
-72.4, -82.0 [40]	-84.3, -89.3 [40]	-91.1, -96.4 [40]	-100.0, -102.0 [40]	

The synthesis of organosilica networks using TEOS as a starting material is indeed a fundamental process. However, studying the formation of organosilica networks from other precursors, such as MTES, DMDES, and TMES, can provide valuable insights. Researchers have therefore studied the spectra of these precursors using ^{29}Si nuclear magnetic resonance to better understand their behaviour.

1.2.2.2 Methyltriethoxysilane, MTES

Following the same logic as the Q notation for TEOS, the T^n notation is used for Methyltriethoxysilane (MTES) to indicate the number of siloxane bridges or crosslinks for each silicon atom. The superscript *n* ranges from 0 to 3, as this molecule only possesses three ethoxy groups that can form crosslinks. The methyl group linked to the silicon atom does not participate

in the sol-gel reactions. Additionally, a subscript indicating the number of hydrolysed groups can be added also in this case. Based on previous reports [41], [42], [43], the signal at -42 ppm is attributed to MTES T^0_{0OH}, while the other peaks between -37 and -42 ppm are attributed to hydrolyzed monomers. MTES can also form a T^2 cyclic trimer in the region -50.8, -51.8 ppm [43]. The hydrolysis and condensation reactions of MTES behave similarly to TEOS. However, consistently with the reasoning reported in paragraph 1.1.3, it has been found that under equal conditions, MTES has higher hydrolysis and initial condensation rates than TEOS [42], [44]. Figure 1.5 and Table 1.2 summarises the *^{29}Si* NMR spectra of MTES.

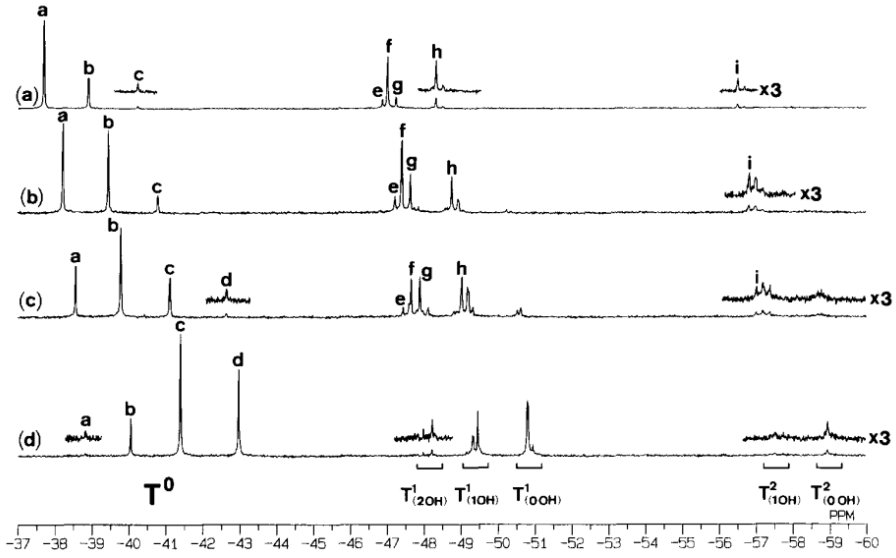

Figure1.6: 29Si NMR spectra of MTES hydrolysed for 2 h in the system of (a) $MTES: EtOH: D_20/H_20: HCl = 1: 4: 6: 10^{-4}$, (b) $MTES: EtOH: D_20/H_20: HCI = 1: 4: 3: 10^{-4}$, (c) $MTES: EtOH: D_20/H_20: HCI = 1: 4: 2: 10^{-4}$, (d) $MTES: EtOH: D_20/H_20: HCI = 1: 4: 1: 10^{-4}$. In the T^0region signal d refers to the non-hydrolysed monomer T^0_{0OH} at -42ppm; c, b and a are respectively $T^0_{1OH}, T^0_{2OH}, T^0_{3OH}$. For the T^1 region, signal f appeared after 30 min at -47 ppm, then g and h were detected after 45 minutes and e after 1 hour; also signal i appeared after one hour in the T^2 region [41].

Table 1.2: ^{29}Si NMR spectra of MTES

T^0	T^1	T^2	T^3
-37.0, -42.0 ppm [41]	-46.0, -49.0 ppm [41]	-56.0, -57.0 ppm [41]	
-39.2, -44.7 ppm [40]	-48.5, -52.1 ppm [40]	-54.7, -60.1 ppm [40]	
-40.9, -42.1 ppm [43]	-48.9, -50.2 ppm [43]	-56.8, -58.4 ppm [43]	
		-54.0, -59.3 ppm [35]	-64.5, -66.4 ppm [35]

1.2.2.3 Dimethyldiethoxysilane, DMDES

In the case of DMDES, the monomer is a unit with the formula $(CH_3)_2Si(OC_2H_5)_2$, which means that each monomer can form a maximum of two cross-links because the other two groups attached to the silicon atom are methyl groups which do not react. The notation D^n is used with

the same rules as for TEOS and MTES. Specifically, D^0 refers to monomeric species, where two OR groups are attached to the silicon atom, the non-hydrolysed monomer D^0_{0OH} can be identified at -2.4 ppm. The symbol D^1 corresponds to end groups, indicating that only one OR group is attached to the silicon atom; these end groups are located at the terminal positions of the molecular chain. Finally, D^2 represents middle groups, which are double cross-linked and located inside the molecular chain [45]. The values of the ^{29}Si NMR spectra for DMDES are reported in Figure 1.6 and Table 1.3 below.

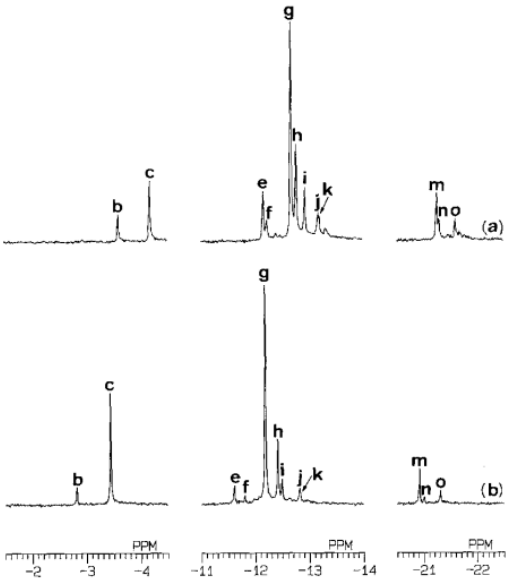

Figure 1.7: ^{29}Si NMR spectra of (a) DMDES hydrolysed in the system of $DMDES: EtOH: D_20/H_20: HCI = 1:2:2:10^{-4}$ for 2 h, and (b) DMDES hydrolysed in the system of $DMDES: EtOH: D20/H_2O: HCI = 1:2:4:10^{-4}$ for 3 h. Signals (a) D^0_{0OH}, (b) D^0_{1OH} and (c) D^0_{2OH} are respectively at -2.4, -3.0, and -3.5 ppm. Signal (a) indicating the non-hydrolysed monomer disappeared after few minutes. Six signals were observed in the D^1 region (e), (g), (h), (i), (j), and (k). In the D^2 region the signals (m), (n), (o) can be identified [45].

Table 1.3: ^{29}Si NMR spectra of DMDES

D^0	D^1	D^2
-3.1, -3.6 ppm [45]	-11.6, -12.4 ppm [45]	-20.7, -21.3 [45]
-5.0 ppm [40]	-13.4 ppm [40]	-21.9 ppm [40]
-16.4, -17.2 ppm [35]	-19.0 ppm [35]	-21.1, -21.3 ppm [35]

1.2.2.4 Trimethylethoxysilane, TMES

Trimethylethoxysilane (TMES) presents challenges in the formation of silica sol gel due to its single hydrolysable group, failing to result in a large network structure. The crosslinking of TMES molecules is intricate, and the resulting oligomers may lack essential properties for most applications. The ^{29}Si NMR data for this molecule are presented in Table 1.4.

Table 1.4: ^{29}Si NMR spectra of TMES

Me_3SiOEt	Me_3SiOH	$Me_3SiOSiMe_3$
+16.8 ppm [46] +14.5 ppm [47]	+13.9 ppm [46]	+7.2 ppm [46] +6.9 ppm [47]

In summary, the synthesis of organosilica networks is a complex research challenge due to factors such as incomplete hydrolysis, intramolecular reactions leading to unavoidable loops, and diffusion limitations causing viscosity effects [28]. These processes result in a heterogeneous mixture of different molecules rather than a single large network molecule. By understanding how the choice of precursors influences the nature of the resulting networks, the final properties can be tailored to specific requirements.

1.3 Kinetic Modelling of polymerization processes

Predicting polymerization reactions is crucial in tailoring the properties of synthesized polymers for industrial process control, safety, and quality assurance [48]. Mathematical models are being developed to describe these intricate processes, aiming to simulate polymer microstructures as a function of monomer conversion and polymerization conditions. However, polymerization processes are inherently complex and require a deep understanding of the underlying mechanisms, as they involve numerous species with a wide range of apparent reactivities at the microscale. In polymerization processes, it is typically necessary to calculate chain length distributions (CLDs) or at least average CLD characteristics [48].

Ideally, every species formed in a polymerization reactor should be tracked spatially over time, accounting for diffusivity and chemical reactivity. This ideal solution, however, is computationally expensive, therefore mathematical models emerged to simplify the chemical description and the hydrodynamics of the process [49].

There are two major classes for mathematical modelling of polymer processes: deterministic and stochastic modelling. Deterministic modelling is based on mass balance principles and preserves reaction history, it considers factors such as monomer consumption and species formation. In contrast, stochastic modelling is based on probabilistic theories, with statistical models solving reconstructed problems; in this case, the reaction history is not taken into account and the focus is on the overall behaviour [50].

Deterministic modelling can be divided into two categories: numerical methods that simulate only the averages of the CLD as a function of monomer conversion, and the so called full CLD methods.

Among the methods that calculate only the average properties, the most important is the method of moments, which is used to predict molecular weight and branching density, sacrificing detailed information about individual polymer chains for faster computation. Because of its simplicity and computational efficiency, it is often used to develop kinetic models in various polymerisation contexts. For example, it is widely employed in industrial settings where knowledge of average chain properties is usually sufficient [50].

Full CLD methods, on the other hand, simulate the full CLD and capture detailed information; theoretically they require solving an infinite number of equations, but in practice truncation of chain lengths reduces the computational complexity. Among the full CLD methods, the most important are the extended method of moments, the fixed pivot method, and the discrete weighted Galerkin method [48].

Unlike deterministic methods, statistical modelling, such as Monte Carlo, doesn't involve solving coupled differential equations. Instead, different species are tracked within a representative microscopic volume and reactions occur discretely over stochastic time steps. While this is an effective method, it ignores the history of reaction, which may result in significant discrepancies from the reality. The combination of statistical and deterministic approaches gives rise to powerful methods, such as kinetic Monte Carlo (*k*MC) model, coupled with Gillespie's algorithm [50], [51].

1.3.1 The kinetic Monte Carlo model coupled with Gillespie's algorithm

Monte Carlo is a diverse family of approaches united by a simple central idea: solving complex problems using random numbers. Monte Carlo-based methods have become widely used in computational chemistry and materials science because of their versatility and their ability to address not only equilibrium problems, but also dynamic phenomena. In contemporary research, *k*MC is a powerful tool for investigating diverse processes, including transport of materials, physical structures and properties, and both equilibrium and non-equilibrium chemistry [49].

Gillespie's algorithm [45], which emerged in 1977, is now the most widely used algorithm in the investigation of polymerization processes. The use of *k*MC coupled with Gillespie's algorithm will be examined, with a specific focus on the research conducted by De Keer *et al.* [52]. The cited study combines kinetic Monte Carlo simulations with molecular dynamics simulations (MD) to predict the chemical and physical interactions between building blocks over time and in three-dimensional space during the entire network formation process. This approach captures molecular information at any given synthesis time *t*, providing details on individual segment compositions, functional groups, bond lengths and angles, and structural defects. The model was also applied to the synthesis of organosilica networks, starting with a sufficiently large number of TEOS molecules. As previously stated, TEOS molecules undergo multiple hydrolysis steps and participate in condensation reactions, resulting in crosslinks; these crosslinking reactions can be categorized as either intermolecular or intramolecular. Intermolecular reactions lead to larger network molecules, but they also reduce linear molecules by incorporating them as dangling chains. In contrast, intramolecular reactions increase the crosslinking degree within a given network molecule. As polymer network yields increase, intramolecular reactions become more likely, which can lead to structural defects.

The aim of the matrix-based *k*MC algorithm is to fully describe the evolution of the network during the reaction. By combining *k*MC and MD simulations, it is even possible to visualize the evolution of each building block over time. The main steps of the *k*MC algorithm are depicted in Figure 1.7. To facilitate the description of the method each step is examined in the following subparagraphs.

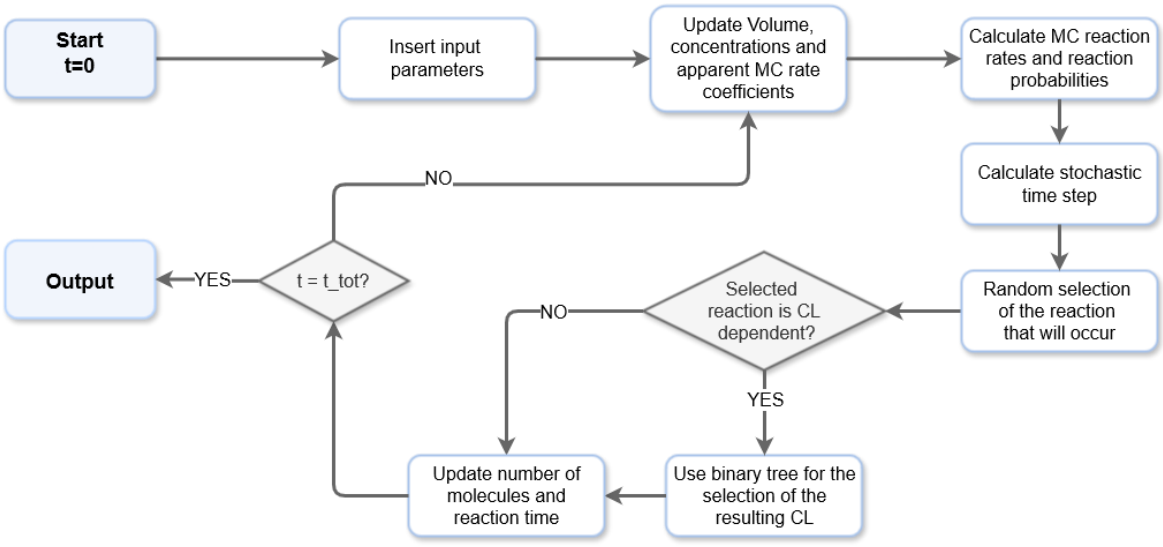

Figure 1.8: simplified scheme representing the main steps of the matrix-based kMC algorithm.

1.3.1.1 Input parameters

The matrix-based kinetic Monte Carlo (*k*MC) algorithm initiates at time t = 0 s. This algorithm is built on several key inputs:

- A comprehensive list of reaction types based on the functional groups involved.
- The functionalization degrees (*fd* values) of monomers or building blocks allowing crosslinking. For instance, TEOS is a tetrafunctional monomer with a *fd* value of 4, MTES is trifunctional (*fd*=3) and DMDES is bifunctional (*fd*=2).
- Polymerization temperature T_p and pressure p_p.
- Intrinsic kinetic information (Arrhenius parameters) to calculate the chemical rate constants k_{chem}.
- Initial concentrations, C_0.
- The initial total number of molecules $n_{tot,0}$, which allows for the calculation of the initial Monte Carlo simulation volume V_0. It is important to verify that $n_{tot,0}$ is sufficiently high to achieve a statistically accurate representation of the process.
- Total simulation time t_{tot} and plotting times t_{plot}.
- Initial physicochemical properties, including individual densities and molar masses of all molecule types.

This kinetic modelling approach also has the ability to distinguish between main and side reactions and accommodate a large number of reaction types. Additionally, the chemical rate constant values (k_{chem}) are defined based on the functional groups involved. For example, if a molecule has four functional groups of the same chemical composition, it can react four times with the same k_{chem}, assuming no local environmental effects (this is the case for TEOS). However, if there are local environmental influences, the molecule may react with four different k_{chem} values.

1.3.1.2 Initialization

After entering all relevant parameters, an initialisation process takes place. During this process, all matrix elements associated with the composition of network molecules, specifically molecules with connected chemical points, are set to zero as no network molecules exist at this stage. Also, the initial number of molecules, concentrations of all molecule types, and individual initial number of functional groups (FGs) are calculated.

1.3.1.3 Calculation of reactions probabilities using Gillespie algorithm

In the context of chemical reactions, each step is defined by the functional groups (FGs) involved and characterized by a chemical rate coefficient denoted as k_{chem}. These coefficients are determined through regression analysis against isothermal (NMR) experimental data. It is important to note that in the case of TEOS polymerization, diffusivity issues are disregarded due to the dominance of linear species.

The probability of a reaction occurring is then calculated by computing the microscopic Monte Carlo rates for individual reaction types. These rates are evaluated at a given time *t*, with the first entry occurring at *t=0 s*, followed by subsequent entries per stochastic time step τ. Rates are expressed in units of s^{-1}, indicating how many times a specific reaction type is expected to occur per second. To achieve this, k_{chem} values are converted to k_{mic} values so that the resulting rates are expressed as a turnover frequency in s^{-1}.

The initial input conditions at $t = 0\ s$ are summarised below:

- The concentration X_i is expressed numerically using as input parameters volume and initial concentration giving the number of molecules of type i: $X_i = C_i V N_A$
- For unimolecular reactions: $k_{mic} = k_{chem}$
- For bimolecular reactions involving two different species: $k_{mic} = \frac{k_{chem}}{V N_A}$
- Correction factors can also be used to address complexities such as bimolecular reactions between identical species: $k_{mic} = \frac{2k_{chem}}{V N_A}$

The time step τ is then calculated, which represents the interval between successive reactions and allows the total time to be updated after each reaction has been completed. To calculate the time step, a random number is divided by the total reaction rate, in this way larger total reaction rates correspond to smaller time steps. The probability of the different possible reactions to occur is then calculated by dividing each individual reaction rate by the total rate. The calculated probabilities are transformed into a cumulative probability distribution within a range of 0 to 1. This representation assigns each potential reaction a distinct vertical interval, with reactions having the highest likelihood covering a wider range of values, consistently with the principles of the Gillespie algorithm [51].

At this point the selection of a specific reaction occurs, a random number between 0 and 1 is generated and the vertical interval containing this number corresponds to the selected reaction.

Following this, the concentration X_i and time t are updated. The mathematical steps for this procedure are summarized below:

- Calculate reaction rates based on numerical inputs, $r(v) = k_{v,mic} X_i X_j$
- Determine the time step for subsequent reactions, $\tau = [\sum_{v=1}^{M} r(v)\,]^{-1}\, log(-r_1)$
- Evaluate probabilities by comparing individual rates to the total, $P(v) = r(v)/\sum_{v=1}^{M} r(v)$
- Randomly select a reaction using cumulative probabilities, $\sum_{v=1}^{\mu-1} P(v) \leq r_2 \leq \sum_{v=1}^{\mu} P(v)$
- Update X_i for the reaction event μ and the overall time $t = t + \tau$
- Start again recalculating the rates with the updated values.

1.3.1.4 Stochastic identification of the reactants

This step aims to identify the species containing functional groups (FGs) linked to the microscopic Monte Carlo rates selected in the previous stage, as these FGs are the ones that will react. The first FG, referred to as A, must be stochastically selected from the entire population of such groups. To achieve this, a FG binary sampling tree is used, each leaf node in the bottom row of the tree represents a molecule and the numerical value associated with each leaf node corresponds to the amount of free, unreacted functional groups within that particular molecule. Furthermore, a FG sampling matrix RA is introduced to complement the tree, this matrix includes numbers that indicate the location of the FGs in the topology matrix. To select the second FG, denoted as B, the same approach is used, but with a different initial step depending on whether the chosen reaction is intermolecular or intramolecular. If an intermolecular reaction is chosen, it is automatically verified whether this second group belongs to a different molecule. For intramolecular reactions, it is necessary to check if the two selected functional groups are part of the same molecule. If they are, an additional step is required to ensure that the FGs are at the correct distance to allow the molecule to rearrange and bring the FGs close enough to react.

In the context of silica sol gels, such as TEOS, group A refers to the OR group, which reacts with the second functional group, B. To handle the complexity resulting from different numbers of OR groups in a molecule, matrices and trees RA4/3/2/1 are used; these structures help differentiate between molecules based on their specific OR group counts (RA4 indicates molecules with 4 alkoxy groups and so on). Furthermore, the general matrix and tree, labelled

RA, represent the overall aggregate of OR groups. This systematic approach helps to capture the complexity of silica sol gels and their reactive behaviour.
In summary, this process involves identifying species with the reacting functional groups, stochastically selecting the first FG (A) using a binary tree and a sampling matrix, and then selecting the second FG (B) with the same method, ensuring compatibility based on the type of reaction.

1.3.1.5 Updating the topology matrix

The topology matrix is an important element in Monte Carlo simulations. It updates the chemical network by storing the connectivity and composition of all molecules, serving as a memory of the local chemical environment surrounding the FGs.
The composition of the molecules is stored in the body of the matrix, while the connectivities between all segments are stored in two vertical arrays, CA1 and CA2. When discussing intermolecular crosslinking, a new segment is identified by updating the corresponding vertical arrays. In contrast, intramolecular reactions require a more complex process. Before updating the topology matrix, an examination is conducted to confirm that the selected FGs are at the appropriate distance for a physical reaction to occur. To determine this, a fundamental distance rule is applied. If the functional groups are not sufficiently far apart, the algorithm repeats its steps and randomly selects two reacting FGs again.

1.3.1.6 Updating the number of molecules and concentrations

The objective of this final step is to update the number of molecules and their concentrations to refresh the reaction probabilities as we move from time t to $t + \tau$. If the newly calculated time matches the value of the final synthesis time t_{tot}, which is an input parameter, the main internal loop is closed. Otherwise, there is a backtrack to the calculation of the new volume, concentrations, and apparent rate coefficients. Using these recalculated parameters the updated reaction probabilities are obtained, and the simulation proceeds with other reactions, following the same steps as previously explained.

In conclusion, *k*MC simulations are a versatile tool for investigating a wide range of processes. Specifically, the use of Gillespie's algorithm, coupled with *k*MC, has been of great importance in the study of polymerisation processes. The research by De Keer *et al.* [52] exemplifies this,

combining *k*MC with molecular dynamics simulations to predict interactions during network formation. This approach captures detailed molecular information, providing insights into segment compositions, functional groups, bond lengths and angles, and structural defects. The combination of kMC and MD simulations provides a powerful tool for visualising the evolution of building blocks over time, enhancing the understanding of complex chemical systems. This method has been successfully applied to the synthesis of organosilica networks, revealing the dynamics of crosslinking reactions and their impact on network structure.

1.4 Rheological behaviour of organosilica during sol-gel synthesis

Rheology is the scientific discipline that studies the flow and deformation characteristics of materials. It examines how substances respond under the influence of a mechanical force. Rheometry refers to a set of experimental techniques used to determine the rheological properties of materials [53].

Materials can exhibit different behaviours: viscous behaviour implies that all the energy applied is dissipated as heat whereas elastic behaviour implies that all the energy applied is stored in the material. Some materials can exhibit both behaviours and are therefore referred to as viscoelastic materials. Rheological studies and the characterization of viscoelastic properties are crucial for various applications since the flow behaviour of materials is an essential quality control tool for the maintenance of the product value [53], [54].

1.4.1 Rheometry

A rheometer is a laboratory instrument used to study the flow and deformation behaviour of substances in both solid and liquid states. Unlike viscosimeters, which provide a single viscosity value, rheometers allow the investigation of multiple parameters by subjecting samples to external forces and providing a valuable understanding of their response, particularly when acting as fluids.

The flow of a material can be defined as a continuous deformation over a period of time. Different materials exhibit different flow behaviours. Newtonian flow is a type of fluid flow where viscosity remains constant regardless of shear rate, whereas non-Newtonian flow occurs when viscosity varies with shear rate. There are two main types of non-Newtonian flow

behaviour: shear thickening, where viscosity increases with increasing shear rate, and shear thinning, where viscosity decreases with increasing shear rate [53].

Rheological measurements are important in both industrial production and scientific research. The most commonly used techniques for determining viscosity and rheological properties can generally be divided into three broad categories:

(i) Capillary technique, where viscosity is determined from measurements of both flow rate and pressure drop.

(ii) The rotational technique, where viscosity is calculated from measurements of torque and rotor speed, and

(iii) the falling/rolling ball technique, where the viscosity is derived from the time required for a ball of known density to roll or fall a certain distance in the fluid being tested [55].

The focus in this work will be on the rotational technique, in particular the parallel plate geometry. This geometry, first proposed by Mooney in 1934, describes the behaviour of viscoelastic materials sandwiched between two plates. In this arrangement, the sample is placed on the stationary lower plate. The upper plate, connected to the rheometer motor by a shaft, is lowered until it reaches a pre-defined gap. The top plate is then rotated at a fixed speed (shear rate, $\dot{\gamma}$) and the resulting force (shear stress, τ) is measured. In this way, the viscosity (η) is obtained from the ratio of shear stress to shear rate, reflecting the material's resistance to shear flow [54].

The parallel plate geometry may introduce errors due to secondary flows, edge effects, and shear heating; however, these errors can be effectively reduced by operating at small gaps [53]. Despite these potential errors, this geometry offers key advantages, such as simplifying the process of preparing and loading samples, particularly for highly viscous materials and soft solids. Compared to cone and plate or concentric cylinders, the parallel disk rheometer is especially effective in collecting viscosity and normal stress data at high shear rates. The shear rate can be increased by adjusting either the rotation rate or decreasing the gap when using this geometry [53], [56]. Specifically, as the gap between the plates decreases, the shear rate increases for a given rotational speed. This is because the shear rate is defined as the velocity gradient across the gap. When the gap is smaller, the velocity difference between the moving plate and the stationary one is distributed over a shorter distance, leading to a higher shear rate. Conversely, a larger gap would distribute the velocity difference over a greater distance, resulting in a lower shear rate [53].

The parallel plate geometry is a powerful tool for characterizing viscous fluids and understanding viscoelastic behaviours. Therefore, it is the preferred method for measuring viscoelastic material properties [57].

1.4.2 Rheology of organosilica sol-gel systems

Understanding the rheology of the solution is essential for predicting the final material properties in the context of sol-gel synthesis. To achieve this, the solution's behaviour is systematically examined at different reaction times and under varying catalyst concentrations. This will provide insights into how the rheological properties evolve with changing conditions and ultimately guide the development of tailored sol-gel materials. In particular, rheological characterization is crucial for optimal performance of electrospinning [58].

Electrospinning is a modern and versatile technique to produce fibers that has been evolving since the late 1990s. It uses an electric field to generate microscopic filaments with diameters in the nanometer range [59]. These nanofibers have numerous applications in fields such as textile engineering [60], battery development [61], [62], biotechnology [63], [64], and gas sensors [65]. This process involves injecting a charged liquid, either a melt or a solution, through a fine needle, the electric field causes the liquid to stretch and the repulsion between the charges results in the formation of ultrafine fibers. Researchers can modify the morphology of electrospun fibers for practical applications [66], [67]. Studies on the electrospinning of ceramic nanofibers have significantly increased in the last decade; specifically interesting is electrospinning based on silica sol-gel systems, for which TEOS has been widely used, since it can be easily produced at low temperatures. Typically, a polymer is added to the TEOS-based spinning solution to achieve the necessary rheological properties for successful electrospinning. However, this polymer is later burned out, often resulting in fibers with poor morphology and mechanical characteristics. More recently, direct electrospinning approaches have been explored to overcome these limitations [68].
Intrinsic viscosity analysis is a key parameter for assessing polymer solution properties, particularly in relation to fiber thickness and entanglement, since lower viscosity values can result in electro-spraying, which generates droplets rather than fibers [69]. Rheological analysis is essential in controlling viscosity during the electrospinning of sol-gel systems, enabling the production of nanofibrous membranes with specific properties.

Considering the rotational rheometer with the parallel plate geometry, the viscosity is determined by shearing the sample and measuring its resistance to the shear. In the case of TEOS and other silica or organosilica precursors also a solvent trap can be used to avoid excess evaporation of ethanol during the analysis [70].

To improve the understanding of the correlation between rheological properties and material synthesis and expand the industrial potential of nanofibrous materials for various applications, it is logical to progress towards electrospun organosilica membranes. This can be achieved by exploring a wider range of Si-based precursors beyond TEOS. With this aim, rheological properties of different organosilica precursors have been investigated to determine their distinct behaviours; the purpose is to analyze how the viscosity of a solution changes under varying conditions [69]. A rheological screening of sol-gel systems using different precursors (trialkoxymethylsilane, tetraethoxysilane, bis(trialkoxysilyl)methane, and bis(trialkoxysilyl)ethane) was conducted [69] using an MCR 702 rheometer from Anton Paar, equipped with a parallel plate setup featuring 5cm diameter discs and a 1mm gap, under a relaxation time of 1 minute and a temperature of 283K. The systems were analyzed based on reaction time, with shear rate varying stepwise from 0.1 to $1000s^{-1}$.

Despite the slight differences in precursor reactivity under initial conditions, a consistent trend emerged across all systems. As the reaction time increased, the dynamic viscosity also increased due to the higher cross-linking density within the sol-gel network. In agreement with previous studies [71], [72] Newtonian flow behaviour was observed over the tested shear range up to 1000 s^{-1} at viscosities below 1000 mPa s.

However, beyond 1000 mPa s, shear thinning was observed from a shear rate of 100 s^{-1}, with this effect becoming more pronounced at longer reaction times.

In conclusion, during the initial electrospinning phase, it is possible to consider a Newtonian flow behaviour, as low viscosities are required for the electrospinning of organosilica sols, then the sol changes from Newtonian to shear thinning near the gel point [69], [72].

Researchers are expanding the range of Si-based precursors used beyond TEOS, facilitating the production of electrospun organosilica membranes with diverse macroscopic properties and applications without the need to add polymer to the spinning solution. However, additional investigation into the behaviour of different precursors is still needed.

Chapter 2

Materials and methods

The preparation of the sols and the various analyses performed on the sols require many pieces of equipment and different procedures. This chapter provides technical information on the instrumentation used and the detailed protocol followed during the experimental part. A brief insight into the code used for the kinetic modelling is also included.

2.1 Materials

For the sol-gel synthesis of (organo)silica sol, the alkoxide precursors tetraethyl orthosilicate (TEOS, ≥99%), methyltriethoxysilane (MTES, ≥99%) and hydrochloric acid (HCl, 37%) were purchased from Sigma-Aldrich. HCl and distilled water (ISO 3696) were combined to form the catalyst solution. The solvent/reactant ethanol (EtOH absolute, ≥ 99.8 %) was obtained from VWR International. For NMR analysis, deuterated water (D2O) from Eurisotop was used as solvent. Liquid nitrogen was used to quench the reaction mixture.

2.2 Methods

2.2.1 Sol preparation

2.2.1.1 Ratios used for the preparation of the sols

The composition of the solution is varied according to the specific experiments. Two different molar ratios of the reactants are used: the Pouxviel ratio and the electrospinnable ratio. Pouxviel conducted experiments with TEOS [27] using the molar ratio [TEOS]:[EtOH]:[H2O]:[HCl] = 1:3.8:4:0.000227, with the water and HCl combined first to form a solution with a pH of 2.5. The same ratio is also applied to MTES, taking into account that it has three reacting functional groups instead of four. This resulted in the ratio [MTES] : [EtOH] : [H2O] : [HCl] = 1:2.85:3:0.00017. The second ratio used is that required for an electrospinnable solution, namely [MTES]:[EtOH]:[H2O]:[HCl]=1:2:2:0.01; this ratio is also used for [TEOS]:[EtOH]:[H2O]:[HCl].

2.2.1.2 Isothermal preparation

To prepare a sol isothermally at 25°C, the reagents are simply reacted in an open beaker on a stir plate. For isothermal synthesis at higher temperatures, the oven and oil bath are preheated to the selected temperature. The precursor and ethanol are preheated by submersion in the oil bath in a closed flask to avoid ethanol evaporation, the catalyst is preheated in a disposable bottle in the oven. When all the reagents are at the correct temperature, the sample is added to the preheated flask with the catalyst and the reagents are mixed, the sample remaining in the closed flask inside the oil bath for the selected time. In both cases, when the desired reaction time is reached, the sample is quenched in liquid nitrogen to drastically slow down the reactions prior to the NMR analysis. The isothermal experiments were always carried out with a Pouxviel ratio.

2.2.1.3 Non-isothermal preparation

For the non-isothermal synthesis an open set up consisting of a 200 ml beaker with a stir bar is used. The preparation of the sol involves several steps. Before adding H_2O and HCl, the precursor and the ethanol are well mixed. After adding the catalyst, the solution is mixed for 5 minutes at 25°C and then submerged in an oil bath preheated to 90°C on a heating plate to reach the desired temperature. When the desired reaction time is reached, the sample is quenched in liquid nitrogen to drastically slow down the reactions prior to the NMR analysis. For the non-isothermal synthesis a starting volume of 60ml is always used and both ratios are analysed.

2.2.2 NMR analysis

For NMR analysis 500 µL of diluted polymer solution (90 v% as retrieved at a given synthesis time and 10 v% D2O added) was put in a 5 mm NMR tube. The one-dimensional ^{29}Si NMR spectra were subsequently recorded on a 400 MHz Avance NEO Bruker Spectrometer equipped with a BBI probe at the NMR Expertise Centre at Ghent University. The spectrometer was operated at a ^{1}H and ^{29}Si frequency of 400.15 MHz and 79.50 MHz, respectively. The sample temperature was set to 298 K, hence, further reaction during analysis could take place, the extent in a first instance assessable via the earlier data of Pouxviel *et al* [27]. A “zgig” gradient spin echo pulse sequence was used to maximize the signal intensities. The acquisition time was set to 1.31 s, the spectral width to 315 ppm, the number of scans to 120, and the number of dummy

scans to 2. This lead to a total measurement time of 84 min per sample. A typical error bar of 5% has been selected. The software TopSpin 4.4.0 was used to analyse the ^{29}Si NMR spectra. The spectrum was subsequently Fourier transformed and calibrated using the corresponding calibrated 1H NMR spectrum as a secondary reference. Both a zero and first order phase correction were performed.

Figure 2.1: 400 MHz Avance NEO Bruker Spectrometer equip- ped with a BBI probe at the NMR Expertise Centre at Ghent University.

2.2.3 Rotational rheometer

The primary instrument used for the rheology measurements in this thesis is the Anton Paar MCR 702 MultiDrive rotational rheometer, as shown in Figure 2.1. This state-of-the-art model is one of the most advanced and versatile rheometers available, with a range of plate geometries and an integrated oven for high temperature testing. Data from the rheometer was analysed using Anton Paar's RheoCompass software.

For the experiments, the setup included two parallel 50 mm diameter plates (PP-50) and a solvent trap to prevent solvent evaporation and maintain a near saturated local atmosphere around the sample. Before starting the measurements, the sol was allowed to equilibrate in the geometry for one minute to improve the structural recovery (relaxation time), before being adjusted to 25°C for testing.

The rheometer was employed to conduct a two-part test. Initially, a constant shear rate $\dot{\gamma} = 1\ s^{-1}$ was maintained for 180 seconds. This was followed by a second constant shear rate $\dot{\gamma} = 100\ s^{-1}$ for 60 seconds. Data were specifically selected from around 120 seconds when the shear rate is $\dot{\gamma} = 1\ s^{-1}$. At this low shear rate the viscosity remains constant due to Newtonian flow and the measurements stabilise, providing a reliable indication of the behaviour of the sol.

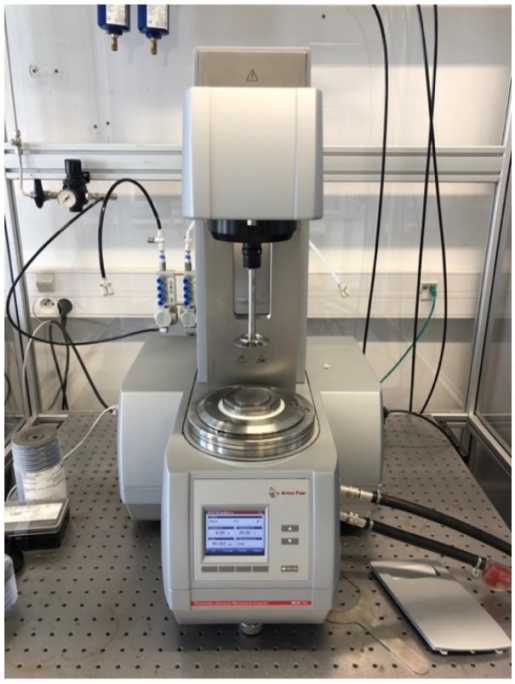

Figure 2.2: Anton Paar's MCR 702 Multidrive rotational rheometer in use at Ghent University laboratory.

2.2.4 Modelling section

The main principles of the kinetic Monte Carlo (kMC) framework to simulate TEOS crosslinking kinetics under both isothermal and non-isothermal conditions have been previously examined in Section 1.3, with specific focus on the contributions of De Keer *et al* [52].

Under non-isothermal conditions the temperature profile is incorporated into the code and solvent evaporation is formally modelled using a zero-order reaction with the corresponding "k_{chem}" tuned based on experimental measurements.

The initial number of monomers employed was always a minimum of 10000, with higher values utilized in cases where the reaction occurred under conditions that facilitated accelerated kinetics.

Modifications were introduced into the code to account for the different number of reacting functional groups in the two alkoxide precursors used (MTES and TEOS).

Chapter 3

Kinetic modelling

This chapter is dedicated to investigating the kinetics of the MTES and TEOS sol-gel synthesis, via kinetic modelling and ^{29}Si NMR. The ratio of [TEOS]:[EtOH]:[H2O]:[HCl] = 1:3.8:4:0.000227, based on the work of Pouxviel et al who performed a pioneering kinetic study of TEOS sol-gel crosslinking. [source] For MTES, this ratio was corrected for the number of reactive groups in the precursor (3 ethoxy groups instead of 4 (TEOS)), resulting in [MTES] : [EtOH] : [H2O] : [HCl] = 1:2.85:3:0.00017. This way, it is possible to compare the two precursors, taking into account their different number of reactive groups.

The kinetic modelling process for both isothermal and non-isothermal reactions involves the following key steps:

(i) The sol is synthesised in the laboratory in accordance with the procedures described in Chapter 2.

(ii) The analysis of these sols at various reaction times using NMR is employed to determine the fractions of differently condensed molecules (for MTES: T^0, T^1, T^2, T^3; for TEOS: Q^0, Q^1, Q^2, Q^3, Q^4; the superscript corresponds with the number of condensed groups Si atom).

(iii) The reactivity ratios and activation energies are tuned within the code to fit the experimental data obtained from the NMR analysis.

These steps constitute the basis of the kinetic modelling performed, and the results are presented in the following paragraphs.

3.1 Isothermal reaction

For the isothermal synthesis, the temperatures analysed are 25°C, 40°C, and 55°C. The reactivity ratios and activation energies for TEOS have already been determined and published in the literature [28]. However, for MTES, adjustments to these parameters are necessary,

starting with the values obtained for TEOS in the previous study [28]. The reactivity ratios are calibrated using the 25°C experiment as a reference. Optimal tuning is achieved when the model accurately predicts the fractions of differently hydrolysed molecules, as determined by NMR analysis of the sols. Once the reactivity ratios are properly calibrated for the 25°C experiment, the higher temperatures are examined to refine the activation energies for the various reactions, and to derive the corresponding Arrhenius parameters.

3.1.1 Isothermal reaction of MTES at 25°C

The reaction of MTES at room temperature is optimally tuned with the values of the reactivity ratios summarised in Table 3.1.

Table 3.1: comparison between the reactivity ratio published for TEOS and the tuned reactivity ratios obtained for MTES.

Reaction considered	**Reference from TEOS** [28]	**Tuned values for MTES**
$k_{hydro}[L/(mol\ s)]$	$7.20 \cdot 10^{-5}$ *	$5.52 \cdot 10^{-3}$
$k_{hydro,rev}[L/(mol\ s)]$	$2.40 \cdot 10^{-6}$	$1.00 \cdot 10^{-3}$
$k_{water\ cond,bi}[L/(mol\ s)]$	$1.00 \cdot 10^{-5}$	$1.40 \cdot 10^{-5}$
$k_{water\ cond,uni}[1/s]$	$1.00 \cdot 10^{-9}$	$1.00 \cdot 10^{-9}$
$k_{alcohol\ cond,bi}[L/(mol\ s)]$	$7.00 \cdot 10^{-6}$	$6.90 \cdot 10^{-6}$
$k_{alcohol\ cond,uni}[1/s]$	$1.00 \cdot 10^{-9}$	$1.00 \cdot 10^{-9}$

* $7.20 \cdot 10^{-5} = 1.20 \cdot 10^{-5} \cdot 6$, *in this case, the hydrolysis reactivity ratio for TEOS is multiplied by six, as it was originally calculated for four non-hydrolyzed groups. Since MTES has only three non-hydrolyzed groups, the reference reactivity ratio for TEOS with three groups is used rather than that for TEOS with four groups. Specifically, this reference ratio is six times the value for the four-group scenario.*

From the values in the table it can be concluded that for MTES the hydrolysis reaction is considerably faster, on the other hand, condensation reactions are just slightly faster, this result is in accordance with previous studies [46], [73]. In particular, existing work [8], [74] confirms that acid catalysed hydrolysis is faster in methylethoxysilanes $(CH_3)_x\ (C_2H_5O)_{4-x}Si$; due to inductive effects the hydrolysis rate increases with the degree of substitution x, of electron donating alkyl groups.

The resulting tuning can be visualized in Figure 3.1 and it achieves a good correspondence with the experimental data.

In the plot the continuous lines represent the data obtained from the code and the dotted lines represent the data from the NMR analysis. It should be noted that the NMR measurement time (1 hour and 24 minutes at 25°C) was also incorporated into the code as a reaction time, given that the sol continues to react throughout the course of the procedure.

The experimental data is represented by circles, which correspond to the NMR results and are connected by dotted lines for visualization. In contrast, the plotted points generated by the code represent the calculated fraction of each moiety approximately every six seconds resulting in smoother lines since more frequent data are available.

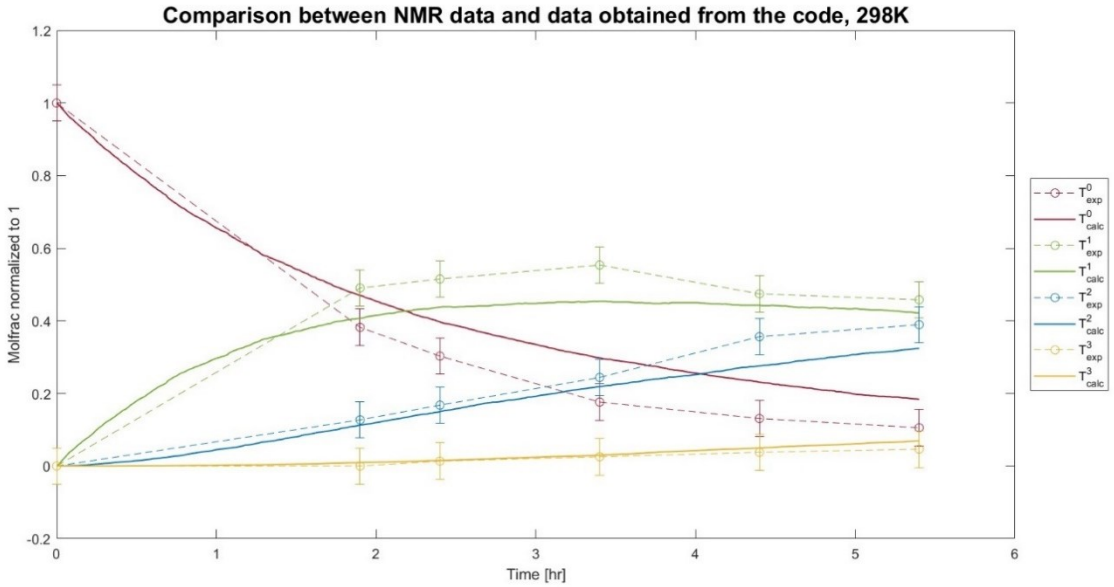

Figure 3.1: Comparison between experimental data (dotted lines) and data obtained from the code (continuous lines) at 25°C. The plot shows the evolution of the different moieties of MTES over reaction time. Typical error bars of 5% have been used.

3.1.2 Isothermal reaction of MTES at higher temperatures

In the analysis of the isothermal reaction at higher temperatures, the reactivity ratios determined at 25°C (see Table 3.1) are used. However, for temperatures above 25°C, it is necessary to tune also the activation energies. This adjustment is required because temperature influences the reactivity ratios in accordance with the Arrhenius law [75]:

$$\ln \frac{k_1}{k_2} = \frac{E_a}{R} \cdot \left(\frac{1}{T_2} \cdot \frac{1}{T_1} \right) \tag{3.1}$$

Where:

T_1= temperature in [K], in this context $T_1 = 328K$;

T_2= temperature in [K], in this context $T_2 = 313K \; or \; 328K$;

k_1= reactivity ratio at T_1, in this context corresponding at the values in Table 3.1;

k_2= reactivity ratio at T_2;

E_a= activation energy, these are the values that need tuning for MTES starting from the values found for TEOS in previous research [28];

$R = 8.314 \; \frac{J}{mol \, K}$, universal gas constant.

In order to guarantee that the model incorporates temperature effects in an accurate manner, the code is modified to include the temperature profile. During the course of the reaction, the temperature is maintained at either 40°C or 55°C and is then reduced to 25°C for the duration of the NMR analysis. Furthermore, the activation energies for each reaction are added as inputs into the code and employed to compute the reactivity ratios in accordance with the Arrhenius law, as detailed in equation [3.1].

Although ethanol may evaporate at higher temperatures, this factor is not considered in the code due to the reaction being conducted in a sealed flask at temperatures well below the boiling point of ethanol. This aspect will be addressed in the non-isothermal synthesis phase, where temperature variations are more complex and reach the boiling point of ethanol, and the loss of ethanol must be accounted for. This careful calibration ensures that the model will remain robust and accurate across different experimental conditions.

The reaction of MTES at higher temperatures is optimally tuned with the values of the activation energies summarised in Table 3.2. These values were estimated by starting from the values used for TEOS in previous research [28], and considering the values already proposed in the literature for MTES [76].

The data presented in Table 3.2 indicates that MTES displays a heightened sensitivity to temperature fluctuations in comparison to TEOS. While temperature has a minimal impact on the already rapid hydrolysis reactions, it significantly influences the condensation reactions as evidenced by the higher activation energies for these reactions. This observation aligns with the results of our laboratory experiments, in which we found that MTES networks formed at a considerably faster rate at higher temperatures, resulting in a highly adhesive solid material. As a result, the reaction became more difficult to control, leading to faster gelation and less manageable processes. This highlights the importance of carefully monitoring and adjusting temperature when working with MTES to ensure controlled synthesis.

Table 3.2: comparison between the activation energies published for TEOS and the tuned activation energies obtained for MTES.

Reaction considered	**Reference from TEOS** [28] [J/mol]	**Tuned values for MTES** [J/mol]
Hydrolysis	$39.2 \cdot 10^3$	$34.5 \cdot 10^3$
Reverse hydrolysis	$39.2 \cdot 10^3$	$34.5 \cdot 10^3$
Water condensation, bimolecular	$30.0 \cdot 10^3$	$49.2 \cdot 10^3$
Water condensation, unimolecular	$30.0 \cdot 10^3$	$49.2 \cdot 10^3$
Alcohol condensation, bimolecular	$30.0 \cdot 10^3$	$49.2 \cdot 10^3$
Alcohol condensation, unimolecular	$30.0 \cdot 10^3$	$49.2 \cdot 10^3$

Using the tuned reactivity ratios (Table 3.1) and activation energies (Table 3.2), the model provides an accurate prediction of MTES reaction behaviour at both 40°C and 55°C. The results demonstrate that the tuned parameters successfully capture the dynamics of the reaction under these conditions. This accuracy can be clearly observed in Figures 3.2 and 3.3, where the predicted reaction profiles align well with the experimental data at the respective temperatures. These findings confirm the effectiveness of the tuning process in modelling MTES behaviour.
To construct these plots, each data point was individually modelled and then connected to create a continuous representation. The crosses on the plots represent the data points that were modelled using the computational code, and these are connected by continuous lines to show the overall trend. Modelling each point separately was necessary because the temperature profile had to be updated for every data point to account for both the selected reaction time and the NMR time. The experimental data are represented by dots on the plots, which are connected with dotted lines to differentiate them from the modelled data.

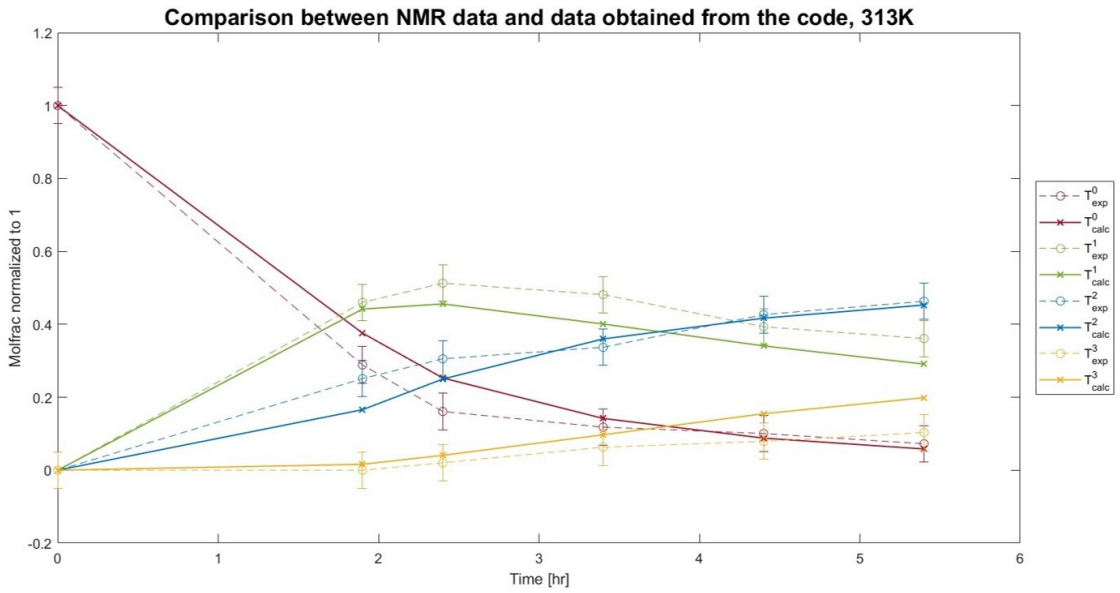

Figure 3.2: Comparison between experimental data (dotted lines) and data obtained from the code (continuous lines) at 40°C. The plot shows the evolution of the different moieties of MTES over reaction time. Typical error bars of 5% have been used.

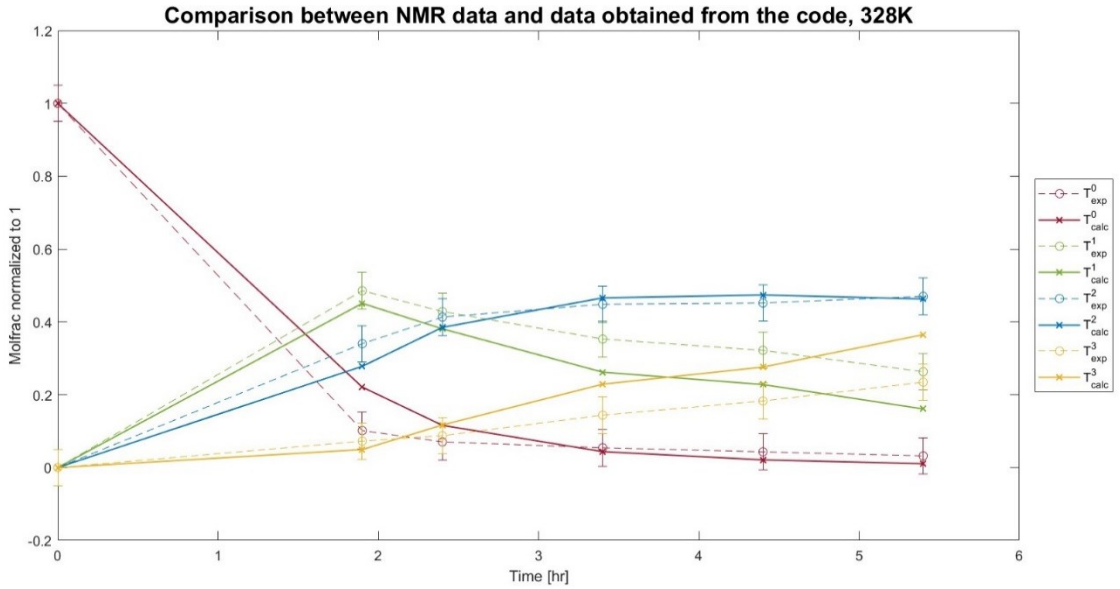

Figure 3.3: Comparison between experimental data (dotted lines) and data obtained from the code (continuous lines) at 55°C. The plot shows the evolution of the different moieties of MTES over reaction time. Typical error bars of 5% have been used.

In order to gain a deeper insight into the influence of NMR time at 25°C on the overall reaction, Figures 3.4 and 3.5 present a comparison of data obtained under two distinct conditions: firstly, when the code is executed isothermally at 40°C and 55°C without taking NMR time into account; and secondly, when the NMR time is incorporated. In the latter case, each reaction time is modelled separately, requiring updates to the temperature profile for each data point. The resulting data are connected by dotted lines. Conversely, when the code is executed

isothermally at a single temperature, the data are generated at approximately six-second intervals, resulting in the production of smoother, continuous lines.

Figure 3.4, which examines the reaction at 40°C, shows that including the NMR time leads to greater overall reaction progress, especially for shorter reaction times. This occurs because the shorter exposure to the higher temperature makes the 1 hour and 24 minutes spent in the NMR at 25°C more significant.

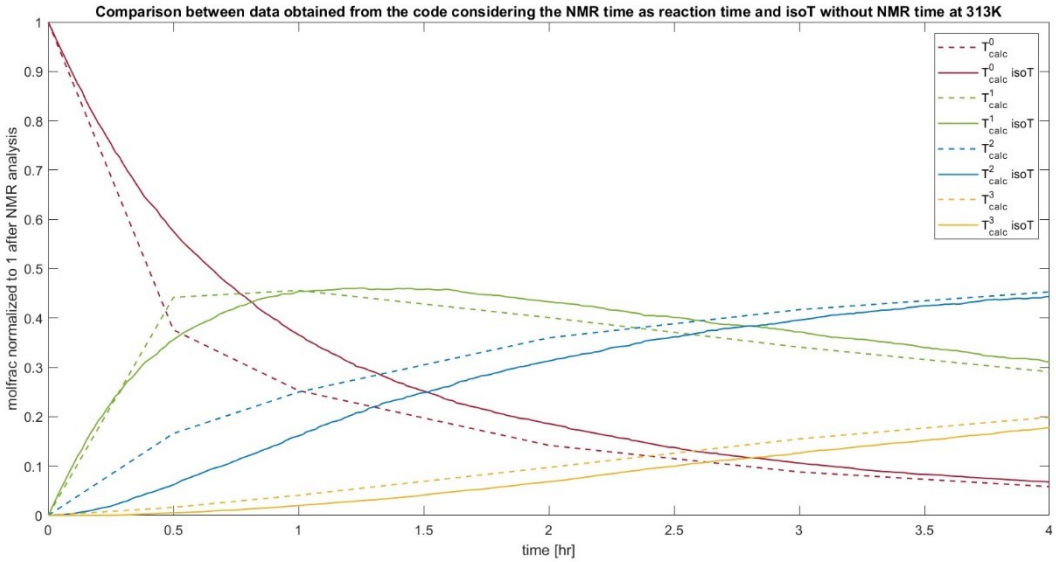

Figure 3.4: compare data obtained under two conditions: when the code is run isothermally at 40°C without considering NMR time (continuous lines), and when the NMR time, namely 1hour and 24 minutes at 25°C, is included (dotted lines), however to consistently compare the data the time on the x-axis is the reaction time in the beaker also for the experimental data including the NMR time. The plot shows the evolution of the different moieties of MTES over reaction time.

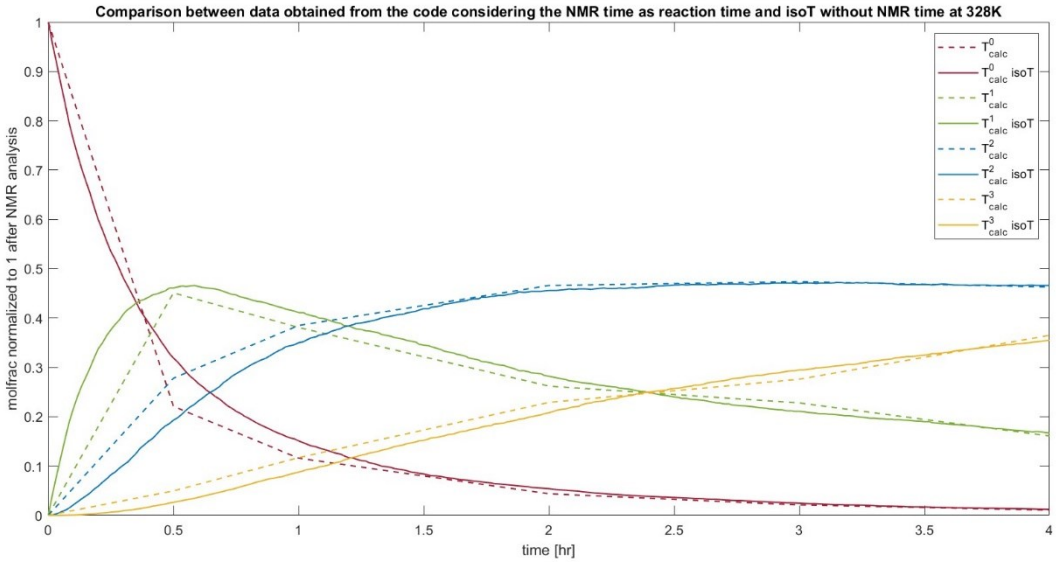

Figure 3.5: comparison of the data obtained under two conditions: when the code runs isothermally at 55°C without considering NMR time (continuous lines), and when the NMR time, namely 1hour and 24 minutes at 25°C, is included (dotted lines), however to consistently compare the data the time on the x-axis is the reaction time in the beaker also for the experimental data including the NMR time. The plot shows the evolution of the different moieties of MTES over reaction time.

In Figure 3.5, which focuses on the reaction at 55°C, the additional NMR time at room temperature has a reduced effect, as the higher laboratory reaction temperature predominates, thereby reducing the impact of the NMR time.

Having obtained a robust fit for both reactivity ratios and activation energies at 25°C and higher temperatures, it is now possible to obtain the Arrhenius plot.
This plot is a graphical method used to illustrate the correlation between reactivity ratios and temperature. The plot is constructed by plotting the natural logarithm of the reactivity ratios against the inverse of the temperature. The relationship between these variables is governed by the Arrhenius equation, as previously introduced in equation 3.1. From this equation, it can be derived that the slope of the line on the Arrhenius plot is equal to $-E_a/R$ and it provides a direct measure of the activation energies.
A plot with a steeper slope indicates a higher activation energy, thereby suggesting that the reaction rate is highly sensitive to temperature changes. Conversely, an inferior slope indicates a lower activation energy and a reduced sensitivity to temperature.
For the reactions under study, the derived Arrhenius plot reveals that the slopes are consistent across different reactions. In particular, all reactions display a similar level of sensitivity to temperature fluctuations, suggesting that their respective activation energies are comparable.

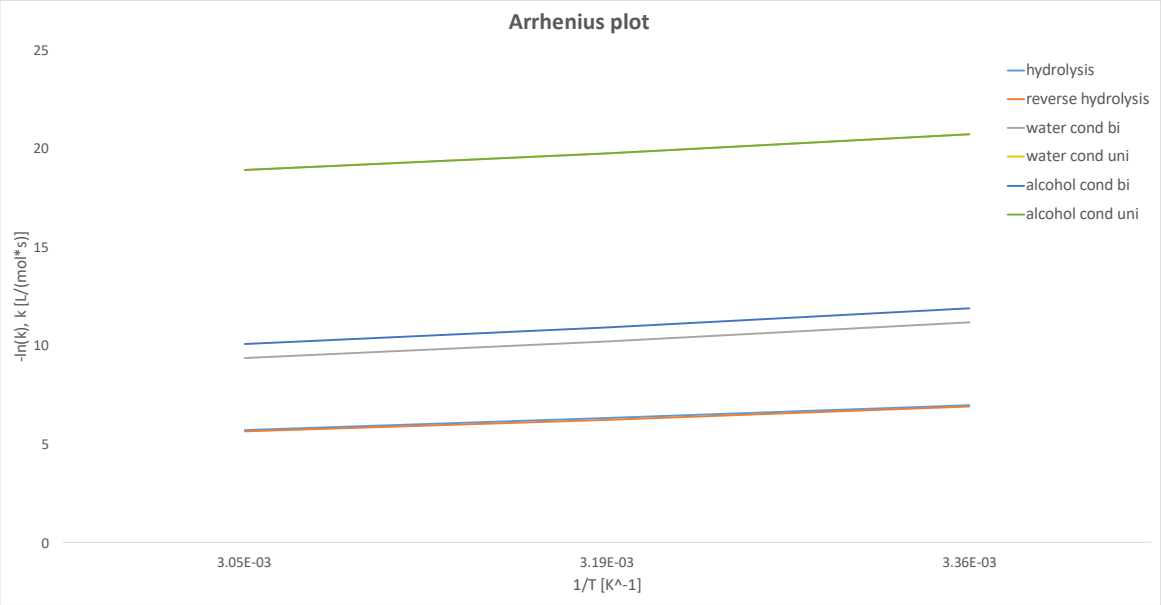

Figure 3.6: The Arrhenius plot is used to visualize the relationship between reactivity ratios and temperature. It is constructed by plotting the natural logarithm of the reactivity ratios against the inverse of the temperature.

3.1.3 Comparison of MTES with TEOS under isothermal conditions

Firstly, a comparison between TEOS and MTES at 25°C is conducted to illustrate their distinct behaviours at room temperature. Figure 3.7 provides a visual representation of this comparison, with TEOS depicted by dotted lines and MTES shown with continuous lines. The red line on the plot represents T^0 for MTES and a combination of Q^0 and Q^1 for TEOS.

The plot reveals that MTES undergoes hydrolysis more rapidly than TEOS. This is evident from the faster consumption of T^0 and the more rapid formation of T^1 for MTES. This accelerated initial hydrolysis is consistent with previous observations detailed in Table 3.1, which indicate that MTES hydrolyzes more quickly. It is also important to note that the red line for MTES represents only T0, while for TEOS, it encompasses both Q0 and Q1. Therefore, the longer time required for TEOS is due also to the combined hydrolysis of both Q0 and Q1, which contributes to the lower slope of the red dotted line.

For molecules with one remaining non-hydrolyzed group, T2 in MTES and Q3 in TEOS, MTES continues to exhibit a slightly faster reaction rate.

When nearly all ethoxy groups have been hydrolyzed, the reaction pathways for TEOS and MTES converge. Despite the faster initial hydrolysis of MTES, the overall progression towards complete hydrolysis shows a similar trajectory for both compounds.

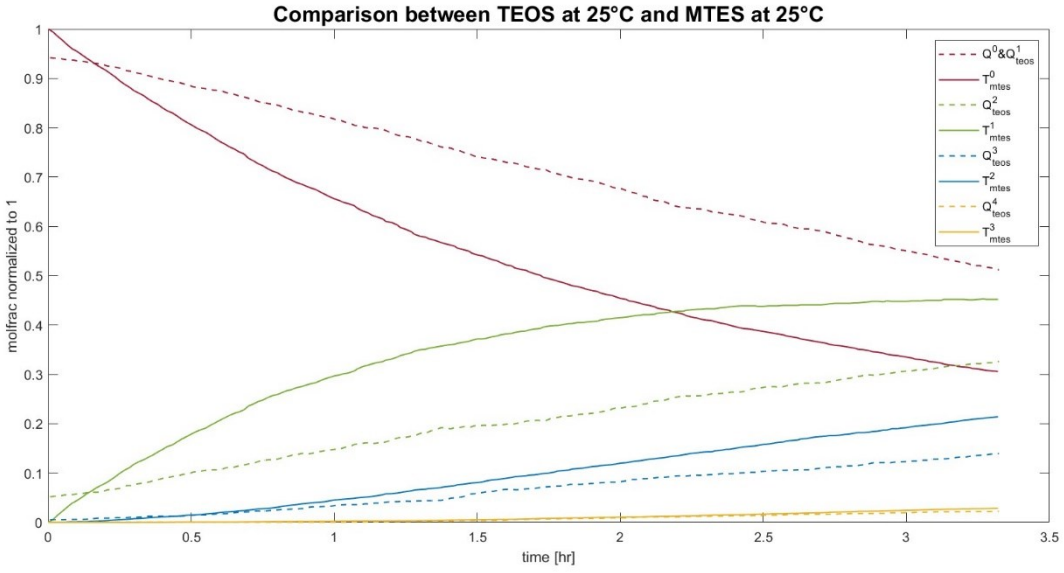

Figure 3.7: Comparison between data obtained from the code for two different precursors both at 25°C. In particular, MTES is represented by the continuous lines and TEOS by the dotted lines. Note that the red line on the plot represents T^0 for MTES and a combination of Q^0 and Q^1 for TEOS.

The evaluation of the conditions under which TEOS and MTES exhibit similar hydrolysis behaviours is illustrated in Figure 3.8. The plot shows that TEOS at 40°C and MTES at 25°C exhibit comparable reaction pathways. This indicates that the hydrolysis behaviour of TEOS under these conditions is analogous to that of MTES. This plot employs the same graphical approach to compare the two precursors as that used in Figure 3.7.

This observed similarity between the two analyzed precursors can be explained by the influence of temperature on reaction kinetics. At 40°C, the increased thermal energy accelerates the hydrolysis process of TEOS, resulting in a reaction rate that approaches that of MTES at 25°C. Conversely, MTES, which has a different chemical structure, exhibits a higher hydrolysis rate at the lower temperature of 25°C, resulting in a hydrolysis rate comparable to TEOS at the higher temperature of 40°C.

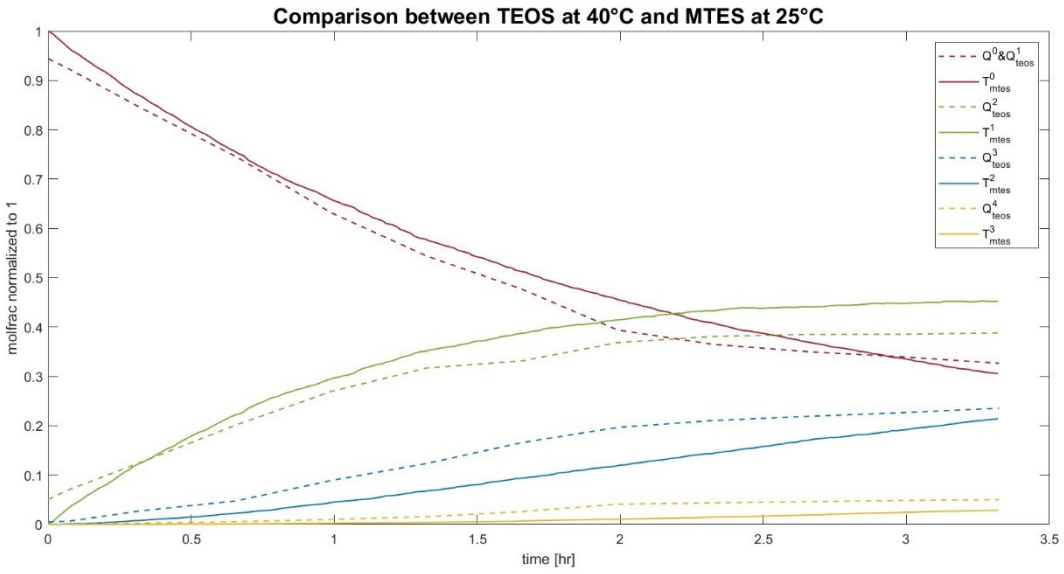

Figure 3.8: Comparison between data obtained from the code for two different precursors. In particular, MTES reacted at 25°C is represented by the continuous lines and TEOS reacted at 40°C by the dotted lines. Note that the red line on the plot represents T^0 for MTES and a combination of Q^0 and Q^1 for TEOS.

3.2 Non-isothermal reaction, Pouxviel ratio

In modelling a non-isothermal synthesis like used for electrospinning using the code, it is essential to incorporate both the temperature profile and the evaporation of ethanol. While the temperature profile was already considered in the isothermal synthesis at higher temperatures, the non-isothermal process introduces additional complexity due to the high temperature above the boiling point of ethanol and the open-beaker setup, which allows ethanol to evaporate as detailed in Chapter 2. To ensure an accurate simulation of the evaporation of ethanol, several

modifications were implemented in the code, the details of which will be provided in the following paragraph.

The temperature profile for the non-isothermal synthesis starts with the sol being maintained at 25°C for 5 minutes. Subsequently, the solution is heated by placing it in an oil bath, resulting in an increase in temperature.

A temperature sensor was employed to monitor this increase, which eventually reached 79°C, the boiling point of ethanol. Additionally, the NMR time (1 hour and 24 minutes) is considered as reaction time at 25°C.

Given the necessity of updating the temperature profile at each reaction time point, the code must be run separately for each time step, as already done for the isothermal case at higher temperatures. The resulting data are then linked to form a continuous representation. In the figures provided in the next paragraphs, crosses on the plots indicate data points generated by the computational model, which are connected by continuous lines to illustrate the overall trend. As each data point had to be modelled separately, the lines may appear less smooth. Experimental data from the NMR analysis are depicted as dots on the plots, with dotted lines connecting them.

3.2.1 Evaporation rate of Ethanol

In order to evaluate the evaporation rate of ethanol during the non-isothermal experiment described in the previous chapter, the volume of the solution was systematically measured at seven-minutes intervals. This approach was selected in order to accurately quantify the amount of ethanol evaporating over time and to determine the corresponding rate of evaporation. By monitoring the changes in volume at regular intervals, it was possible to gain a precise understanding of the evaporation process. As hypothesised, the evaporation followed a linear trend, thus enabling the calculation of the rate constant, represented by the symbol $k_{evap,\ EtOH}$, which denotes the rate at which ethanol was evaporating under the specified experimental conditions. Figure 3.9 depicts the quantity of ethanol that has evaporated over time during the preparation of a MTES sol with a Pouxviel ratio.

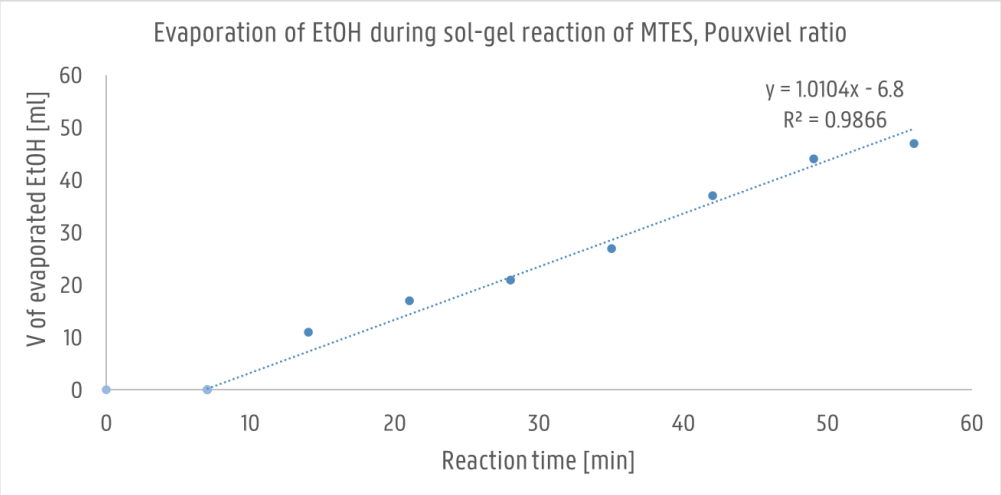

Figure 3.9: Evaporation of EtOH during sol-gel reaction of MTES, the sol is prepared using the Pouxviel ratio, the plot shows the volume of ethanol evaporated over the reaction time.

The value of the evaporation rate can be obtained from these measurements, but it is dependent on the number of initial molecules considered. Consequently, in the code used to describe the process, the value must be updated depending on the initial number of monomers used. Table 3.3 below provides a summary of the calculated values of $k_{evap,\ EtOH}$ for the various cases.

Table 3.3 calculated rate of evaporation for varying numbers of initial monomers of MTES, considering the Pouxviel ratio.

MTES monomers:	5000	10 000	15 000	20 000
$k_{evap,\ EtOH}$:	9.58 s^{-1}	19.17 s^{-1}	28.75 s^{-1}	38.33 s^{-1}

The same procedure was applied to MTES, considering the electrospinnable ratio. However, the results did not show significant variations. Therefore, in the code, the evaporation rates used are consistently those corresponding to the Pouxviel ratio presented in Table 3.3.

Similarly, the same experiment and calculations are conducted for TEOS, and the results for the Pouxviel ratio are presented in Figure 3.10 and Table 3.4 below.

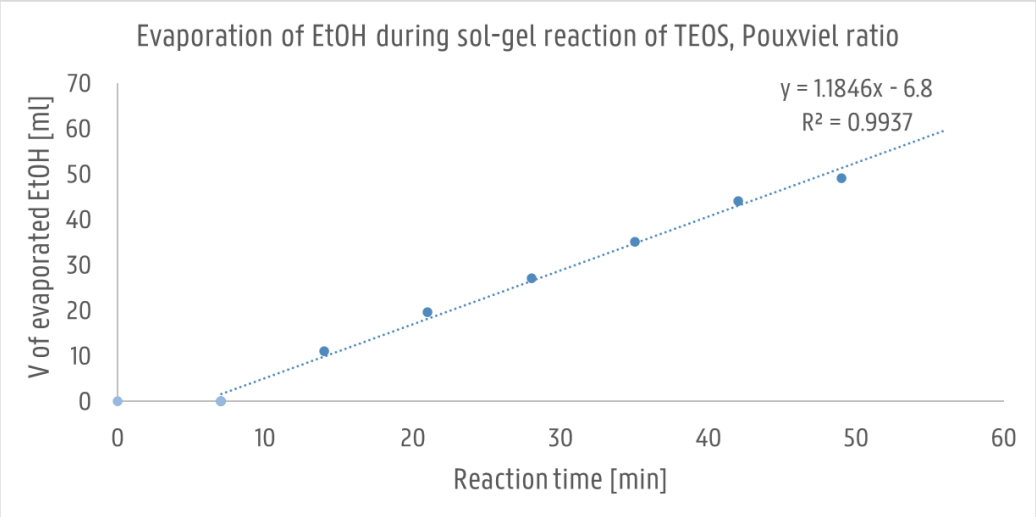

Figure 3.10: Evaporation of EtOH during sol-gel reaction of TEOS, the sol is prepared using the Pouxviel ratio, the plot shows the volume of ethanol evaporated over the reaction time.

Table 3.4 calculated rate of evaporation for varying numbers of initial monomers of TEOS, considering the Pouxviel ratio.

TEOS monomers:	5000	10 000	15 000	20 000
$k_{evap,\ EtOH}$:	$14.36\ s^{-1}$	$28.73\ s^{-1}$	$43.09\ s^{-1}$	$57.46\ s^{-1}$

Likewise, the results for TEOS in the case of the electrospinnable sol closely resemble those obtained for the Pouxviel ratio. Due to this minor difference, only the evaporation rates from the Pouxviel sol are employed in the code to simulate the reaction.

3.2.2 Modelling results of MTES and TEOS

Since the Pouxviel ratio is maintained in these experiments, the reactivity ratios and activation energies employed remain consistent, namely the tuned values from Table 3.1 and Table 3.2 for MTES and the values taken from literature for TEOS [28]. The precision of the results achieved supports the efficacy of the preceding tuning process. Figures 3.11 and 3.12 below compare the experimental data and the modelling results for MTES and TEOS, respectively.

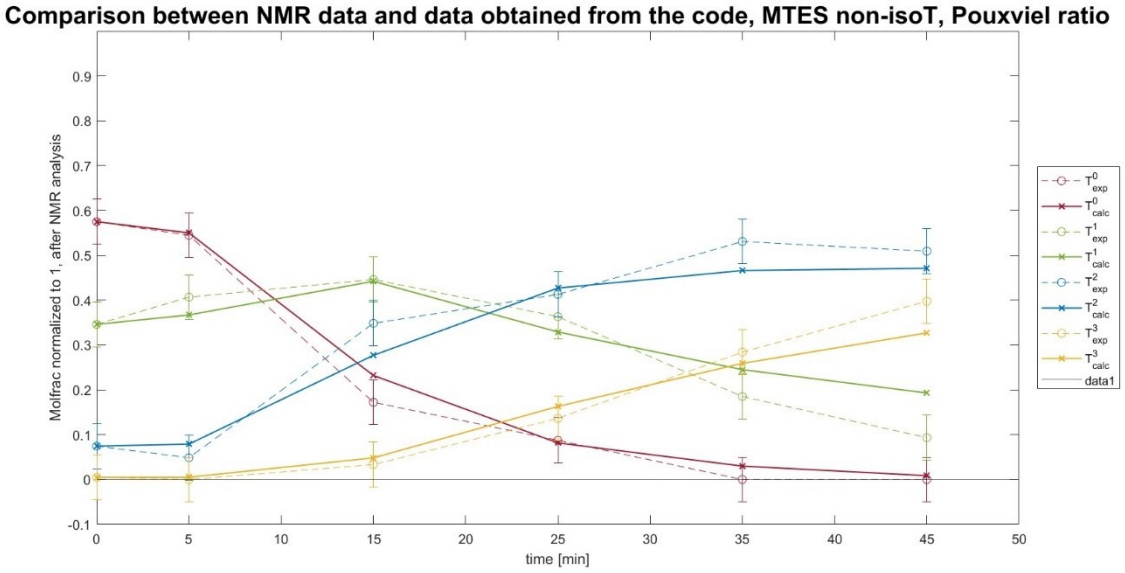

Figure 3.11: Comparison between experimental data (dotted lines) and data obtained from the code (continuous lines) for a non-isothermal synthesis. The plot shows the evolution of the different moieties of MTES over reaction time. Typical error bars of 5% have been used.

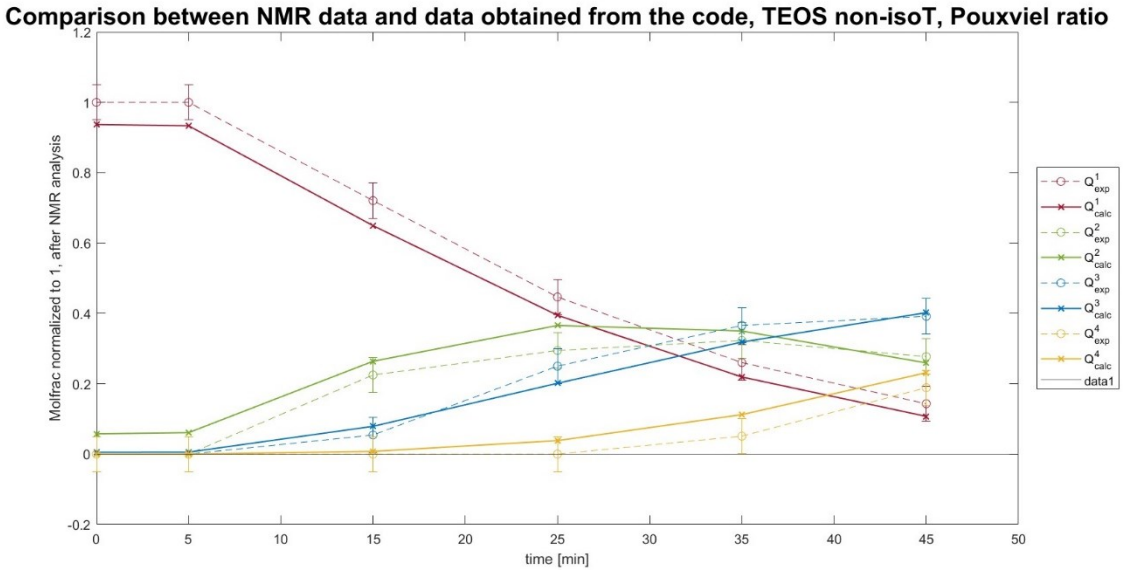

Figure 3.12: Comparison between experimental data (dotted lines) and data obtained from the code (continuous lines) for a non-isothermal synthesis. The plot shows the evolution of the different moieties of TEOS over reaction time. Typical error bars of 5% have been used.

Comparing sols prepared with the Pouxviel ratio offers significant advantages over those made with the electrospinnable ratio because the Pouxviel ratio accounts for the number of functional groups by adjusting the reagent proportions accordingly. This approach ensures a more precise balance of reactive components, leading to more accurate modelling of the sol-gel process.

With the robust fit that has been established for both MTES and TEOS, the code can simulate various time and temperature profiles effectively, allowing for a comprehensive comparison of

these two precursors. The upcoming figures illustrate the behaviour of MTES and TEOS reactions under non-isothermal conditions using the Pouxviel ratio. To thoroughly evaluate their behaviour, several key parameters were analysed, including conversion rates, the number of molecules present, the formation of inter- and intra-molecular bonds, and the normalized count of different functional groups involved in the reactions.

By examining these parameters, the simulations provide insights into how each precursor reacts, offering a deeper understanding of the similarities and differences in their behaviour. This detailed analysis is crucial for optimizing synthesis conditions and predicting the performance of the final materials based on the chosen precursor and reaction conditions.

In order to normalise the values for the number of hydroxyl groups, ethoxy groups, and oxygen bridges, the maximum possible number of each group was used as a reference point. In the case of MTES, the process of normalization was based on a maximum of 30,000 groups when the initial quantity of monomers was 10,000, or 45,000 groups with 15,000 monomers. In the case of TEOS, the normalization process employed 40,000 groups for an initial 10,000 monomers or 60,000 groups for 15,000 monomers.

In order to normalise the number of molecules and the extent of inter- and intra-molecular linkages, the initial number of monomers was used as reference.

This approach ensures consistency in the analysis, thus allowing for a precise and direct comparison of reaction dynamics and precursor behaviour. This is exemplified in the following figures.

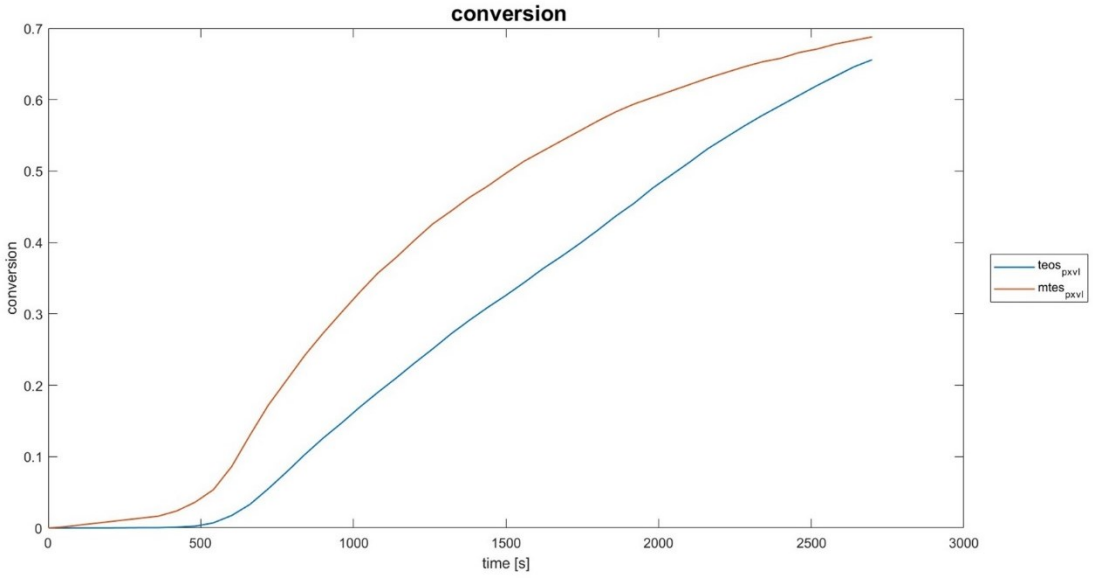

Figure 3.13: Comparison between MTES (red) and TEOS (blue) conversion during a non-isothermal reaction with a Pouxviel ratio. The plotted points were modelled using the tuned reactivity ratios and activation energies (see Table 3.1 and 3.2).

In Figure 3.13 it is possible to compare how conversion increases during the reaction of MTES and TEOS. The conversion in the computational model is calculated considering the sum of the oxygen bridges and the total number of monomers as shown in the following equations.

$$\text{conversion} = \frac{2 \cdot oxygen\ bridges}{3 \cdot total\ monomers} \text{ for MTES, conversion} = \frac{2 \cdot oxygen\ bridges}{4 \cdot total\ monomers} \text{ for TEOS.}$$

The definition of conversion was adjusted for MTES to consider its different number of hydrolysable groups (3 for MTES instead of 4 for TEOS). For each of the precursors, the number of oxygen bridges are counted twice because each oxygen bridge is shared by two silicon atoms.

From the plot it is clear that MTES conversion increases at a faster rate, this is due to the higher reactivity ratios and activation energies found for this precursor compared to the ones for TEOS. As a consequence of the definition used for conversion, the plots including the number of oxygen bridges (Figure 3.16) and the one for overall conversion (Figure 3.13) follow the same path. This alignment is a consequence of the direct correlation between conversion and the formation of oxygen bridges.

Figure 3.14 analyses the total number of molecules involved in the reaction. As already observed, when comparing MTES and TEOS, it is evident that MTES reactions proceed at a faster rate, as evidenced by the higher rate of decay in the number of molecules compared to TEOS. This conclusion aligns with the observations made in the discussion of Figure 3.13.

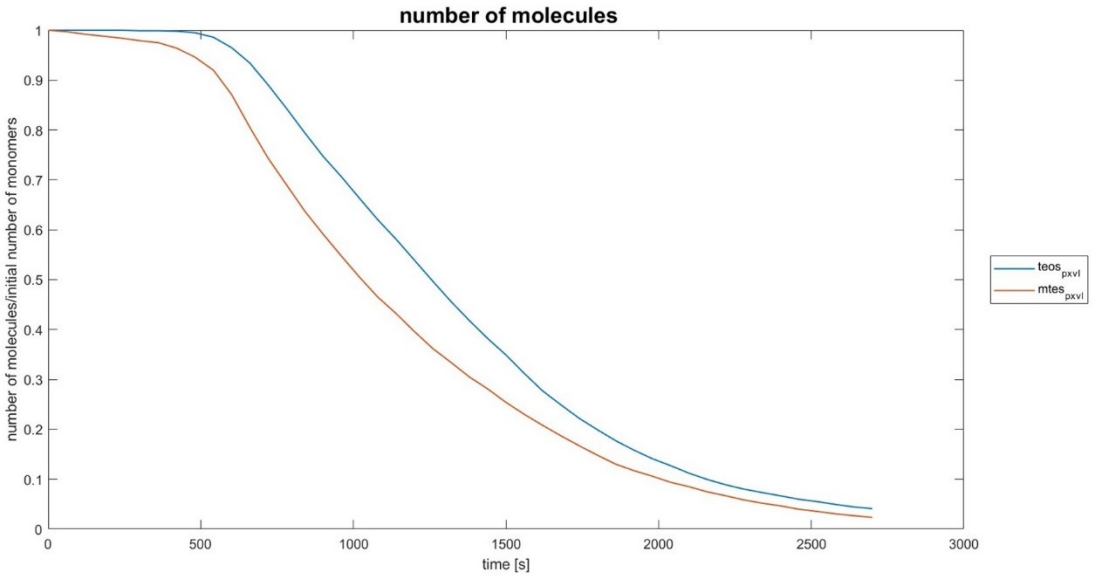

Figure 3.14: Comparison between MTES (red) and TEOS (blue) number of molecules during a non-isothermal reaction with a Pouxviel ratio. The plotted points were modelled using the tuned reactivity ratios and activation energies (see Table 3.1 and 3.2).

Figure 3.15 presents the normalized number of inter- and intra-molecular links formed during the reactions. The formation of inter-molecular links follows a similar trend observed earlier, where MTES shows a faster reaction rate. This rapid progression is consistent with the faster hydrolysis and condensation processes of MTES, leading to quicker formation of cross-links between different molecules.

However, in the formation of intra-molecular bonds TEOS exhibits a grater tendency to form intra-molecular links than MTES. This difference can likely be attributed to the structural characteristics of the TEOS molecule, which possesses four reactive groups, compared to the three in MTES. The additional reactive group in TEOS allows for a more complex molecular network, facilitating the rearrangement of the molecule to form bonds within itself. This increased intra-molecular bonding in TEOS suggests the formation of a more viscous and potentially more entangled polymeric network. This will be discussed in greater detail in the following chapter, where rheological results will be examined and compared. This behaviour could influence the final properties of the material, such as its rigidity and mechanical strength.

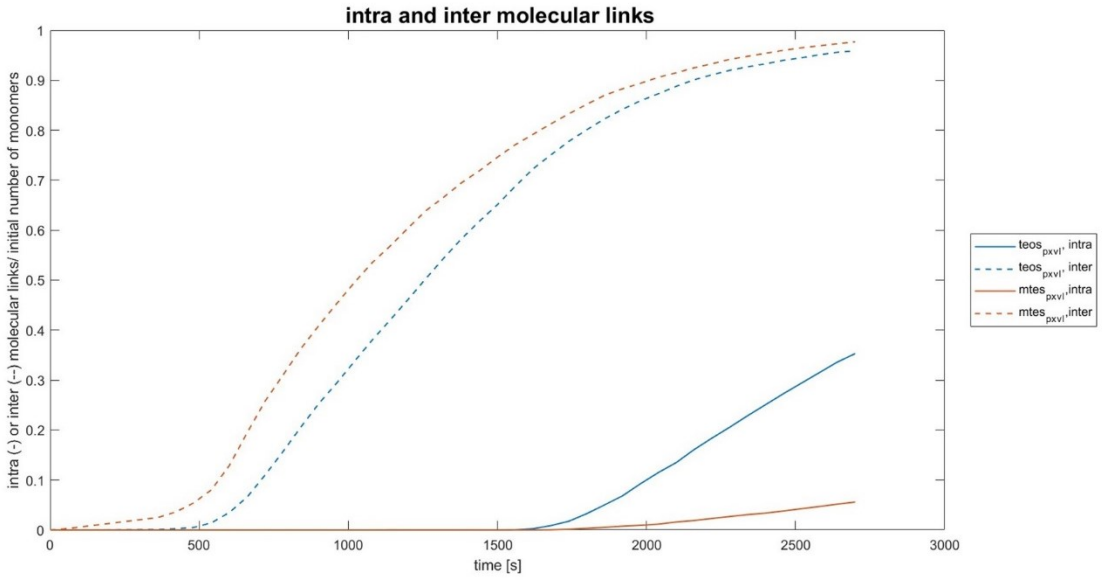

Figure 3.15: Comparison between MTES (red) and TEOS (blue) intra and inter molecular links during a non-isothermal reaction with a Pouxviel ratio. The plotted points were modelled using the tuned reactivity ratios and activation energies (see Table 3.1 and 3.2).

In analyzing Figure 3.16 that shows the normalized number of ethoxy groups (OEt), hydroxyl groups (OH), and oxygen bridges (O), it is important to note that the sum of the normalized number of these functional groups, counting the oxygen bounds twice, remains constant at 1 throughout the reaction, namely $OEt + OH + 2 \cdot O = 1$. This highlights the evolution of the

functional groups as the reaction progresses. The plotted number of oxygen bridges in Figure 3.16 is multiplied by two to make it visually clear that the sum of the functional groups is one. A comparison between TEOS and MTES, considering a Pouxviel ratio, reveals differences in the rate at which ethoxy groups decrease in favor of hydroxyl groups and oxygen bridges. The rapid decline of OEt groups, particularly in MTES, indicates a faster hydrolysis process, where ethoxy groups are quickly replaced by hydroxyl groups, as expected from the values of the reactivity ratios. Concurrently, the formation of oxygen bridges indicates the progress of condensation reactions. This shift from OEt to OH and subsequently to O-bridges reflects the sequential stages of hydrolysis and condensation, with MTES demonstrating a more rapid progression compared to TEOS.

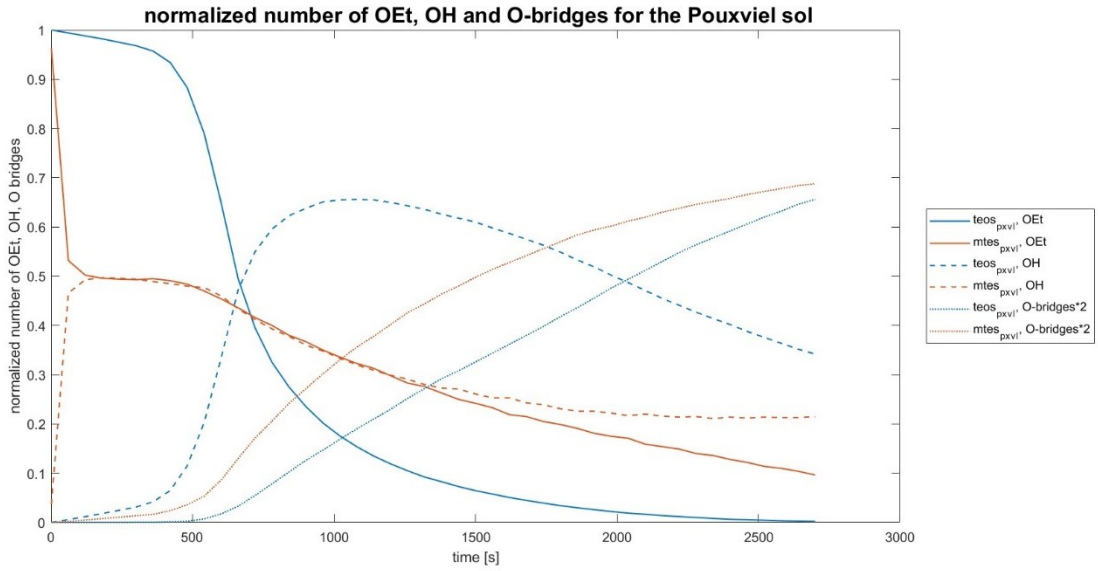

Figure 3.16: Comparison between MTES (dotted lines) and TEOS (continuous lines) normalized number of functional groups during a non-isothermal reaction with a Pouxviel ratio. Note that the normalized number of oxygen bridges is multiplied by two. The plotted points were modelled using the tuned reactivity ratios and activation energies (see Table 3.1 and 3.2).

The results presented in this chapter are highly significant as they facilitate a comprehensive comparison between two distinct precursors, MTES and TEOS. Following the tuning of the model with experimental data obtained from NMR analysis, the computational code has proven to be an invaluable tool for predicting and analyzing the behaviour of these precursors under various reaction conditions.

The optimization of the code through tuning with NMR data enhances its accuracy, enabling it to generate precise and detailed information throughout the entire reaction process. This capability allows for a precise examination of how MTES and TEOS behave under different

conditions, offering deep insights into their respective polymerization mechanisms and network formation.

The code's precision in capturing these details provides valuable information on how each precursor contributes to the formation of the polymer matrix, influencing properties such as network density, cross-linking efficiency and overall material performance. Consequently, this detailed analysis not only advances the understanding of the behaviour of each precursor, but also informs the optimization of synthesis conditions to achieve the desired material properties. In particular, the next chapter focuses on the relationship between these properties, which the code can capture in detail, and the electrospinnability and flow behaviour of the sol

Chapter 4

Linking network characteristics to flow behaviour and electrospinnability

The second objective of this thesis is to establish a connection between the structural characteristics of (organo)silica networks and the flow behaviour of the sol, which is a critical parameter influencing the sol's electrospinnability. The flow behaviour of the sol is highly sensitive to the conditions under which it is synthesized, and thus constitutes an essential factor in determining the feasibility of electrospinning.

As previously discussed, the combination of experimental ^{29}Si NMR analysis with kinetic modelling provides a means of extracting intrinsic network characteristics, including conversion rates and the distribution of functional groups. The objective of this chapter is to gain a deeper understanding of these intrinsic parameters and to examine their relationship with viscosity data. By establishing a correlation between network characteristics and flow behaviour, it becomes possible to evaluate the suitability of different precursors for electrospinning applications.

This approach not only enhances the understanding of the rheological properties of silica and organosilica sols but also provides valuable insights into their processability into nanofibers. By correlating the structural parameters of the network with the sol's flow behaviour, this chapter seeks to contribute to the optimization of synthesis conditions, ultimately improving the electrospinnability and quality of the resulting nanofibers.

4.1 Analysis of the electrospinnable solution

4.1.1 Kinetic modelling of the electrospinnable solution

In the preceding chapter, the analysis focused on the Pouxviel sol, which was formulated using the reactivity ratio initially established by Pouxviel for TEOS [27], with subsequent adjustments made for MTES to account for its distinctive number of reactive functional groups. This approach permitted a comprehensive comparison between the two precursors within a consistent framework. However, the focus of this chapter is on the electrospinnable solutions

to produce (organo)silica nanofibers, prepared with a different initial molar ratio of reagents than the Pouxviel ratio.

Previous studies have investigated the electrospinning regions for both TEOS and MTES, identifying specific ratios of reagents that yield electrospinnable sols. It was demonstrated that the use of an optimised ratio, referred to as the electrospinnable ratio, resulted in the production of sols that could be successfully electrospun into nanofibers for both precursors [28], [29], [69].

The ratio used to produce the electrospinnable sol is the following: [MTES]:[EtOH]:[H2O]:[HCl]=1:2:2:0.01; the same initial composition is also used for TEOS: [TEOS]:[EtOH]:[H2O]:[HCl]=1:2:2:0.01.

This ratio differs from the Pouxviel one mainly in its higher concentration of catalyst, specifically a greater amount of HCl in the catalyst solution, it is also more concentrated in the precursor as it contains less water and EtOH than the Pouxviel sol. An increase in the concentration of HCl has a significant impact on the properties of the sol, necessitating a reassessment of the reactivity ratios used to describe the reactions. On the other hand, the same activation energies are used since the effect of temperature on the reaction kinetics remains the same.

The sols produced with this ratio have the potential to form a robust network suitable for electrospinning. Given the importance of this electrospinnable ratio, it is important to update the code to capture the behaviour of TEOS and MTES in this specific case.

The retuning process was initiated with an analysis of the results obtained from the ^{29}Si NMR analysis, which provided insights into the reaction kinetics.

For MTES, the NMR data indicated that the bimolecular condensations were considerably faster, and that the hydrolysis reactions were slightly accelerated in comparison to the Pouxviel sol. The higher catalyst concentration markedly accelerates the condensation reactions, whereas the hydrolysis reactions, which were already rapid, exhibit only a slight increase in speed under these new conditions.

The newly calibrated reactivity ratios for MTES, specifically tailored to the electrospinnable sol, are shown in Table 4.1. These adjustments ensure that the computational model accurately predicts the formation and behaviour of the polymeric network under conditions suitable for successful electrospinning. The calibration assumes that both hydrolysis and reverse hydrolysis

reactions are accelerated equally, as is generally observed in catalysis, and that water and alcohol condensation reactions are accelerated by the same factor.

Table 4.1: Comparison between the reactivity ratio for MTES for the Pouxviel ratio and the newly tuned reactivity ratios for the electrospinnable ratio.

Reaction considered	MTES, Pouxviel	MTES, electrospinnable	Electrospinnable/Pouxviel
$k_{hydro}[L/(mol\ s)]$	$5.52 \cdot 10^{-3}$	$8.28 \cdot 10^{-3}$	1.50
$k_{hydro,rev}[L/(mol\ s)]$	$1.00 \cdot 10^{-3}$	$1.50 \cdot 10^{-3}$	1.50
$k_{water\ cond,bi}[L/(mol\ s)]$	$1.40 \cdot 10^{-5}$	$9.80 \cdot 10^{-5}$	7.00
$k_{water\ cond,uni}[1/s]$	$1.00 \cdot 10^{-9}$	$1.00 \cdot 10^{-9}$	1.00
$k_{alcohol\ cond,bi}[L/(mol\ s)]$	$6.90 \cdot 10^{-6}$	$4.83 \cdot 10^{-6}$	7.00
$k_{alcohol\ cond,uni}[1/s]$	$1.00 \cdot 10^{-9}$	$1.00 \cdot 10^{-9}$	1.00

The results of applying the newly optimised reactivity ratios to model the electrospinnable sol can be seen in Figure 4.1.

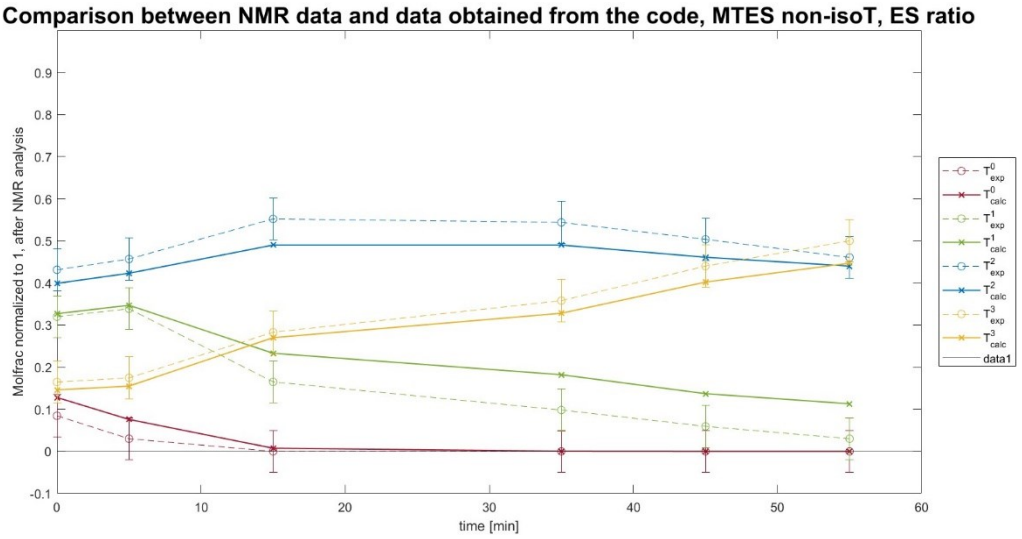

Figure 4.1: Comparison between experimental data (dotted lines) and data obtained from the code (continuous lines) for a non-isothermal synthesis of MTES with the electrospinnable ratio. The plot shows the evolution of the different moieties of MTES over reaction time. Typical error bars of 5% have been used. The x-axis shows reaction time without including the additional NMR time to ensure a clearer visualization and prevent the plot from shifting too far to the right. However, the plotted data points do take NMR time into account, so the plot does not begin at 0 for T^3, T^2, and T^1 or at 1 for T^0. Instead, the values have been interpolated to represent the conditions after the NMR time.

The plot above clearly shows that the resulting fit has a good precision. This level of accuracy indicates that the model effectively captures the underlying dynamics of the reactions.

Furthermore, the curves show that the reactions proceed at a significantly accelerated rate when this ratio is used. In particular, the rapid consumption of T^0 moieties is evident, leading to a significant increase in the final fraction of T^3 moieties through condensation reactions compared to what is observed with the Pouxviel ratio. This suggests that the new ratio results in a higher concentration of T^3 moieties, with important implications for the properties of the resulting material.

Following a similar approach for TEOS, the NMR analysis in this case shows that the hydrolysis reactions occur at an accelerated rate, with the bimolecular condensation reactions proceeding only slightly faster. Also in this case, the use of the electrospinnable ratio results in a more dynamic reaction environment than previously observed. To reflect these findings, the reactivity ratios have been adjusted and the new values are presented in Table 4.2.

Table 4.2: Comparison between the reactivity ratio for TEOS for the Pouxviel ratio and the newly tuned reactivity ratios for the electrospinnable ratio.

Reaction considered	**TEOS, Pouxviel**	**TEOS, electrospinnable**	**Electrospinnable/Pouxviel**
$k_{hydro}[L/(mol\ s)]$	$1.20 \cdot 10^{-5}$	$8.4 \cdot 10^{-5}$	7.00
$k_{hydro,rev}[L/(mol\ s)]$	$2.40 \cdot 10^{-6}$	$1.68 \cdot 10^{-5}$	7.00
$k_{water\ cond,bi}[L/(mol\ s)]$	$1.00 \cdot 10^{-5}$	$1.50 \cdot 10^{-5}$	1.50
$k_{water\ cond,uni}[1/s]$	$1.00 \cdot 10^{-9}$	$1.00 \cdot 10^{-9}$	1.00
$k_{alcohol\ cond,bi}[L/(mol\ s)]$	$7.00 \cdot 10^{-6}$	$1.05 \cdot 10^{-5}$	1.50
$k_{alcohol\ cond,uni}[1/s]$	$1.00 \cdot 10^{-9}$	$1.00 \cdot 10^{-9}$	1.00

Compared to what is observed for the Pouxviel sol, the Q^0 moieties in this system are rapidly consumed, leading to a faster formation of Q^4 moieties. However, even with this increased rate of Q^4 moiety formation, the reaction kinetics remain less aggressive than those of the MTES sol, indicating a more gradual reaction progression. This difference can be attributed to the ratio of reagents used: although the same ratio is used for both MTES and TEOS, TEOS has four reactive groups, which results in less water and catalyst per reactive group, thus slowing down the reaction. These characteristics are clearly visualized in Figure 4.2.

This difference in reaction dynamics could play a crucial role in determining the final structural and material properties of the sols obtained with these two different precursors.

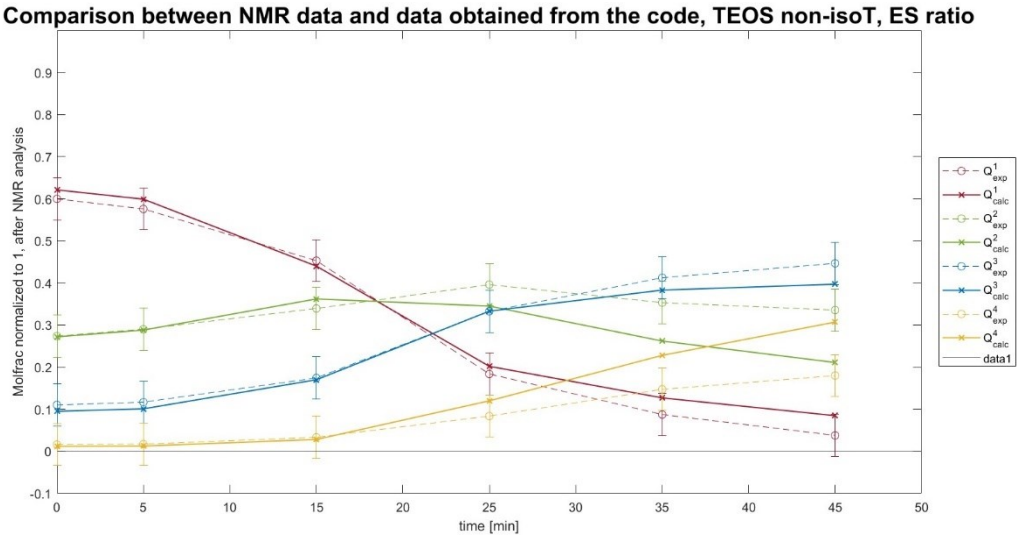

Figure 4.2: Comparison between experimental data (dotted lines) and data obtained from the code (continuous lines) for a non-isothermal synthesis of TEOS with the electrospinnable ratio. The plot shows the evolution of the different moieties of TEOS over reaction time. Typical error bars of 5% have been used. The x-axis shows reaction time without including the additional NMR time to ensure a clearer visualization and prevent the plot from shifting too far to the right. However, the plotted data points do take NMR time into account, so the plot does not begin at 0 for T^3, T^2, and T^1 or at 1 for T^0. Instead, the values have been interpolated to represent the conditions after the NMR time.

4.1.2 Comparison of the sols obtained with the electrospinnable ratio and the Pouxviel ratio

With a good fit now established for the electrospinnable ratio for both TEOS and MTES, it becomes possible to compare the behaviour of these two precursors in the context of electrospinning, where they can be used to produce nanofibers and eventually membranes. However, comparing these two molecules is more complex in this scenario because the ratio used is the same for both precursors, despite the different number of reactive groups they contain. This uniform ratio does not fully account for the variations in their reactivity, making it less straightforward to draw conclusions based solely on the trends observed under this ratio. Nevertheless, a comparison of the behaviour of TEOS and MTES under the two different ratios remains of great value to compare their processability into nanofibers. To facilitate this comparison, the computational model is used with the newly adjusted reactivity ratios (Table 4.1 and 4.2), this allows the prediction of key parameters that effectively describe the reaction, such as conversion rates and number of molecules.

Also when comparing electrospinnable and Pouxviel sols, to normalize the values for hydroxyl groups, ethoxy groups, and oxygen bridges, the maximum possible number of each group was used as a reference point. For MTES, normalization was based on 30,000 groups in case of

10,000 monomers or 45,000 groups in case of 15,000 monomers. For TEOS, 40,000 groups in case of10,000 monomers or 60,000 groups in case of15,000 monomers were used. The initial number of monomers was also used to normalize the number of molecules and the extent of molecular linkages.

This interesting comparison between the two different ratios used for TEOS and MTES is shown in Figures 4.3 to 4.5.

Figure 4.3 shows the conversion trend throughout the reaction, where conversion is defined as conversion = $\frac{2 \cdot oxygen\ bridges}{3 \cdot total\ monomers}$ for MTES, or conversion = $\frac{2 \cdot oxygen\ bridges}{4 \cdot total\ monomers}$ for TEOS. As already noticed, this definition results in a trend that closely reflects the normalised number of oxygen bridges.

The figure clearly shows that the conversion rate for MTES is consistently higher than that for TEOS. However, when considering the electrospinnable ratio, both MTES and TEOS show accelerated conversions. In particular, MTES shows a rapid increase in conversion early in the reaction, whereas TEOS shows a more gradual, steady acceleration. Despite these differences in initial reaction behaviour, the final conversion rates for both precursors converge to similar values of about 70%. The key difference lies in the reaction dynamics, with MTES reaching higher conversion levels much earlier in the process compared to TEOS, which progresses at a more consistent rate throughout the reaction.

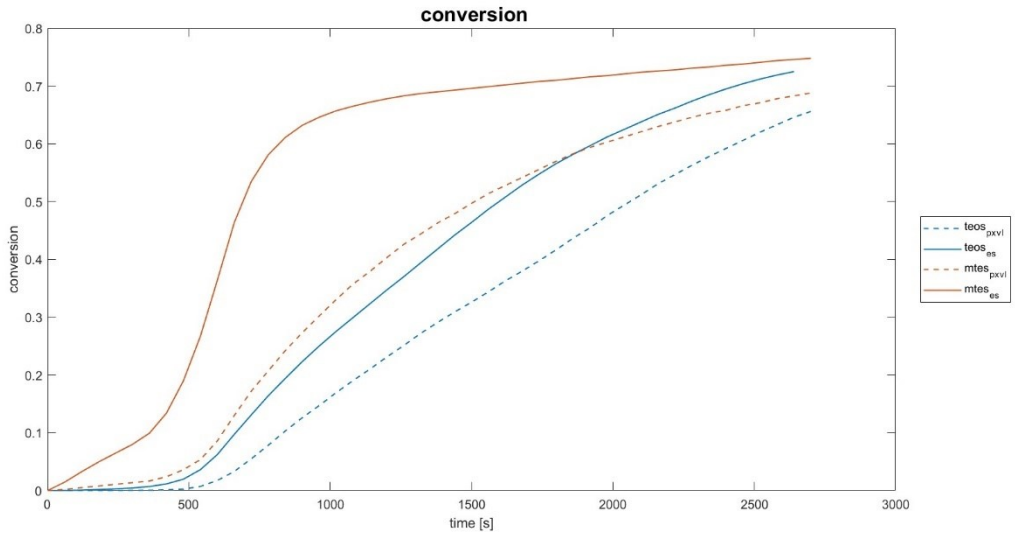

Figure 4.3: Comparison between MTES (red) and TEOS (blue) conversion for both a sol produced with a non-isothermal synthesis using the Pouxviel ratio (dotted lines) and the electrospinnable ratio (continuous lines). The plotted points were modelled using the tuned reactivity ratios (see Table 4.1 and 4.2).

The total number of molecules throughout the reaction can be visualized in Figure 4.4. Similar observations can be made here as for the conversion rate: the number of MTES molecules decreases faster than that of TEOS. The electrospinnable ratio accelerates the reactions for both TEOS and MTES, but in different ways: MTES exhibits a faster decrease early in the reaction, whereas TEOS shows a more gradual consumption of molecules.

Interestingly, the normalized number of molecules for MTES in the electrospinnable sol appears to approach zero, but this is due to the actual number of molecules dropping to just one in the final moments of the reaction. This value is then normalized by the initial total number of molecules, giving the impression of a value close to zero. This rapid reduction suggests that the reaction is extremely fast, with the monomers being consumed so quickly that they form a single, highly entangled molecule.
To better understand this scenario, it would be beneficial to run simulations with a higher initial number of molecules. However, due to the significant computational demand, such simulations would require a supercomputer. This more detailed analysis will be pursued in future studies to provide a clearer understanding of the reaction dynamics under these conditions.

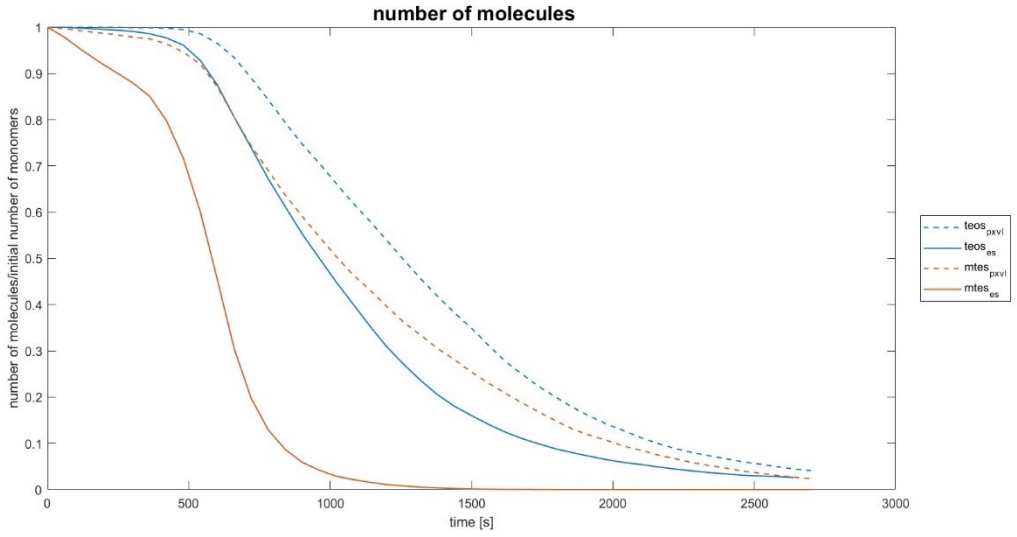

Figure 4.4: Comparison between MTES (red) and TEOS (blue) number of molecules for both a sol produced with a non-isothermal synthesis using the Pouxviel ratio (dotted lines) and the electrospinnable ratio (continuous lines). The plotted points were modelled using the tuned reactivity ratios (see Table 4.1 and 4.2).

Figure 4.5 compares the intra- and inter-molecular bonds in TEOS and MTES. MTES forms inter-molecular bonds faster due to its faster hydrolysis and condensation processes, leading to rapid cross-linking between molecules. for inter-molecular links, as already seen, the

electrospinnable ratio accelerates the reactions of both precursors, but differently: MTES shows a rapid increase early on, while TEOS accelerates more steadily.

However, as observed for the Pouxviel ratio, TEOS shows a greater tendency to form intramolecular bonds than MTES also in the case of the electrospinnable sol. This difference is probably due to the structure of TEOS, which has four reactive groups compared to three in MTES. The extra reactive group in TEOS allows for a more complex and flexible molecular network, which promotes intra-molecular bonding.

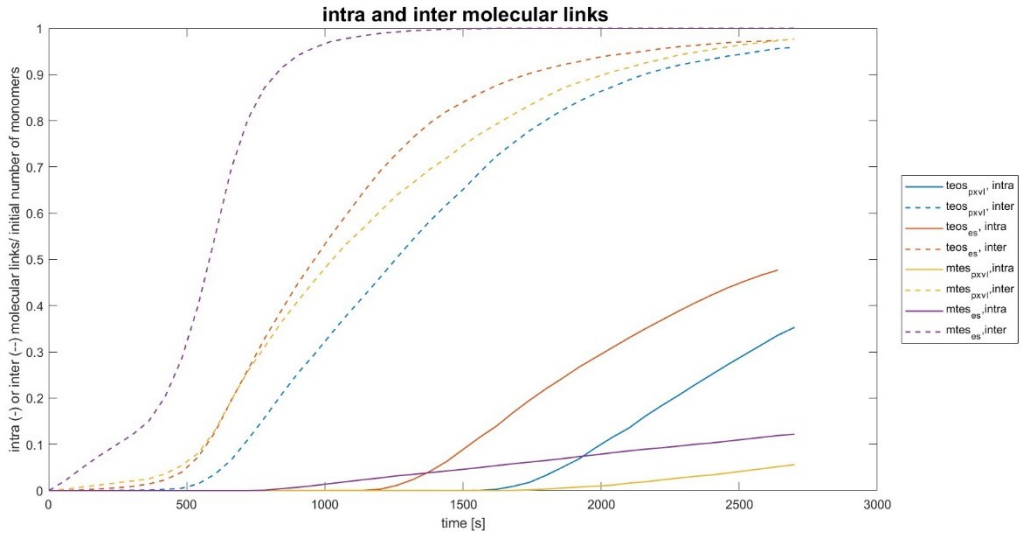

Figure 4.5: Comparison between MTES and TEOS intra-molecular (continuous lines) and inter-molecular (dotted lines) links for both a sol produced with a non-isothermal synthesis using the Pouxviel ratio and the electrospinnable ratio. The plotted points were modelled using the tuned reactivity ratios (see Table 4.1 and 4.2).

Figure 4.6 follows the analysis done in Figure 3.16, focusing only on the electrospinnable ratios. The plot shows the normalized number of ethoxy groups (OEt), hydroxyl groups (OH) and oxygen bridges (O). It is important to note that the sum of these normalized functional groups, counting the oxygen bonds twice, remains constant at one throughout the reaction. The plotted number of oxygen bridges in Figure 3.16 is multiplied by two to make it visually clear that the sum of the functional groups is one.

When TEOS and MTES are compared using the electrospinnable ratio, there are clear differences in the rate at which ethoxy groups decrease, giving way to hydroxyl groups and oxygen bridges. The rapid reduction of OEt groups, particularly for MTES, indicates a faster hydrolysis process, with ethoxy groups being rapidly replaced by hydroxyl groups in accordance with the reactivity ratios. At the same time, the formation of oxygen bridges marks the progress of the condensation reactions. This transition from OEt to OH and then to O-

bridges illustrates the sequential stages of hydrolysis and condensation, with MTES again showing a faster progression than TEOS.

The trends in this plot confirm once more that MTES experiences an earlier acceleration compared to TEOS. However, the final number of oxygen bridges is similar for both molecules, as seen earlier in the conversion analysis.

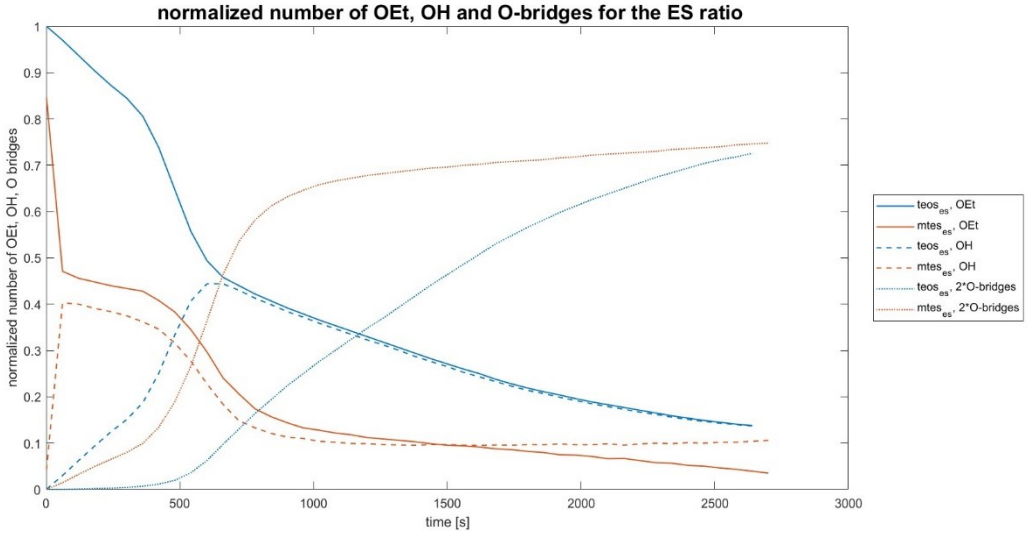

Figure 4.6: Comparison between MTES (dotted lines) and TEOS (continuous lines) normalized number of functional groups during a non-isothermal reaction with an electrospinnable ratio. Note that the normalized number of oxygen bridges is multiplied by two. The plotted points were modelled using the tuned reactivity ratios (see Table 4.1 and 4.2).

After analyzing these plots, it is clear that the main difference between the two precursors when using the electrospinnable ratio lies in their reaction dynamics. MTES shows an earlier acceleration due to the fact that it has only three reactive groups, which allows the catalytic action to be more concentrated, given that the same ratio is applied to both molecules.

As a result, the reaction with MTES starts faster, leading to faster hydrolysis and condensation reactions initially. In contrast, TEOS, with its four reactive groups, experiences a slower initial reaction rate because it has more groups to hydrolyze. This added complexity not only slows down the initial hydrolysis, but also increases the overall reaction time. As a result, while MTES molecules react faster initially, their reaction rate decreases as more of the reactive groups are consumed. Meanwhile, TEOS maintains a more consistent reaction rate over a longer period of time as it continues to hydrolyze and condense more groups.

This difference in reaction timing explains why MTES slows down earlier in the process and why, despite these kinetic differences, the final number of oxygen bridges, and thus the overall conversion, is similar for both TEOS and MTES.

The different behaviour of each precursor during the reaction highlights the importance of understanding the specific kinetics involved when optimizing conditions for electrospinning, where precise control of molecular interactions is crucial.

4.2 Linking network characteristics to flow behaviour

4.2.1 Viscosity measurements

Given that viscosity is critical in determining whether a sol is suitable for electrospinning, both MTES and TEOS sols, prepared at the Pouxviel and electrospinnable ratios, were analysed using a rheometer to obtain accurate measurements of their viscosity changes over time.
A two-parts test was performed: first, a constant shear rate of $\dot{\gamma} = 1\ s^{-1}$ was maintained for 180 seconds, followed by a shear rate of $\dot{\gamma} = 100\ s^{-1}$ for 60 seconds.

The primary objective is to compare the viscosity evolution of MTES and TEOS during their reaction time under two different ratios. To achieve this, samples were taken from the reacting sol at different time intervals during the non-isothermal synthesis carried out in the laboratory. Each sample was quenched in liquid nitrogen to preserve its properties until analysis. The samples were then analysed on the rheometer using the two part test described above. Viscosity values were specifically selected from around 120 seconds when the shear rate is $\dot{\gamma} = 1\ s^{-1}$. At this low shear rate, shear thinning does not take place, providing a reliable comparison between the different samples.

Figure 4.7 shows this data for MTES, using results from a non-isothermal synthesis with a Pouxviel ratio from the first set of experiments. The plot shows that samples with very low viscosity produce oscillatory responses from the instrument, with the mean value used as the accurate measurement. The shear thinning behaviour of the sol also becomes more apparent with higher viscosity samples, reflecting a more advanced stage of the reaction.

Figure 4.7 is just one example of what was also done for TEOS and the electrospinnable ratio. All measurements were repeated in three separate sets of experiments, with additional plots available in the Appendix.

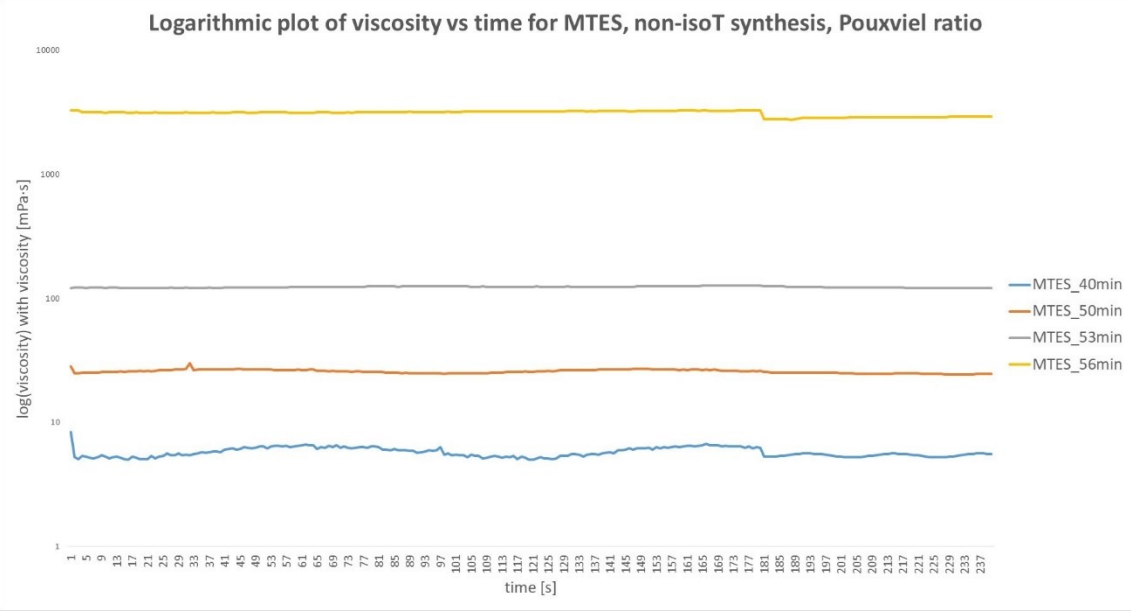

Figure 4.7: Logarithmic plot of viscosity versus reaction time for MTES, non-isothermal synthesis with a Pouxviel ratio considering different reaction times. The data plotted are from the first set of experiments (05/06/2024), for the data from the other experiments see the Appendix.

Figure 4.8 provides a comprehensive summary of all the experimental data collected throughout the study and illustrates the overall trends by averaging the viscosity measurements from the different experiments conducted at each reaction time for both MTES and TEOS under the two different ratios. Each line in the plot represents these averaged trends and provides a clear visualisation of how the viscosity of each precursor evolves over time. For both sols, the viscosity remains low for an extended period before increasing abruptly. The key difference between the sols is the specific point at which this viscosity increase occurs, which depends on their different reaction kinetics and conditions.

However, it is important to note that the use of reaction time on the x-axis does not provide any intrinsic information about the properties of the sol, highlighting a limitation that will be addressed in the following paragraphs.

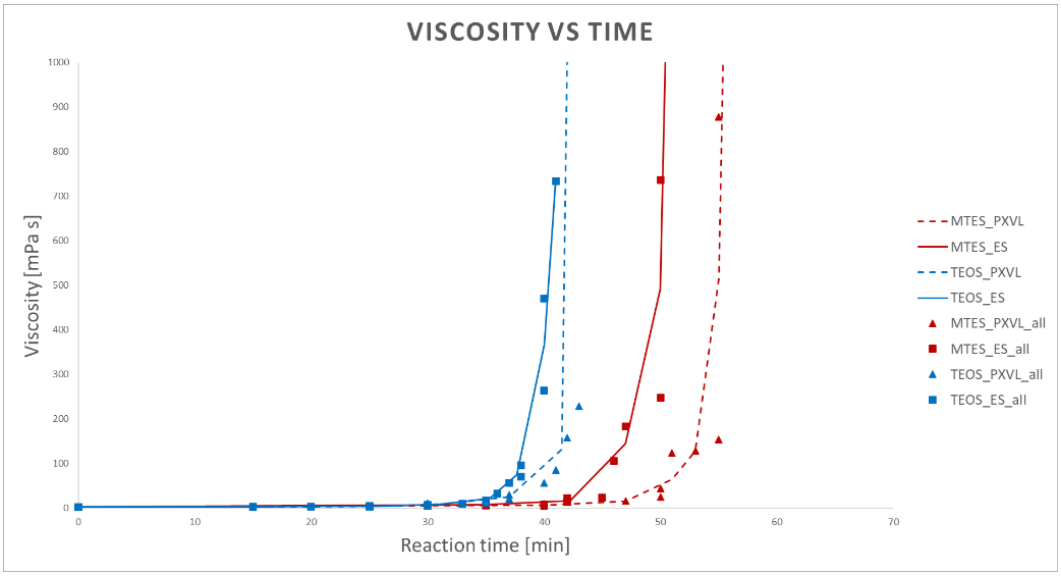

Figure 4.8: Plot of viscosity versus reaction time for TEOS (blue) and MTES (red) sols prepared by non-isothermal synthesis, considering both the Pouxviel ratio (dotted lines) and the electrospinnable ratio (continuous lines). Three different sets of experiments were carried out and the experimental data obtained are represented by the shapes in the plot. The lines represent an overall trend obtained by averaging the different experimental data at each reaction time.

Figure 4.9 shows the same data as Figure 4.8 but using a logarithmic scale for viscosity in the y-axis and thus allowing a better comparison of the curves.

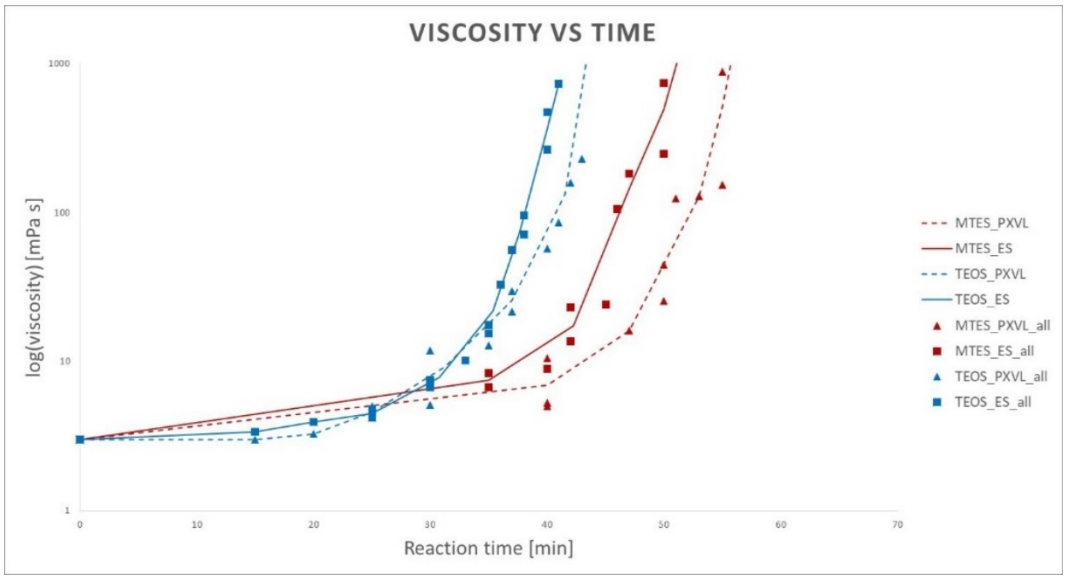

Figure 4.9: Logarithmic plot of viscosity versus reaction time for TEOS (blue) and MTES (red) sols prepared by non-isothermal synthesis, considering both the Pouxviel ratio (dotted lines) and the electrospinnable ratio (continuous lines). Three different sets of experiments were carried out and the experimental data obtained are represented by the shapes in the plot. The lines represent an overall trend obtained by averaging the different experimental data at each reaction time.

Figures 4.8 and 4.9 provide a detailed comparison of the viscosity evolution of MTES and TEOS during the reaction time.

In particular, TEOS viscosity change starts earlier in the reaction time compared to MTES. The early onset of viscosity changes in TEOS can be attributed to its molecular structure, which facilitates the initial formation of intramolecular bonds that gradually evolve into a more complex network, as shown in Figures 4.5 and 3.15.

4.2.2 Linking viscosity to conversion

A significant and innovative advance in this research is to relate viscosity directly to the degree of conversion rather than to the reaction time. This approach represents a novel step forward from the current state of the art and allows a more accurate analysis of the rheological behaviour. By fine-tuning the computational code to accurately predict conversion at each step of the reaction, it becomes possible to correlate viscosity with conversion, effectively decoupling the analysis from the constraints of reaction time.
The primary aim of this method is to compare the rheological properties of TEOS and MTES without the variability introduced by reaction time, which can be affected by factors such as the volume of the solution and the specific conditions of each experiment and has thus limited value in understanding the sol-gel crosslinking behaviour. Reaction time is often a variable closely related to the scale and design of the experiment, making it a less reliable parameter for direct comparisons between different studies or materials. By focusing on conversion, which directly reflects the degree of cross-linking in the sol-gel process, a more standardised, intrinsic and meaningful comparison between the two precursors can be achieved, eliminating the need to account for experimental variables related to time.

Since the computational code associates each reaction time point with a specific degree of conversion, and since the reaction time data is associated with viscosity measurements, it is now possible to directly correlate viscosity with conversion.
Figures 4.10 and 4.11 illustrate this comparison, highlighting how viscosity evolves with conversion rather than reaction time.

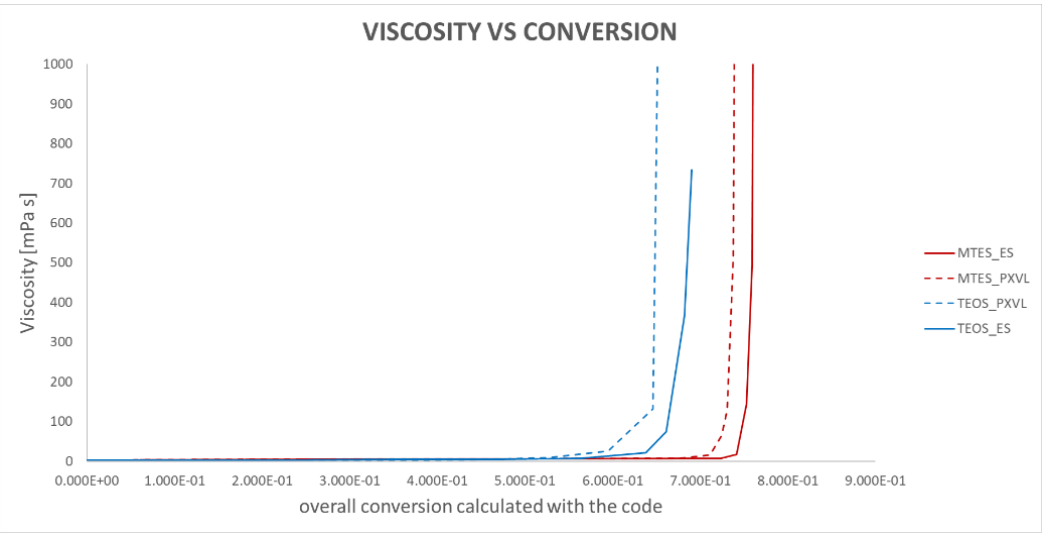

Figure 4.10: Plot of viscosity versus conversion for TEOS (blue) and MTES (red) sols prepared by non-isothermal synthesis, considering both the Pouxviel ratio (dotted lines) and the electrospinnable ratio (continuous lines).

Figure 4.11 shows the same data as Figure 4.10 but using a logarithmic scale for viscosity in the y-axis and thus allowing a better comparison of the curves.

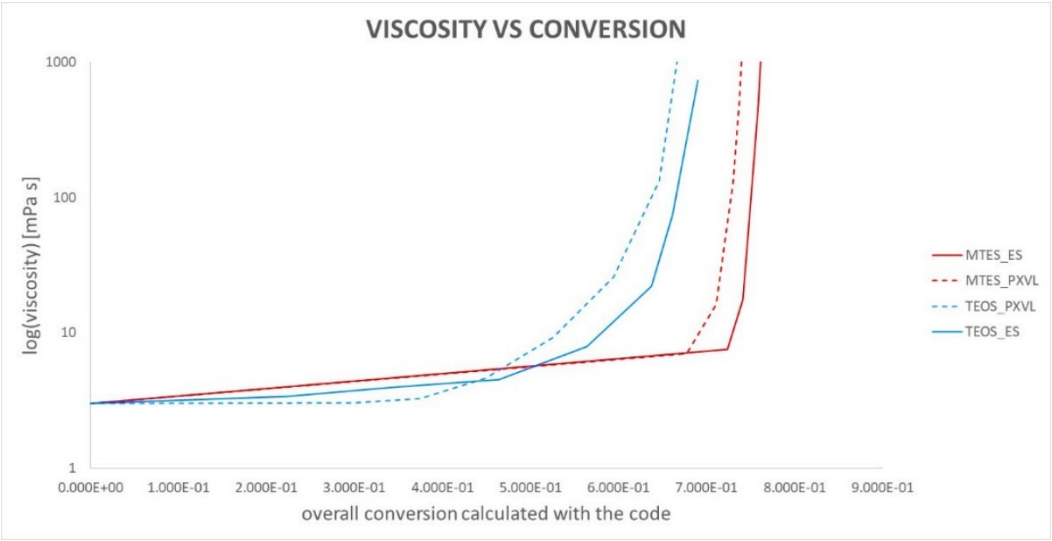

Figure 4.11: Logarithmic plot of viscosity versus conversion for TEOS (blue) and MTES (red) sols prepared by non-isothermal synthesis, considering both the Pouxviel ratio (dotted lines) and the electrospinnable ratio (continuous lines).

From the above figures it can be seen that both MTES and TEOS show a similar overall trend where the viscosity remains low for a long period before increasing sharply once the reaction reaches a critical point. This abrupt increase indicates a rapid transition from a low viscosity state to a highly structured and cross-linked network for both sols, highlighting the fundamental changes that occur during the reaction.

However, when each sol is examined individually, clear differences in reaction kinetics and viscosity evolution become apparent. MTES shows a rapid increase in viscosity after a delayed start, suggesting a more abrupt transition to a higher viscosity state once the reaction reaches a critical moment. This behaviour was also observed experimentally, where MTES quickly became a sticky solid as the viscosity began to increase. With fewer intramolecular bonds than TEOS, MTES takes longer to reach the point of significant viscosity increase, but when it does, the transition is much faster.

In contrast, TEOS begins to thicken earlier in the reaction but at a more moderate rate. The higher propensity of TEOS for intramolecular bonding contributes to this early thickening as these internal bonds gradually form and stabilise the structure. However, due to the gradual nature of this bonding and the slower overall reaction kinetics compared to MTES, the viscosity increase for TEOS remains less aggressive over time. These differences in viscosity evolution are closely related to the different molecular structures and reaction dynamics of the two precursors. However, it is important to note that reaction time alone on the x-axis does not provide intrinsic information about the sol properties, a limitation that will be addressed in the following discussion.

Previously the focus was on comparing the behaviour of TEOS and MTES. The focus now shifts to a comparison of the Pouxviel (PXVL) and Electrospinnable (ES) ratios. Table 4.3 summarises key viscosity, reaction time and conversion data for the different precursors to facilitate a comparison between the two ratios.

Table 4.3: Comparison of TEOS and MTES using both the Pouxviel (PXVL) and Electrospinnable (ES) ratios. Summary of some key data on viscosity, reaction time, and conversion for easier comparison of the two ratios.

MTES, PXVL			**MTES, ES**		
Time [min]	viscosity [mPa s]	conversion	Time [min]	viscosity [mPa s]	conversion
50	65	0.72	50	490	0.76
55	900	0.74	55	5350	0.77
conversion	viscosity [mPa s]		conversion	viscosity [mPa s]	
0.72	65		0.72	7	
0.74	900		0.74	17	

TEOS, PXVL			TEOS, ES		
Time [min]	viscosity [mPa s]	conversion	Time [min]	viscosity [mPa s]	conversion
35	20	0.5	35	22	0.64
40	130	0.63	40	700	0.68
conversion	viscosity [mPa s]		conversion	viscosity [mPa s]	
0.64	132		0.64	22	
0.7	6800		0.7	735	

The data in this table compare the viscosity changes of MTES and TEOS sols for Pouxviel and Electrospinnable ratios, taking into account both reaction time and conversion.

Looking at the viscosity behaviour with respect to reaction time, it is clear that the ES ratio shows a more rapid increase in viscosity compared to the PXVL ratio. This suggests that the ES ratio reaches higher viscosities faster in time.

However, this observation must be interpreted in the context of conversion. For the ES ratio, the viscosity starts to increase when the conversion is already relatively high. As the conversion is already advanced by the time viscosity increases significantly, the absolute change in viscosity is less dramatic in relation to conversion. In contrast, for the PXVL ratio, viscosity starts to increase at a lower conversion. As the conversion is lower when the viscosity starts to increase, the change in viscosity relative to the conversion is more pronounced. This means that the PXVL ratio shows a steeper increase in viscosity as conversion progresses compared to the ES ratio.

In summary, TEOS begins to thicken earlier but at a slightly slower rate, whereas MTES experiences a delayed but rapid increase in viscosity.

When comparing the Pouxviel and electrospinnable ratios, different patterns emerge depending on whether reaction time or conversion is considered.

For the ES ratio, the viscosity increases more rapidly with reaction time, reaching higher values at an earlier stage. However, this rapid increase is observed when the conversion is already relatively high, resulting in a less pronounced relative increase in viscosity with respect to conversion. Conversely, for the PXVL ratio, the viscosity starts to increase at a lower conversion, resulting in a more significant change in viscosity relative to conversion. This

means that the PXVL ratio shows a steeper increase in viscosity with increasing conversion compared to the ES ratio.

These differences highlight the importance of focusing on intrinsic properties such as conversion rather than relying solely on reaction time. While reaction time provides an overview of how viscosity changes over time, conversion provides a more accurate measure of how material properties evolve with crosslinking. This approach allows a clearer and more meaningful comparison, which is critical for applications that require precise control of material properties, such as electrospinning.

The following chapter focuses on establishing a direct correlation between the electrospinnability of a sol and the parameters provided by the code that accurately describe the reaction, for example conversion and number of functional groups.

Chapter 5

The electrospinning region defined by reaction parameters

This chapter focuses on establishing a thorough relationship between the electrospinnability of a sol and the key sol-gel parameters. Electrospinnability, a critical property in the manufacture of nanofibres, is influenced by a number of factors related to the chemical composition and structural evolution of the sol. The existing literature has established a strong relationship between electrospinnability and sol viscosity [69], [77].

Starting from this knowledge, this chapter aims to provide a deeper understanding by linking electrospinnability directly to the intrinsic parameters of the reaction. Using advanced computational modelling, it is now possible to predict how critical reaction parameters evolve during the process. By studying these parameters, it is possible to describe the progression of the sol from a less viscous state to a state suitable for electrospinning, providing a clearer picture of the conditions required to achieve optimal electrospinnability.

Furthermore, by understanding the parameters that govern the formation of the sol's network structure, it becomes possible to better control the manufacturing procedure and tailor the properties of the resulting nanofibres.
This chapter describes how predictive modelling, using parameters derived from the reaction kinetics, enables more effective description of the electrospinnability of the sol.

5.1 Identification of the electrospinning region for MTES, considering different initial ratios

Previous studies have suggested a correlation between viscosity and electrospinnability for both MTES [69] and TEOS [77] sols. Specifically, for MTES, different initial ratios have been

investigated. Starting from the previously analysed electrospinnable ratio (ES) of [MTES]:[EtOH]:[H2O]:[HCl] = 1:2:2:0.01, the initial water concentration [H2O] was varied from 1 to 3 as shown on the x-axis of Figure 5.1.

The electrospinnability of each sol produced from these different ratios was then evaluated based on their viscosity. In Figure 5.1, the blue area represents the electrospinning region, highlighting the conditions under which the sol can be successfully electrospun, the white area shows the range where the sol can be electrosprayed and the grey area shows the range where the sol cannot be used for either purpose.

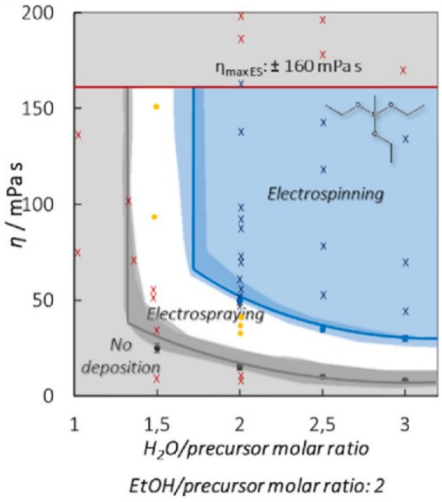

Figure 5.1: Electrospraying and electrospinning operating windows of MTES-based sol-gel systems established after SEM analysis and studies of the dynamic viscosity of the sol-gels with the solid lines as trend lines based on data points. The measured data point are indicated in blue for electrospinnable, yellow for electrosprayable, and red for non-spinnable/sprayable dynamic viscosities [69].

To account for all the different ratios, the code was used to model the behaviour of each sol throughout the reaction process. However, experimental data correlating viscosity with the modelled reaction parameters are only available for the ES ratio (when [H2O] = 2), as detailed in Chapter 4.

To qualitatively compare the other ratios, the established relationship between viscosity and reaction time for the electrospinnable ratio was used to convert the y-axis from viscosity to reaction time, as shown in Table 5.1. This approach also allows the electrospinning region to be identified on the basis of reaction time.

The approximation assumes that since the electrospinning region was initially identified using viscosity, the relationship between reaction time and viscosity (valid only for the ES ratio) must be applied to determine this region using reaction time.

As a result, it was possible to plot key reaction parameters with reaction time on the y-axis, as the code provides reaction time data for each ratio, and also identify the electrospinning region in this plot thanks to the approximation performed.

Although this approach is an approximation, it is considered a reasonable method as the main variation between the different ratios is the initial amount of water, which is not expected to cause significantly large changes in the viscosity of the sol.
However, this method has its limitations and future research will include direct viscosity measurements for the other ratios. This will allow a more accurate and comprehensive analysis of the electrospinning region over all the ratios tested and will provide a deeper understanding of the relationship between reaction parameters and electrospinnability.

Table 5.1: Direct link between viscosity and reaction time, obtained for the ES ratio from the experiments described in Chapter 4.

Viscosity [mPa s]	3	7.53	17.50	144.50	492.24	4700
Reaction time [min]	0	35	42	47	50	53

In Table 5.2 the electrospinning region is described using both viscosity and reaction time. The second row is valid for all ratios as these data are directly taken from Figure 5.1. On the other hand, the third row is only correct for the ES ratio [MTES]:[EtOH]:[H2O]:[HCl] = 1:2:2:0.01, but it is also applied to the other ratios in order to be able to qualitatively describe the electrospinning region using reaction parameters also for all the other cases analysed.

Table 5.2: Identification of the electrospinning region using both viscosity and reaction time. This link is precise only for the ratio [MTES]:[EtOH]:[H2O]:[HCl] = 1:2:2:0.01, but it is applied also to the other ratios to qualitatively compare them.

Region	Non-spinnable/sprayable	Electrospraying	Electrospinning
Viscosity [mPa s]	3-15.6	15.6-51	51-160
Reaction time [min]	0-40	40-43	43-47

The code was run with different ratios of water molecules to identify the parameters associated with the electrospinnability of the sols. Two sets of plots that describe the behaviour of reaction parameters are included in the analysis: those considering in the x-axis the full reaction time

(from 0 to 50 minutes) in Figure 5.2 and those showing a zoomed view (from 38 to 50 minutes) in Figure 5.3.

After extensive testing, the most effective parameters for describing the electrospinning region were found to be conversion, the normalised number of OEt groups, and the T^1 and T^3 fractions, which represents respectively the amount of molecules with just one group hydrolysed and the most hydrolysed molecules. The fraction representing the T^1 moieties was preferred to that representing the T^0 moieties because the latter goes to zero very quickly and does not provide an accurate description of the electrospinning region. Conversion is particularly important as it describes the extent of the reaction and is intrinsically linked to the normalized number of O-bridges as expressed in its definition, $MTES_{conv} = \frac{2 \cdot oxygen\ bridges}{3 \cdot total\ monomers}$. The number of OEt groups indicates the amount of unreacted molecules.

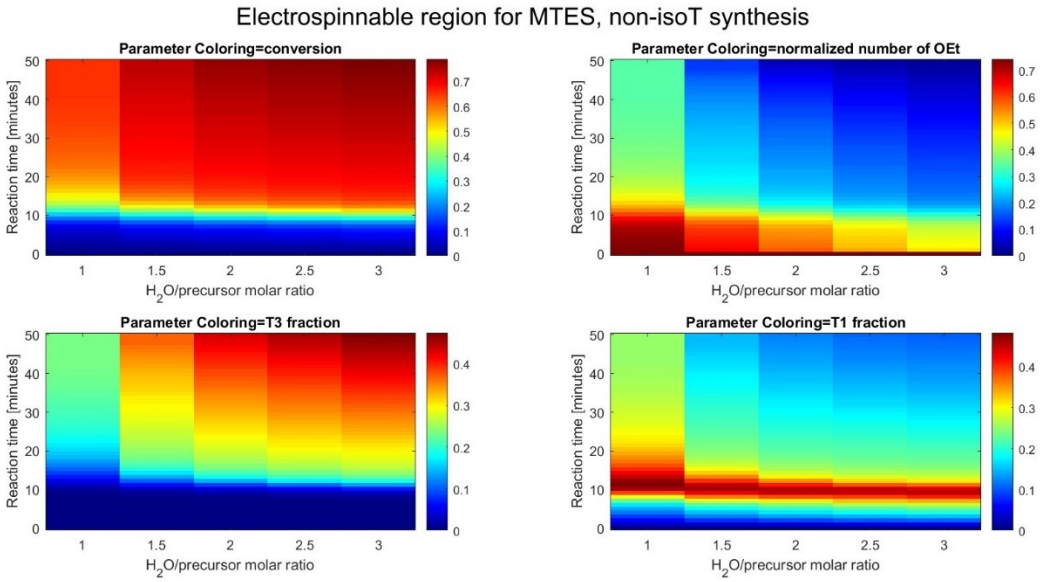

Figure 5.2: Surface plots with reaction time in the y-axis and the initial ratio used in the x-axis ([H2O] changes at each column, while the other initial concentrations remain as in the ES ratio). The synthesis of the MTES sols is done non-isothermally. The colormap changes following a different parameter in each plot, clockwise the parameters used are conversion, normalized number of OEt, T^3 fraction and T^1 fraction.

The initial number of OEt groups is remarkably high, as shown in Figure 5.2, where the data at time 0 seconds is shown in very dark red. This is because these values, around 0.9, are outside the range represented by the colour map. Including these values in the colour map would cause a significant shift in colour shading that would give a poor representation of the overall trend of the data, so the colour map is limited to a maximum of 0.75, even though the original data exceeds this limit.

In Figure 5.2 the electrospinning region can be identified in the upper right part of the plots, where the parameters values tend to become uniform, as indicated by the colour gradient. This is consistent with Figure 5.1, which shows that the ratios in the first two columns, corresponding to [H2O] = 1 and 1.5, are not electrospinnable. The electrospinning region only appears at higher initial water concentrations [H2O] = 2:3, and viscosities above 50 mPa s.

The zoomed-in plots in Figure 5.3 focus on the specific interval where the viscosity approaches the electrospinning region, which begins at about 15 mPa s. This viscosity level is not reached until about 40 minutes into the reaction, according to the data in Table 5.2. As a result, the part of the plot showing short reaction times, which represents the early stages of the reaction before the electrospinning region is reached, is less relevant for analysis. Focusing on the latter part of the reaction is justified as it highlights the most critical phase where the sol enters a viscosity range suitable for electrospinning.

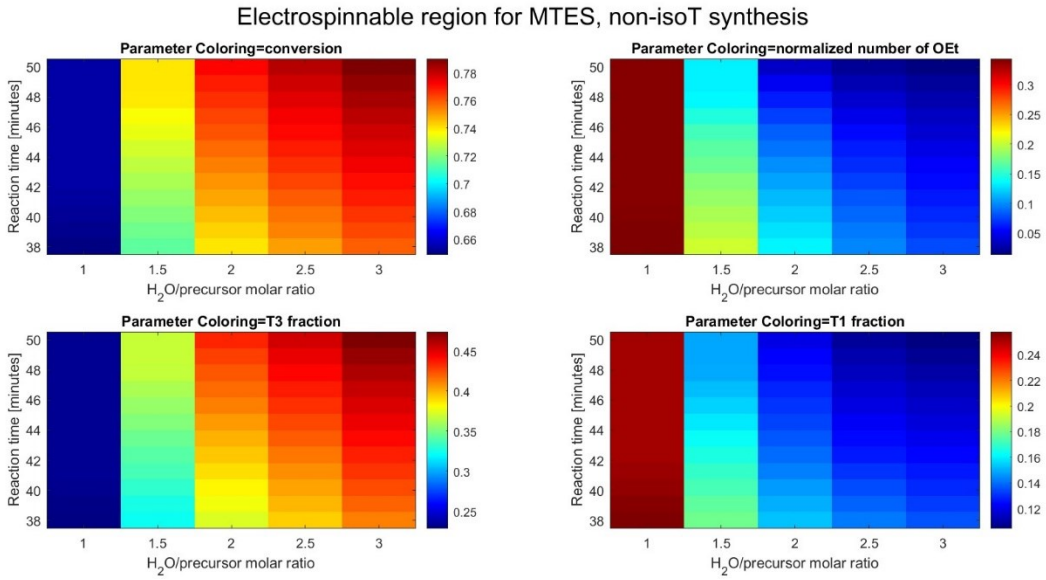

Figure 5.3: Zoomed-in surface plots with reaction time in the y-axis and the initial ratio used in the x-axis ([H2O] changes at each column, while the other initial concentrations remain as in the ES ratio). The synthesis of the MTES sols is done non-isothermally. The colormap changes following a different parameter in each plot, clockwise the parameters used are conversion, normalized number of OEt, T^3 fraction and T^1 fraction.

In the zoomed-in version of the plots, all four parameters: conversion, number of OEt groups and T^1 and T^3 fraction; provide a detailed representation of the electrospinning region. In each plot, the first two columns, corresponding to [H2O] = 1 and 1.5, are clearly different from the others, indicating the non-electrospinnable zones. In contrast, the more uniform shading in the remaining columns accurately represents the electrospinning region. The boundaries of this

region, as suggested by the shading, are not strictly horizontal but show some variation and are identified between approximately 43 and 47 minutes of reaction time, accurately capturing the transition into the electrospinnable region.

All data in Figures 5.2 and 5.3 are plotted with reaction time on the y-axis. However, as discussed in Chapter 4, it is essential to prioritize intrinsic properties over reaction time for a more precise analysis of material behavior. For electrospinning, viscosity is directly linked to the electrospinnable region, as established in the literature [69], [77].
Therefore, using viscosity as an intrinsic property to characterise this region would provide a clearer and more accurate representation of the data, allowing a more meaningful comparison by focusing on a property that directly reflects the suitability of the material for electrospinning, rather than just its evolution over time. Currently, viscosity data is only available for the ES ratio, so this direct correlation can only be made for this ratio at present. Future research will include direct viscosity measurements also for the other ratios, allowing a more accurate and comprehensive analysis of the electrospinning range under different conditions.

5.2 Linking the electrosspinable region for both MTES and TEOS directly to their viscosity

Defining electrospinnability using specific reaction parameters and linking them to an intrinsic property of the sol represents a significant advance in understanding the electrospinning process. This approach allows a more direct and detailed analysis of the evolution of the sol by going beyond simple time-based measurements. Rather than relying solely on reaction time, which can vary depending on experimental conditions, this chapter presents a framework in which electrospinnability is characterised by specific chemical changes within the sol and correlated with viscosity rather than time.

The aim is to establish a direct relationship between viscosity and the reaction parameters that define the electrospinning range. To achieve this, the viscosity values obtained from experiments with MTES using the ES ratio [MTES]:[EtOH]:[H2O]:[HCl] = 1:2:2:0.01 (see Chapter 4 and Appendix) are used. To provide a more consistent description of the viscosity evolution, the viscosity values are interpolated using the experimental values as a reference to match each reaction time point.

Since viscosity changes in a non-uniform manner with reaction time, remaining low for a period of time before rising sharply, as observed in the previous chapter, it is necessary to redefine a set of viscosity data that progresses uniformly. This allows the construction of a y-axis suitable for plotting. Starting with a viscosity of 3 mPa s, corresponding to a reaction time of 0 seconds, viscosity values are selected in increments of 10 mPa s up to 173 mPa s, which is just above the non-electrospinnable limit for MTES.
With this new set of uniformly spaced viscosity data, all the corresponding reaction parameters are interpolated using the original data from the code. After this interpolation, the data are ready to be plotted with viscosity on the y-axis, as the reaction parameters are now related to uniformly scaled viscosity values.

Figure 5.4 shows the data plotted according to the method now described, focusing specifically on the electrospinnable ratio for MTES, where [H_2O] = 2. In these plots, the electrospinning and electrospraying regions are clearly identifiable using the second column labelled 'result'. This identification is based on the data from Figure 5.1 and is further detailed in Table 5.1.

The reaction parameters: conversion, normalised number of OEt groups, T^1 and T^3 fraction; again effectively delineate the electrospinning region.
When the sol is outside the electrospinning region, the reaction parameters show significantly different values. For example, the conversion, and T^3 fraction are significantly lower than required for electrospinning, while the number of OEt groups is excessively high.
The reasoning for the T^1 fraction is slightly different, because this parameter starts very low, increases significantly and then decreases again. This fluctuation occurs because most of the molecules are initially unhydrolysed. As the reaction progresses, many molecules have only one group condensed, leading to a high T^1 fraction. However, as more molecules are hydrolysed, the number of T^1 moieties decreases. As shown in Figure 5.1, the appropriate values for electrospinning are reached when the sol has been reacting for approximately 38 minutes, corresponding to a sol viscosity of 50 mPa s. The corresponding values of T^1 moieties represents an intermediate value that balances the initially low and subsequently high T^1 fractions.
As the sol moves into the electrospraying region, these parameters start to approach the values required for electrospinning, as indicated by the shading in the plots. But the non uniformity in

the shading still indicates that the values are either too high or too low for optimal electrospinning conditions.

It is only when the sol enters the electrospinning region that the parameters reach their appropriate values, which is visually represented by more uniform shading within the electrospinning region of the plots.

However, above a certain viscosity, the parameters again deviate from the ideal values for electrospinning: conversion and T^3 fraction become excessively high, while the number of OEt groups and T^1 fraction falls below the required level. This shift is also evident in the plots, where the colour becomes consistently darker compared to the more balanced shading observed in the electrospinning region, signalling a departure from the optimal conditions required for successful electrospinning.

This visual representation highlights the importance of maintaining certain reaction parameters within specific ranges to achieve the desired electrospinnability.

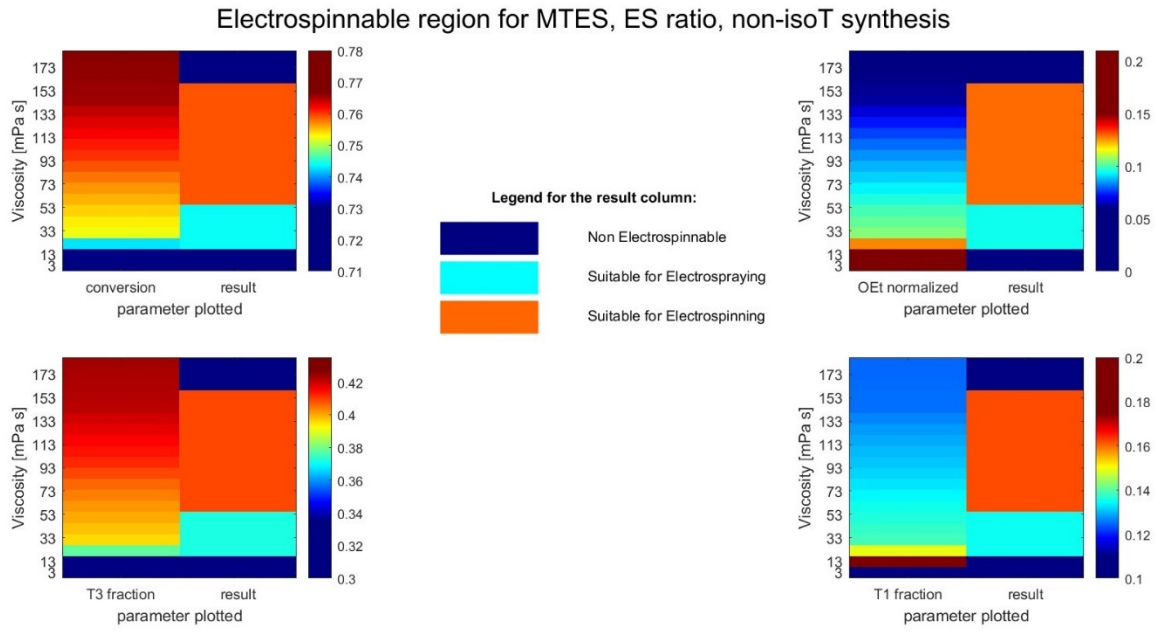

Figure 5.4: Surface plots with viscosity in the y-axis and the parameter used for coloring in the x-axis. [H_2O]=2 in all these plots, as in the ES ratio, the synthesis of the MTES sols is done non-isothermally. The colormap changes following a different parameter in each plot, clockwise the parameters used are conversion, normalized number of OEt, T^3 fraction and T^1 fraction. On the second column of each plot the sol is defined (following literature data [69]) as non electrospinnable, suitable for electrospraying or suitable for electrospinning, as detailed in the legend in the center of the figure.

The same procedure was used for TEOS. However, for TEOS the electrospinnability data available in previous works [77] is limited to the ES ratio, specifically [TEOS]:[EtOH]:[H2O]:[HCl] = 1:2:2:0.01. This is the same ratio for which viscosity data are

available (as detailed in Chapter 4 and in the Appendix), immediately allowing the identification of the electrospinning region using viscosity. The most relevant data from literature [77] describing the electrospinning region for TEOS with the ES ratio are summarised in Table 5.3 below.

Table 5.3 Identification of the electrospinning region for TEOS using viscosity [77]. This link is precise only for the ratio [TEOS]:[EtOH]:[H2O]:[HCl] = 1:2:2:0.01. For the non-spinnable sols, only drops were deposited on the collector plate. For the badly electrospinnable sols electrospinning stability was less stable and beaded fibres or thicker fibres were obtained. For the electrospinnable sols the nanofibers showed to be stable in time, with no further crosslinking taking place [77].

Region	Non-spinnable	Badly electrospinnable	Electrospinnable
Viscosity [mPa s]	17-65	65-82, 260-981	118-198

As the viscosity data is already available for the ES ratio, the plots for TEOS can be constructed directly with viscosity on the y-axis. These plots follow the same method applied for Figure 5.4 where the viscosity data is used to determine the electrospinning region based on specific reaction parameters. The result of this analysis for TEOS is shown in Figure 5.5.

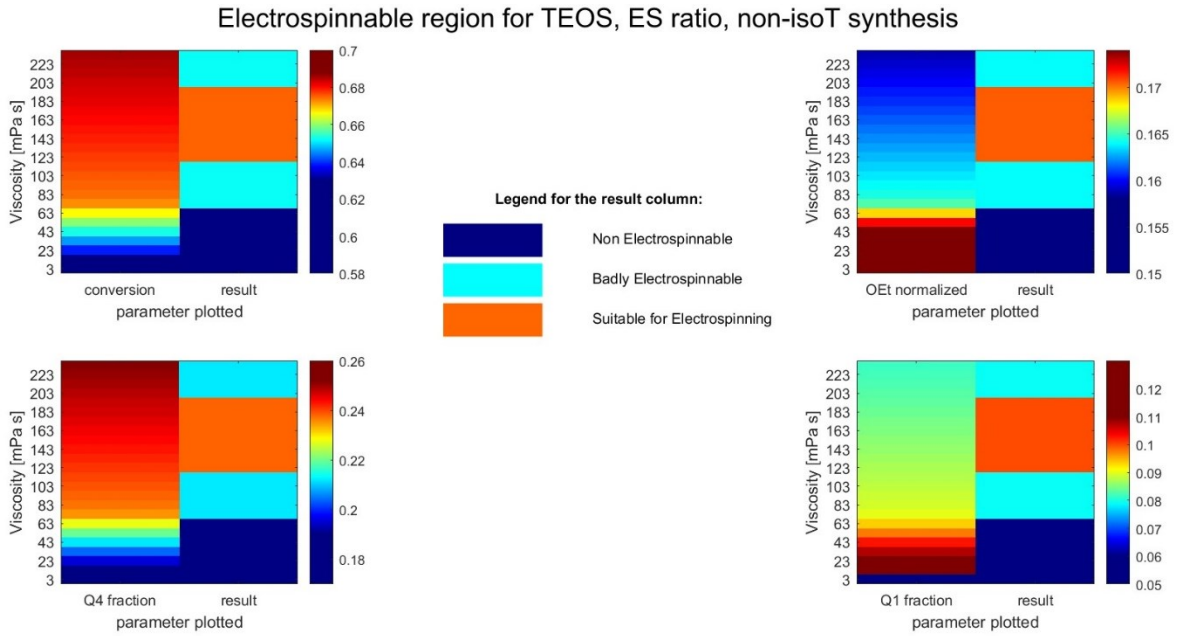

Figure 5.5: Surface plots with viscosity in the y-axis and the parameter used for coloring in the x-axis. [H2O]=2 in all these plots, as in the ES ratio, the synthesis of the TEOS sols is done non-isothermally. The colormap changes following a different parameter in each plot, clockwise the parameters used are conversion, normalized number of OEt, Q^4 fraction and Q^1 fraction. On the second column of each plot the sol is defined (following literature data [77]) as non electrospinnable, badly electrospinnable or suitable for electrospinning, as detailed in the legend in the center of the figure.

To be consistent with what done for MTES, the same parameters are used also to describe the electrospinning region for TEOS, switching from the T^1 and T^3 fractions, to the Q^1 and Q^4

fractions, which still represent the amount of molecules with only one group condensed and the most condensed molecules, respectively.

A similar colour shading pattern to that observed for MTES in Figure 5.4 is also found for TEOS in Figure 5.5. However, in the case of TEOS, the viscosity values that define the different regions: non-electrospinnable, badly electrospinnable and suitable for electrospinning; are higher than those for MTES.

This difference is due to the fact that, at equivalent viscosity levels, TEOS typically has lower conversion values than MTES, and therefore TEOS has higher viscosities for the same conversion value when compared to MTES. As a result, the electrospinning range for TEOS is defined within a higher viscosity range. To further clarify these statements, a selection of data from Chapter 4 is summarised in Table 5.4 below.

The same reasoning applies to the other reaction parameters such as the number of OEt groups, Q^1 and Q^4 fraction. These parameters also shift according to the different viscosities required for TEOS to reach similar states of electrospinnability, highlighting the unique behaviour of each sol based on its intrinsic properties and reaction dynamics.

Table 5.4: Comparison of TEOS and MTES using the electrospinnable (ES) ratios. Summary of some key data on viscosity, reaction time, and conversion for easier comparison of the two ratios.

TEOS, ES			**MTES, ES**		
Time [min]	viscosity [mPa s]	conversion	Time [min]	viscosity [mPa s]	conversion
35	22	0.64	50	490	0.76
40	700	0.68	55	5350	0.77
conversion	viscosity [mPa s]		conversion	viscosity [mPa s]	
0.64	22		0.72	7	
0.7	735		0.74	17	

In summary, the ability to accurately identify the electrospinning region is critical to the production of tailored nanofibers, which can then be used to create membranes with specific properties for a wide range of applications.

By precisely defining the electrospinning region, researchers can optimise the production process to obtain fibres with the desired properties, thereby improving the performance and functionality of the resulting membranes.

In addition, linking the electrospinning region directly to an intrinsic property such as viscosity, rather than reaction time, represents a significant advance in the field. This approach allows a more meaningful comparison of sols produced in different laboratories, as viscosity is an intrinsic property that is not affected by external factors such as solution volume or temperature. By using viscosity as a reference, fibres obtained from different sols can be directly compared, ensuring consistency and reliability across different studies and applications.

This not only facilitates better understanding and optimisation of electrospinning processes, but also promotes greater collaboration and standardisation in the development of advanced nanofiber-based materials.

Conclusions and future work

This work has advanced the understanding of silica sol-gel synthesis and the critical parameters that influence the electrospinnability of sols for the production of nanofibers.
By combining kinetic modelling with experimental techniques such as ^{29}Si NMR and rheometry, the study investigated the behaviour of different precursors, specifically MTES and TEOS, in the formation of silica networks.
The research highlights the importance of linking intrinsic properties such as viscosity, conversion or other reaction parameters to the processability of sols into nanofibers, rather than relying on less informative metrics such as reaction time.

A major achievement of this work is the detailed description of viscosity evolution using conversion as a reference instead of reaction time. Another important advance is the identification and characterisation of the electrospinning region based on intrinsic properties rather than time-based measurements.
These approaches provide a more robust framework for understanding the sol-gel process across different experimental setups, enabling the production of tailored nanofibers with specific properties suitable for different applications.
In addition, the study highlighted the importance of using computational modelling to accurately describe reaction parameters that can serve as intrinsic properties to better characterise sols. By focusing on properties directly related to the structure and cross-linking behaviour of the sol, researchers can make more accurate comparisons between different laboratories and experimental conditions. These findings facilitate the development of standardised and reproducible methods for assessing sol properties, thereby increasing the reliability and scalability of nanofibers production.

Future work should focus on several key areas to build on the results of this thesis:

Secondly, additional experimental work is required to include direct viscosity measurements for sols prepared from other initial ratios to produce MTES sols, as discussed in Chapter 5. Similarly, viscosity and electrospinnability measurements should be carried out for TEOS at different initial ratios. These experiments would provide a more detailed and comprehensive

analysis of the electrospinning region for both MTES and TEOS and improve the understanding of how different initial conditions affect sol viscosity and electrospinnability.
Third, improving the computational modelling code to directly predict viscosity values based on reaction parameters would be an ambitious but valuable goal. This improvement would significantly increase the predictive power of the code, allowing for more precise control of the sol-gel process and nanofibers production. However, achieving this level of modelling would be challenging requiring extensive refinement and validation against experimental data.

Pursuing these future directions will allow the research initiated in this thesis to evolve and contribute to a more in-depth understanding of sol-gel chemistry and its applications in nanofibers production. The advancement of both experimental and computational methods will enable the creation of more refined and tailored nanofibrous materials suitable for a wide range of industrial and scientific applications.

Appendix

Appendix A: Viscosity measurements

Three different sets of experiments have been conducted for TEOS and MTES for both Pouxviel and electrospinning ratios. The first set pf experiment was conducted on the 05/06/2024, the second on the 06/06/2024 and the third on the 07/06/2024. All the results are shown in the figures below.

- First set of experiments, 05/06/2024, MTES

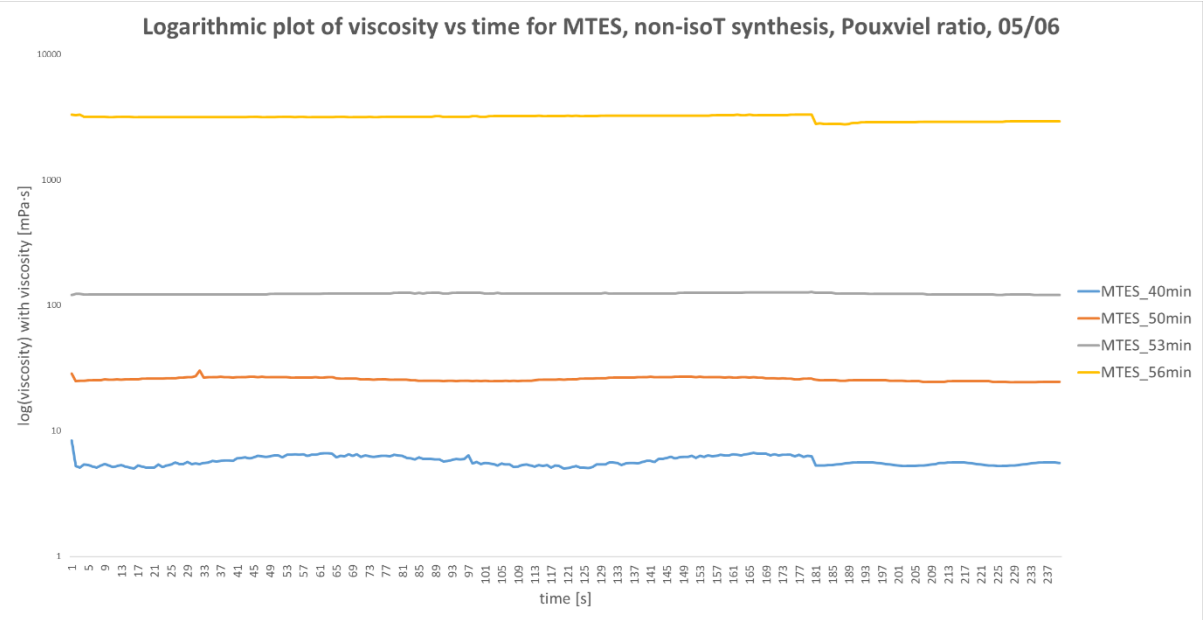

Figure A1: Logarithmic plot of viscosity versus reaction time for MTES, non-isothermal synthesis with a Pouxviel ratio considering different reaction times. The data plotted are from the first set of experiments (05/06/2024).

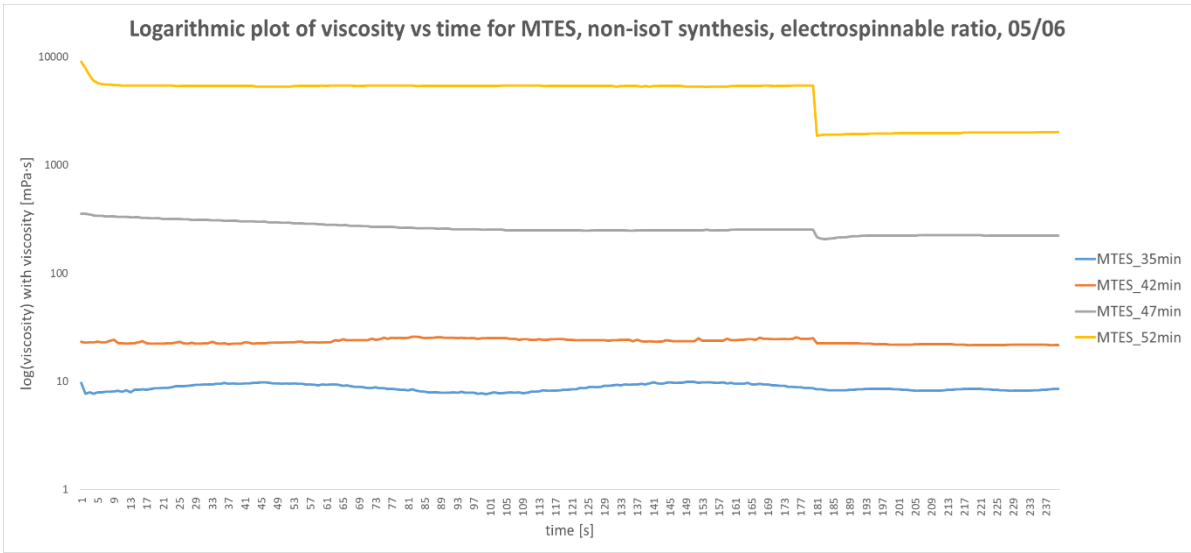

Figure A2: Logarithmic plot of viscosity versus reaction time for MTES, non-isothermal synthesis with an electrospinnable ratio considering different reaction times. The data plotted are from the first set of experiments (05/06/2024).

- First set of experiments, 05/06/2024, TEOS

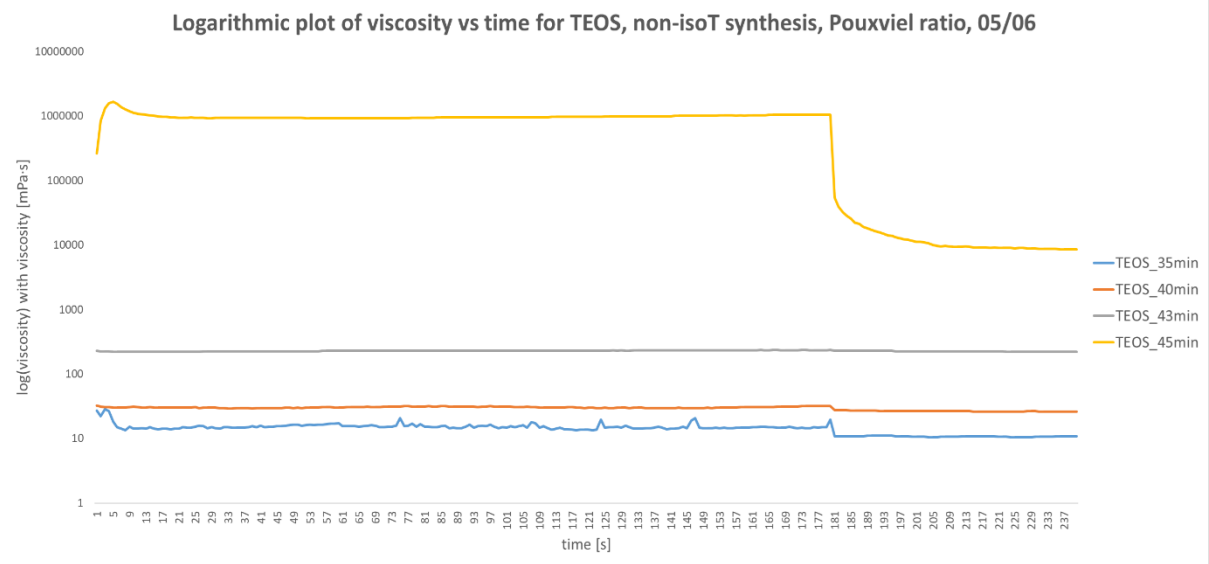

Figure A3: Logarithmic plot of viscosity versus reaction time for TEOS, non-isothermal synthesis with a Pouxviel ratio considering different reaction times. The data plotted are from the first set of experiments (05/06/2024).

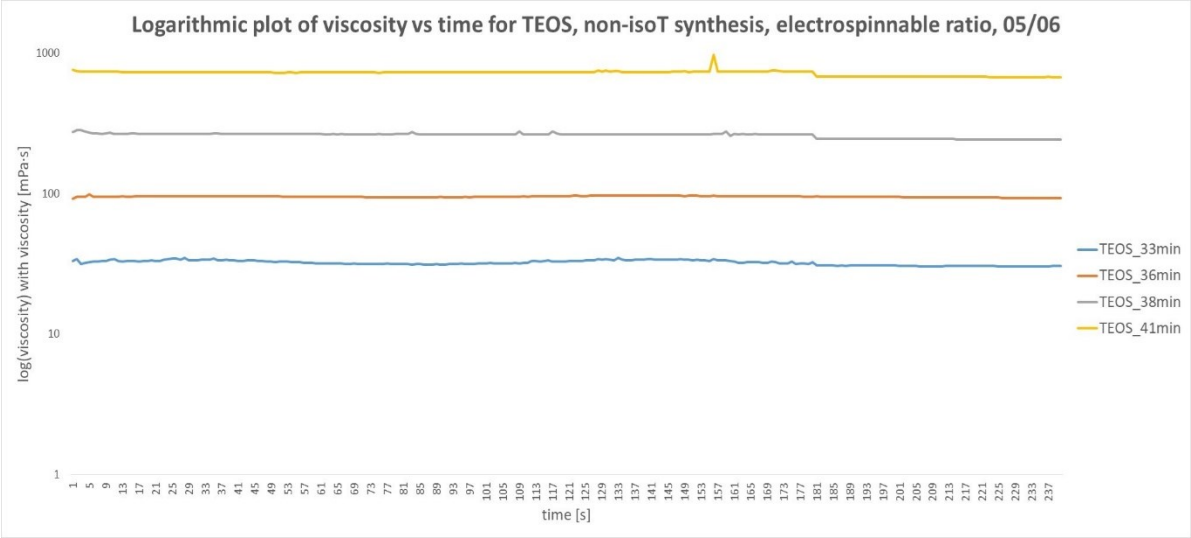

Figure A4: Logarithmic plot of viscosity versus reaction time for TEOS, non-isothermal synthesis with an electrospinnable ratio considering different reaction times. The data plotted are from the first set of experiments (05/06/2024).

- Second set of experiments, 06/06/2024, MTES

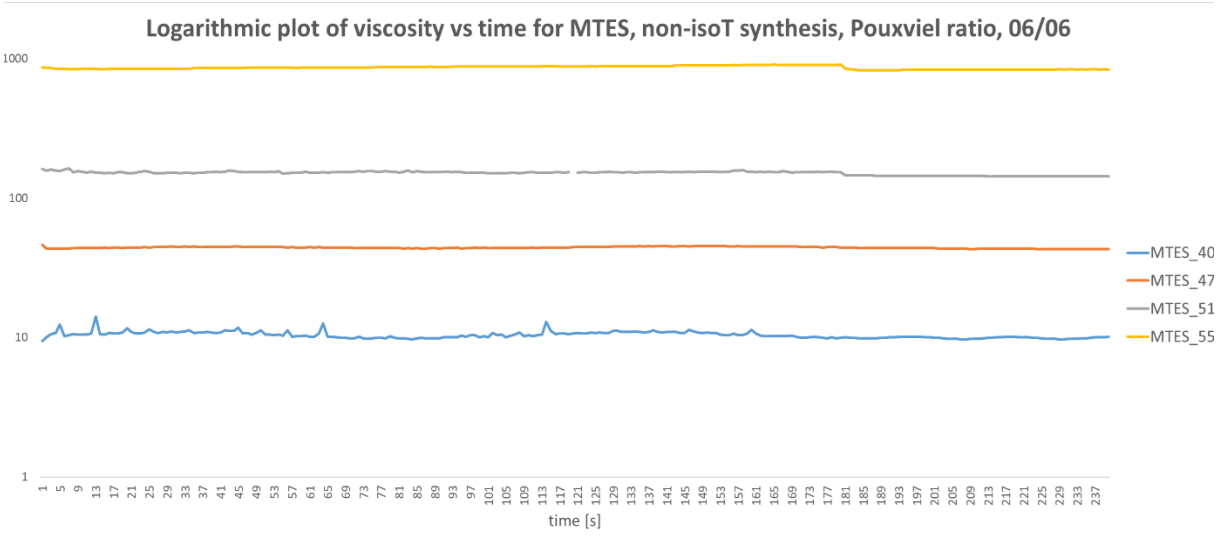

Figure A5: Logarithmic plot of viscosity versus reaction time for MTES, non-isothermal synthesis with a Pouxviel ratio considering different reaction times. The data plotted are from the second set of experiments (06/06/2024).

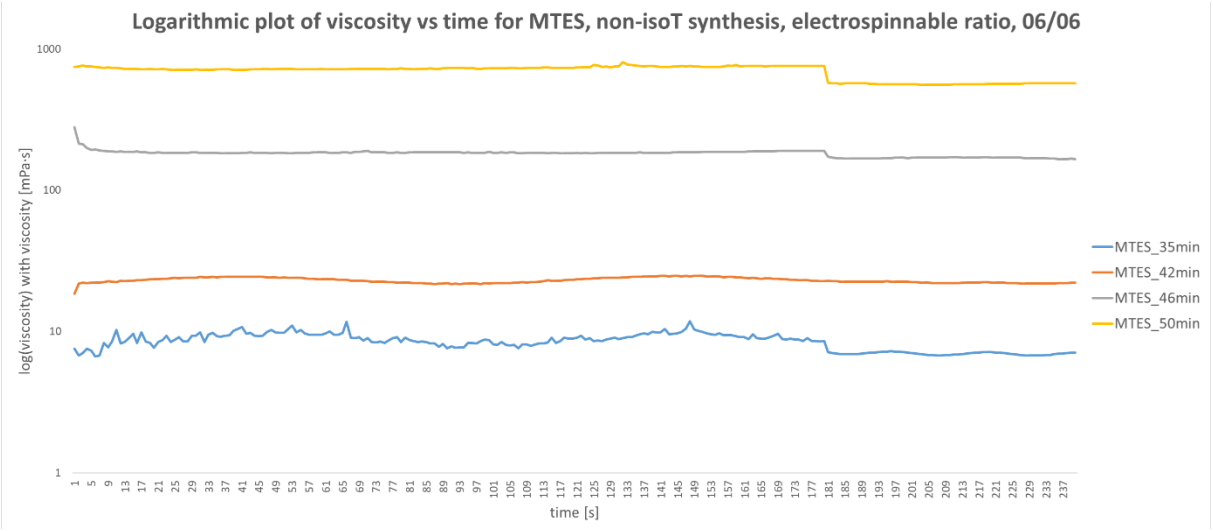

Figure A6: Logarithmic plot of viscosity versus reaction time for MTES, non-isothermal synthesis with an electrospinnable ratio considering different reaction times. The data plotted are from the second set of experiments (06/06/2024).

- Second set of experiments, 06/06/2024, TEOS

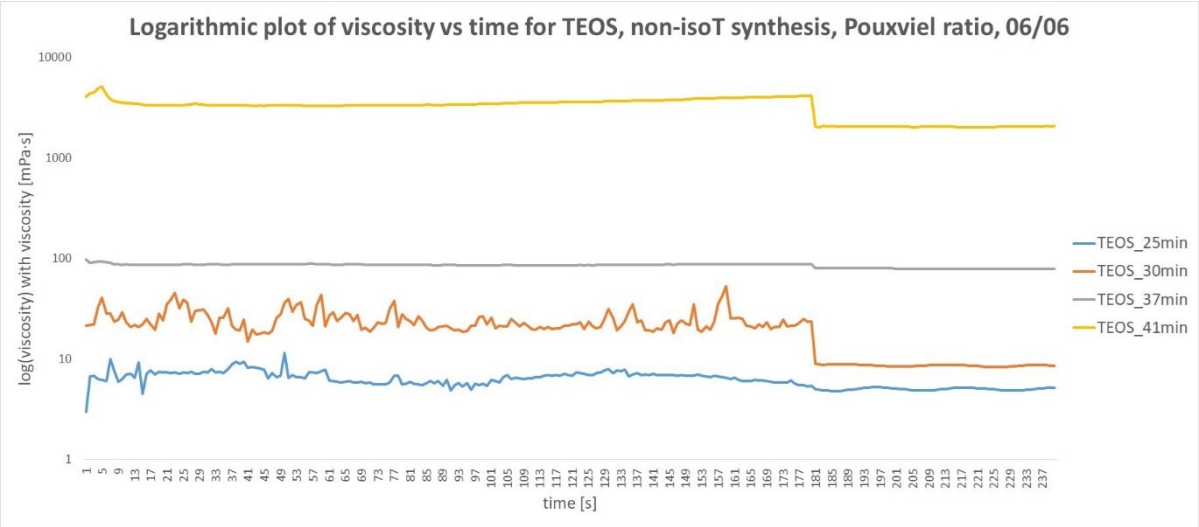

Figure A7: Logarithmic plot of viscosity versus reaction time for TEOS, non-isothermal synthesis with a Pouxviel ratio considering different reaction times. The data plotted are from the second set of experiments (06/06/2024).

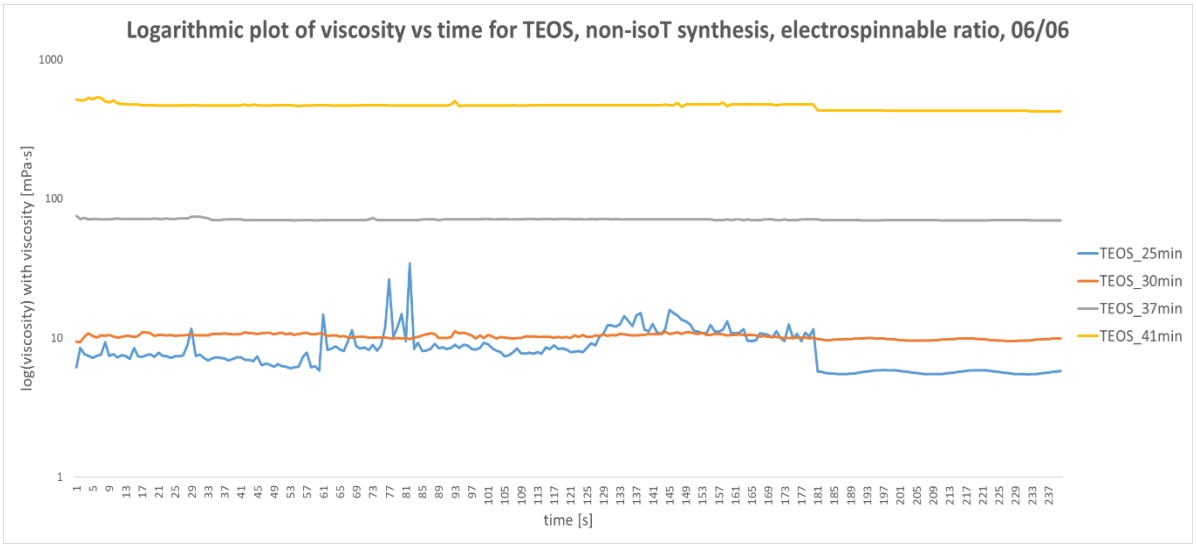

Figure A8: Logarithmic plot of viscosity versus reaction time for TEOS, non-isothermal synthesis with an electrospinnable ratio considering different reaction times. The data plotted are from the second set of experiments (06/06/2024).

- Third set of experiments, 07/06/2024, MTES

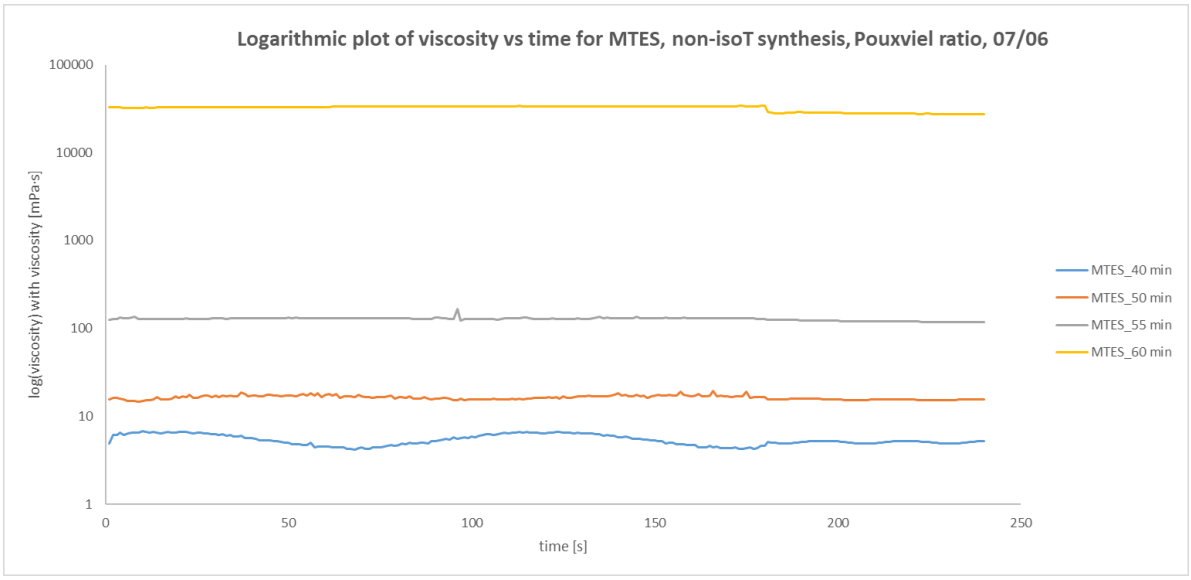

Figure A9: Logarithmic plot of viscosity versus reaction time for MTES, non-isothermal synthesis with a Pouxviel ratio considering different reaction times. The data plotted are from the third set of experiments (07/06/2024).

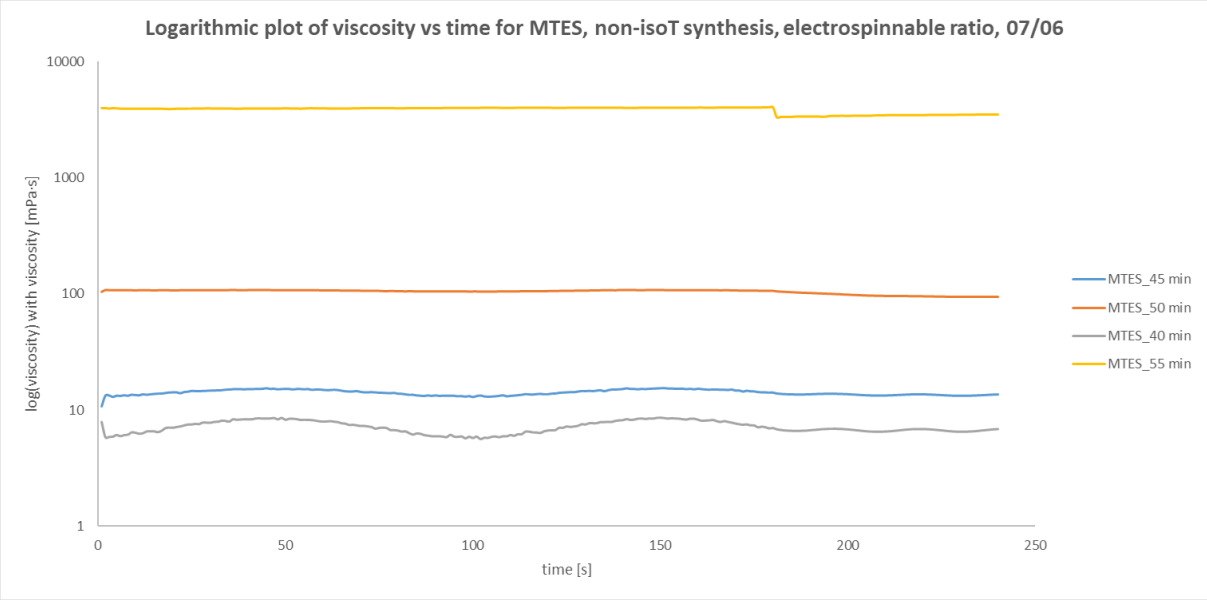

Figure A10: Logarithmic plot of viscosity versus reaction time for MTES, non-isothermal synthesis with an electrospinnable ratio considering different reaction times. The data plotted are from the third set of experiments (07/06/2024).

- Third set of experiments, 07/06/2024, TEOS

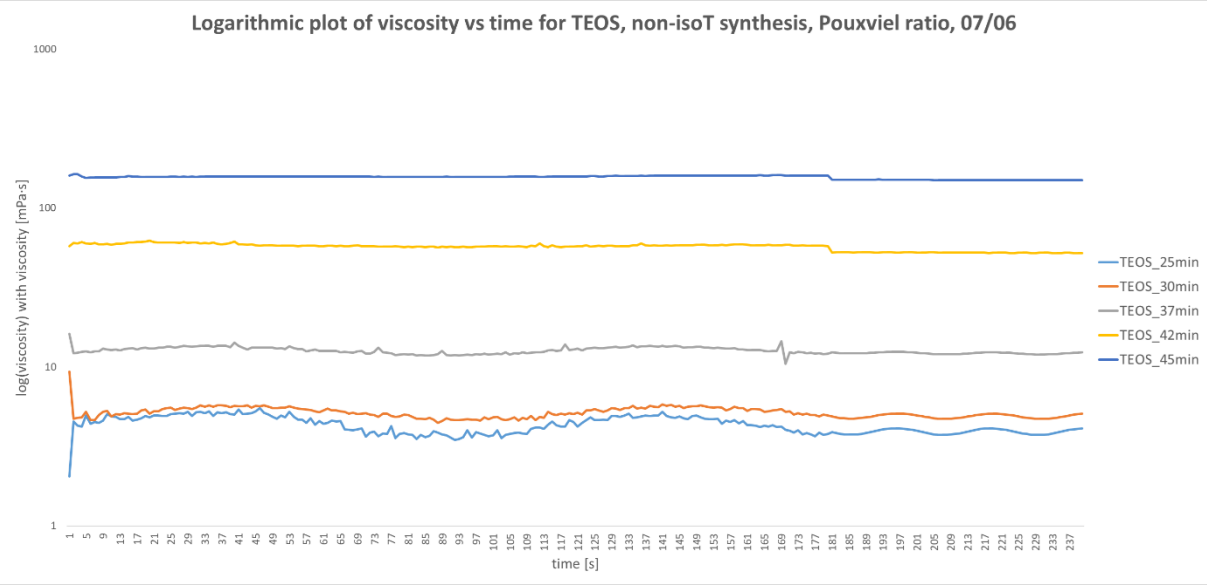

Figure A11: Logarithmic plot of viscosity versus reaction time for TEOS, non-isothermal synthesis with a Pouxviel ratio considering different reaction times. The data plotted are from the third set of experiments (07/06/2024).

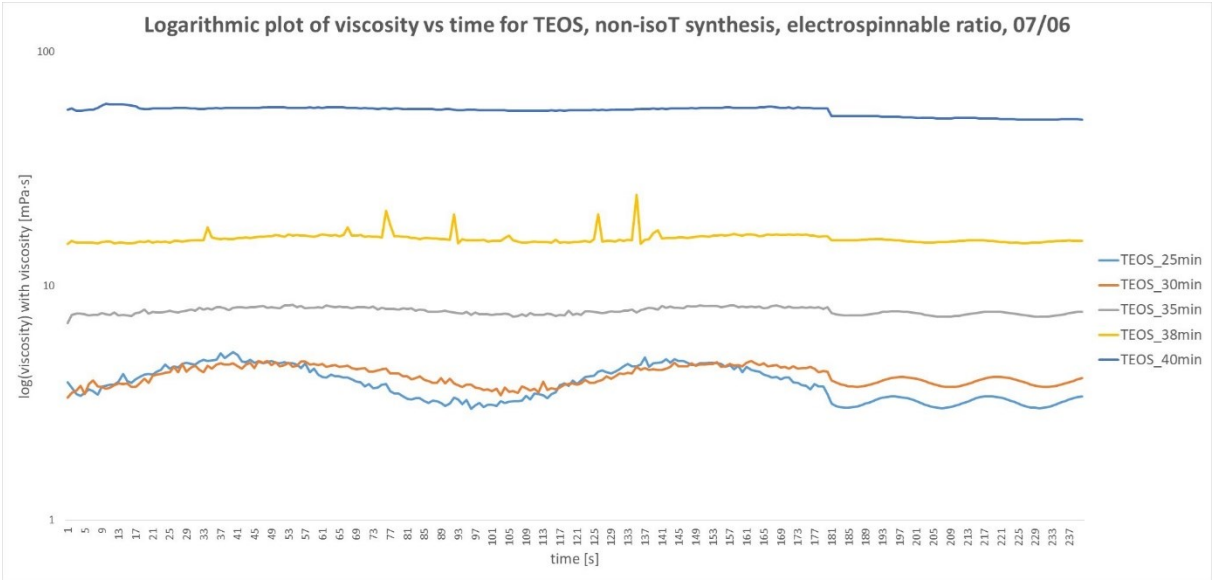

Figure A12: Logarithmic plot of viscosity versus reaction time for TEOS, non-isothermal synthesis with an electrospinnable ratio considering different reaction times. The data plotted are from the third set of experiments (07/06/2024).

List of Figures

List of Tables

Bibliography

[1] A. E. Danks, S. R. Hall, e Z. Schnepp, «The evolution of 'sol–gel' chemistry as a technique for materials synthesis», *Mater. Horiz.*, vol. 3, fasc. 2, pp. 91–112, 2016, doi: 10.1039/C5MH00260E.

[2] B. L. Cushing, V. L. Kolesnichenko, e C. J. O'Connor, «Recent Advances in the Liquid-Phase Syntheses of Inorganic Nanoparticles», *Chem. Rev.*, vol. 104, fasc. 9, pp. 3893–3946, set. 2004, doi: 10.1021/cr030027b.

[3] R. Ciriminna, A. Fidalgo, V. Pandarus, F. Béland, L. M. Ilharco, e M. Pagliaro, «The Sol–Gel Route to Advanced Silica-Based Materials and Recent Applications», *Chem. Rev.*, vol. 113, fasc. 8, pp. 6592–6620, ago. 2013, doi: 10.1021/cr300399c.

[4] A. Kumar, N. Yadav, M. Bhatt, N. K. Mishra, P. Chaudhary, e R. Singh, «Sol-Gel Derived Nanomaterials and It's Applications: A Review», vol. 5, 2015.

[5] Z. Ma *et al.*, «Engineering and optimization of nano- and mesoporous silica fibers using sol–gel and electrospinning techniques for sorption of heavy metal ions», *J. Colloid Interface Sci.*, vol. 358, fasc. 2, pp. 547–553, giu. 2011, doi: 10.1016/j.jcis.2011.02.066.

[6] Z. Ma *et al.*, «Engineering and optimisation of medically multi-functional mesoporous SiO2 fibers as effective wound dressing material», *J. Mater. Chem.*, vol. 21, fasc. 26, pp. 9595–9602, giu. 2011, doi: 10.1039/C1JM11115A.

[7] H. G. Emblem, «Ethyl-silicate-bonded refractories», *Mater. Chem. Phys.*, vol. 8, fasc. 3, pp. 265–277, mar. 1983, doi: 10.1016/0254-0584(83)90039-1.

[8] C. J. Brinker e G. W. Scherer, *Sol-Gel Science: The Physics and Chemistry of Sol-Gel Processing*. Academic Press, 2013.

[9] B. E. Yoldas, «Preparation of glasses and ceramics from metal-organic compounds», *J. Mater. Sci.*, vol. 12, fasc. 6, pp. 1203–1208, giu. 1977, doi: 10.1007/PL00020396.

[10] M. Nogami e Y. Moriya, «Glass formation through hydrolysis of Si(OC2H5)4 with NH4OH and HCl solution», *J. Non-Cryst. Solids*, vol. 37, fasc. 2, pp. 191–201, apr. 1980, doi: 10.1016/0022-3093(80)90150-7.

[11] F. Hoffmann e M. Fröba, «Vitalising porous inorganic silica networks with organic functions—PMOs and related hybrid materials», *Chem. Soc. Rev.*, vol. 40, fasc. 2, pp. 608–620, gen. 2011, doi: 10.1039/C0CS00076K.

[12] M. Barczak, C. Mcdonagh, e D. Wencel, «Micro- and nanostructured sol-gel-based materials for optical chemical sensing (2005–2015)», *Microchim. Acta*, vol. 183, lug. 2016, doi: 10.1007/s00604-016-1863-y.

[13] C. J. Brinker, D. E. Clark, e D. R. Ulrich, «Better ceramics through chemistry II; Proceedings of the Symposium, Palo Alto, CA, Apr. 15-19, 1986», Art. fasc. CONF-860445-,

gen. 1986, Consultato: 14 marzo 2024. [Online]. Disponibile su: https://www.osti.gov/biblio/6325059
[14] S. Sakka e K. Kamiya, «The sol-gel transition in the hydrolysis of metal alkoxides in relation to the formation of glass fibers and films», *J. Non-Cryst. Solids*, vol. 48, fasc. 1, pp. 31–46, mar. 1982, doi: 10.1016/0022-3093(82)90244-7.
[15] H. Schmidt, H. Scholze, e A. Kaiser, «Principles of hydrolysis and condensation reaction of alkoxysilanes», *J. Non-Cryst. Solids*, vol. 63, fasc. 1, pp. 1–11, feb. 1984, doi: 10.1016/0022-3093(84)90381-8.
[16] E. R. Pohl e F. D. Osterholtz, «Kinetics and Mechanism of Aqueous Hydrolysis and Condensation of Alkyltrialkoxysilanes», in *Molecular Characterization of Composite Interfaces*, H. Ishida e G. Kumar, A c. di, in Polymer Science and Technology. , Berlin, Heidelberg: Springer, 1985, pp. 157–170. doi: 10.1007/978-3-662-29084-2_10.
[17] M. G. Voronkov e A. Ya. Deich, «The donor-acceptor properties of the siloxane bond», *J. Struct. Chem.*, vol. 5, fasc. 3, pp. 443–448, mag. 1964, doi: 10.1007/BF00748884.
[18] C. J. Brinker, K. D. Keefer, D. W. Schaefer, R. A. Assink, B. D. Kay, e C. S. Ashley, «Sol-gel transition in simple silicates II», *J. Non-Cryst. Solids*, vol. 63, fasc. 1, pp. 45–59, feb. 1984, doi: 10.1016/0022-3093(84)90385-5.
[19] T. W. Zerda, I. Artaki, e J. Jonas, «Study of polymerization processes in acid and base catalyzed silica sol-gels», *J. Non-Cryst. Solids*, vol. 81, fasc. 3, pp. 365–379, mag. 1986, doi: 10.1016/0022-3093(86)90503-X.
[20] R. Aelion, A. Loebel, e F. Eirich, «Hydrolysis of Ethyl Silicate*», ACS Publications. Consultato: 15 marzo 2024. [Online]. Disponibile su: https://pubs.acs.org/doi/pdf/10.1021/ja01168a090
[21] «The hydrolysis and polycondensation of tetra alkoxysilanes - Aelion - 1950 - Recueil des Travaux Chimiques des Pays-Bas - Wiley Online Library». Consultato: 15 marzo 2024. [Online]. Disponibile su: https://onlinelibrary.wiley.com/doi/abs/10.1002/recl.19500690109
[22] S. Sfameni, G. Rando, e M. Plutino, «Sustainable Secondary-Raw Materials, Natural Substances and Eco-Friendly Nanomaterial-Based Approaches for Improved Surface Performances: An Overview of What They Are and How They Work», *Int. J. Mol. Sci.*, vol. 24, p. 5472, mar. 2023, doi: 10.3390/ijms24065472.
[23] C. J. Brinker, E. P. Roth, G. W. Scherer, e D. R. Tallant, «Structural evolution during the gel to glass conversion», *J. Non-Cryst. Solids*, vol. 71, fasc. 1, pp. 171–185, mag. 1985, doi: 10.1016/0022-3093(85)90286-8.
[24] R. K. Iler, «The Colloid Chemistry of Silica and Silicates», *Soil Sci.*, vol. 80, fasc. 1, p. 86, lug. 1955.
[25] R. A. Assink e B. D. Kay, «Sol-gel kinetics I. Functional group kinetics», *J. Non-Cryst. Solids*, vol. 99, fasc. 2, pp. 359–370, feb. 1988, doi: 10.1016/0022-3093(88)90441-3.

[26] B. D. Kay e R. A. Assink, «Sol-gel kinetics: II. Chemical speciation modeling», *J. Non-Cryst. Solids*, vol. 104, fasc. 1, pp. 112–122, ago. 1988, doi: 10.1016/0022-3093(88)90189-5.
[27] J. C. Pouxviel, J. P. Boilot, J. C. Beloeil, e J. Y. Lallemand, «NMR study of the sol/gel polymerization», *J. Non-Cryst. Solids*, vol. 89, fasc. 3, pp. 345–360, mar. 1987, doi: 10.1016/S0022-3093(87)80277-6.
[28] «A dedicated protocol to capture orthosilicate crosslinking kinetics and Arrhenius parameters - ScienceDirect». Consultato: 9 marzo 2024. [Online]. Disponibile su: https://www.sciencedirect.com/science/article/pii/S1385894723004321
[29] E. Loccufier, J. Geltmeyer, L. Daelemans, D. R. D'hooge, K. De Buysser, e K. De Clerck, «Silica Nanofibrous Membranes for the Separation of Heterogeneous Azeotropes», *Adv. Funct. Mater.*, vol. 28, fasc. 44, p. 1804138, 2018, doi: 10.1002/adfm.201804138.
[30] J. L. Lippert, S. B. Melpolder, e L. M. Kelts, «Raman spectroscopic determination of the pH dependence of intermediates in sol-gel silicate formation», *J. Non-Cryst. Solids*, vol. 104, fasc. 1, pp. 139–147, ago. 1988, doi: 10.1016/0022-3093(88)90193-7.
[31] C. A. M. Mulder e A. A. J. M. Damen, «Raman analysis of the initial stages of the hydrolysis and polymerization of tetraethylorthosilicate», *J. Non-Cryst. Solids*, vol. 93, fasc. 1, pp. 169–178, ago. 1987, doi: 10.1016/S0022-3093(87)80036-4.
[32] H.-L. Wang, E.-M. You, R. Panneerselvam, S.-Y. Ding, e Z.-Q. Tian, «Advances of surface-enhanced Raman and IR spectroscopies: from nano/microstructures to macro-optical design», *Light Sci. Appl.*, vol. 10, fasc. 1, p. 161, ago. 2021, doi: 10.1038/s41377-021-00599-2.
[33] A. M. Wands e J. J. Kohler, «Recent Developments in Designing Compact Biological Photoprobes», in *Photoaffinity Labeling for Structural Probing Within Protein*, Y. Hatanaka e M. Hashimoto, A c. di, Tokyo: Springer Japan, 2017, pp. 45–78. doi: 10.1007/978-4-431-56569-7_3.
[34] D. W. Schaefer e K. D. Keefer, «STRUCTURE OF RANDOM SILICATES: POLYMERS, COLLOIDS, AND POROUS SOLIDS*», in *Fractals in Physics*, L. Pietronero e E. Tosatti, A c. di, Amsterdam: Elsevier, 1986, pp. 39–45. doi: 10.1016/B978-0-444-86995-1.50009-3.
[35] A. Jitianu *et al.*, «29Si NMR and SAXS investigation of the hybrid organic-inorganic glasses obtained by consolidation of the melting gels», *Dalton Trans. Camb. Engl. 2003*, vol. 46, fasc. 11, pp. 3729–3741, mar. 2017, doi: 10.1039/c6dt04394a.
[36] H. S. N. Jayawardena, S. H. Liyanage, K. Rathnayake, U. Patel, e M. Yan, «Analytical Methods for Characterization of Nanomaterial Surfaces», *Anal. Chem.*, vol. 93, fasc. 4, pp. 1889–1911, feb. 2021, doi: 10.1021/acs.analchem.0c05208.
[37] R. A. Assink e B. D. Kay, «Study of Sol-Gel Chemical Reaction Kinetics by NMR», *Annu. Rev. Mater. Sci.*, vol. 21, fasc. 1, pp. 491–513, 1991, doi: 10.1146/annurev.ms.21.080191.002423.

[38] L. W. Kelts, N. J. Armstrong, C. J. Brinker, D. E. Clark, e D. R. Ulrich, «Better Ceramics Through Chemistry III», in *Materials Research Society Symposium Proceedings, Pittsburgh, PA*, 1988.
[39] T. Iwamoto, K. Morita, e J. D. Mackenzie, «Liquid state 29Si NMR study on the sol-gel reaction mechanisms of ormosils», *J. Non-Cryst. Solids*, vol. 159, fasc. 1, pp. 65–72, giu. 1993, doi: 10.1016/0022-3093(93)91282-8.
[40] «29Si NMR Kinetic Study of Tetraethoxysilane and Ethyl-Substituted Ethoxysilane Polymerization in Acidic Conditions | Industrial & Engineering Chemistry Research». Consultato: 12 marzo 2024. [Online]. Disponibile su: https://pubs.acs.org/doi/full/10.1021/ie950246q
[41] Y. Sugahara, S. Okada, S. Sato, K. Kuroda, e C. Kato, «29Si-NMR study of hydrolysis and initial polycondensation processes of organoalkoxysilanes. II. Methyltriethoxysilane», *J. Non-Cryst. Solids*, vol. 167, fasc. 1, pp. 21–28, gen. 1994, doi: 10.1016/0022-3093(94)90362-X.
[42] M. J. van Bommel, T. N. M. Bernards, e A. H. Boonstra, «The influence of the addition of alkyl-substituted ethoxysilane on the hydrolysis—condensation process of TEOS», *J. Non-Cryst. Solids*, vol. 128, fasc. 3, pp. 231–242, mag. 1991, doi: 10.1016/0022-3093(91)90461-E.
[43] I. Hasegawa, S. Sakka, Y. Sugahara, K. Kuroda, e C. Kato, «Polymerization of Hydrolysis Products of Methyltriethoxysilane in Aqueous Solutions», *J. Ceram. Soc. Jpn.*, vol. 98, fasc. 1139, pp. 647–652, 1990, doi: 10.2109/jcersj.98.647.
[44] H. Castricum *et al.*, «Structure of hybrid organic–inorganic sols for the preparation of hydrothermally stable membranes», *J. Sol-Gel Sci. Technol.*, vol. 48, pp. 11–17, nov. 2008, doi: 10.1007/s10971-008-1742-z.
[45] Y. Sugahara, S. Okada, K. Kuroda, e C. Kato, «29Si-NMR study of hydrolysis and initial polycondensation processes of organoalkoxysilanes. I. Dimethyldiethoxysilane», *J. Non-Cryst. Solids*, vol. 139, pp. 25–34, gen. 1992, doi: 10.1016/S0022-3093(05)80802-6.
[46] R. J. Hook, «A 29Si NMR study of the sol-gel polymerisation rates of substituted ethoxysilanes», *J. Non-Cryst. Solids*, vol. 195, fasc. 1, pp. 1–15, feb. 1996, doi: 10.1016/0022-3093(95)00508-0.
[47] R. K. Harris e B. E. Mann, «NMR and the Periodic Table», *No Title*, 1978, Consultato: 14 marzo 2024. [Online]. Disponibile su: https://cir.nii.ac.jp/crid/1130000793828342272
[48] D. R. D'hooge, P. H. M. V. Steenberge, P. Derboven, M.-F. Reyniers, e G. B. Marin, «Model-based design of the polymer microstructure: bridging the gap between polymer chemistry and engineering», *Polym. Chem.*, vol. 6, fasc. 40, pp. 7081–7096, 2015, doi: 10.1039/C5PY01069A.
[49] M. Andersen, C. Panosetti, e K. Reuter, «A Practical Guide to Surface Kinetic Monte Carlo Simulations», *Front. Chem.*, vol. 7, apr. 2019, doi: 10.3389/fchem.2019.00202.

[50] «Method of moments: A versatile tool for deterministic modeling of polymerization kinetics - ScienceDirect». Consultato: 20 marzo 2024. [Online]. Disponibile su: https://www.sciencedirect.com/science/article/pii/S0014305715002347
[51] D. T. Gillespie, «A general method for numerically simulating the stochastic time evolution of coupled chemical reactions», *J. Comput. Phys.*, vol. 22, fasc. 4, pp. 403–434, dic. 1976, doi: 10.1016/0021-9991(76)90041-3.
[52] L. De Keer *et al.*, «Computational prediction of the molecular configuration of three-dimensional network polymers», *Nat. Mater.*, vol. 20, fasc. 10, pp. 1422–1430, ott. 2021, doi: 10.1038/s41563-021-01040-0.
[53] C. W. Macosko, *Rheology: principles, measurements, and applications*. in Advances in interfacial engineering series. New York: VCH, 1994.
[54] H. Ramli, N. F. A. Zainal, M. Hess, e C. H. Chan, «Basic principle and good practices of rheology for polymers for teachers and beginners», *Chem. Teach. Int.*, vol. 4, fasc. 4, pp. 307–326, dic. 2022, doi: 10.1515/cti-2022-0010.
[55] S. Marsh e F. Rummel, «Rheometry and Rheological Characterisation», in *Food Texturology: Measurement and Perception of Food Textural Properties*, A. Rosenthal e J. Chen, A c. di, Cham: Springer International Publishing, 2024, pp. 195–216. doi: 10.1007/978-3-031-41900-3_10.
[56] G. A. Davies e J. R. Stokes, «On the gap error in parallel plate rheometry that arises from the presence of air when zeroing the gap», *J. Rheol.*, vol. 49, fasc. 4, pp. 919–922, lug. 2005, doi: 10.1122/1.1942501.
[57] E. Broyer e C. W. Macosko, «COMPARISON OF CONE AND PLATE, BICONE AND PARALLEL PLATES GEOMETRIES FOR MELT RHEOLOGICAL MEASUREMENTS.: SPE Tech Conf, 33rd Annu, Proc», 1975, pp. 343–345. Consultato: 2 aprile 2024. [Online]. Disponibile su: http://www.scopus.com/inward/record.url?scp=0016424008&partnerID=8YFLogxK
[58] J. Geltmeyer, L. Van der Schueren, F. Goethals, K. De Buysser, e K. De Clerck, «Optimum sol viscosity for stable electrospinning of silica nanofibres», *J. Sol-Gel Sci. Technol.*, vol. 67, fasc. 1, pp. 188–195, lug. 2013, doi: 10.1007/s10971-013-3066-x.
[59] A. Das *et al.*, «Electrospinning: The State of Art Technique for the Production of Nanofibers and Nanofibrous Membranes for Advanced Engineering Applications», in *Electrospinning for Advanced Energy Storage Applications*, N. T. M. Balakrishnan e R. Prasanth, A c. di, Singapore: Springer, 2021, pp. 23–71. doi: 10.1007/978-981-15-8844-0_2.
[60] A. Baji, K. Agarwal, e S. V. Oopath, «Emerging Developments in the Use of Electrospun Fibers and Membranes for Protective Clothing Applications», *Polymers*, vol. 12, fasc. 2, Art. fasc. 2, feb. 2020, doi: 10.3390/polym12020492.

[61] X. Gao *et al.*, «Flame-Retardant Nano-TiO2/Polyimide Composite Separator for the Safety of a Lithium-Ion Battery», *ACS Appl. Polym. Mater.*, vol. 4, fasc. 7, pp. 5125–5133, lug. 2022, doi: 10.1021/acsapm.2c00645.

[62] Q. Liu, J. Zhu, L. Zhang, e Y. Qiu, «Recent advances in energy materials by electrospinning», *Renew. Sustain. Energy Rev.*, vol. 81, pp. 1825–1858, gen. 2018, doi: 10.1016/j.rser.2017.05.281.

[63] S. Y. Chew, Y. Wen, Y. Dzenis, e K. W. Leong, «The Role of Electrospinning in the Emerging Field of Nanomedicine», *Curr. Pharm. Des.*, vol. 12, fasc. 36, pp. 4751–4770.

[64] L. R. Manea, A. Popa, e A. P. Bertea, «Medical Applications of Functional Electrospun Nanofibers - A Review», *Key Eng. Mater.*, vol. 752, pp. 132–138, 2017, doi: 10.4028/www.scientific.net/KEM.752.132.

[65] B. Zhang *et al.*, «In/Fe Cospinning Nanowires for Triethylamine Gas Sensing», *ACS Appl. Nano Mater.*, vol. 5, fasc. 7, pp. 9554–9566, lug. 2022, doi: 10.1021/acsanm.2c01778.

[66] G. K. Sharma, N. R. James, G. K. Sharma, e N. R. James, «Electrospinning: The Technique and Applications», in *Recent Developments in Nanofibers Research*, IntechOpen, 2022. doi: 10.5772/intechopen.105804.

[67] F. J. García-Mateos, R. Ruiz-Rosas, J. M. Rosas, J. Rodríguez-Mirasol, e T. Cordero, «Controlling the Composition, Morphology, Porosity, and Surface Chemistry of Lignin-Based Electrospun Carbon Materials», *Front. Mater.*, vol. 6, mag. 2019, doi: 10.3389/fmats.2019.00114.

[68] E. Loccufier, J. Geltmeyer, D. Esquivel, D. R. D'hooge, K. D. Buysser, e K. D. Clerck, «2B4_0505_ ELECTROSPINNING OF SILICA NANOFIBERS WITHOUT CARRIER POLYMER FOR ADVANCED ENGINEERING APPLICATIONS», *Proc. 19th World Text. Conf. - Autex 2019*, fasc. 0, Art. fasc. 0, ago. 2019, Consultato: 6 agosto 2024. [Online]. Disponibile su: https://openjournals.ugent.be/autex/article/id/63768/

[69] «A broad spectrum of electrospun organosilica membrane properties by tuning the chemical nature of the precursor building block - ScienceDirect». Consultato: 1 aprile 2024. [Online]. Disponibile su: https://www.sciencedirect.com/science/article/pii/S2468519424000569?casa_token=A95QrIRl9i0AAAAA:RuV5gckitEA07-wpCWSDeCSNDKRuVk0jZDQyYG8hDumEj5UZJj34yHYFGlP3IvIKubsNU9mXMA

[70] X. Zhu, Y. Yang, Z. Zheng, B. Xiang, e X. Cui, «Multiwave rheology and dynamic light scattering characterizations for a two-step sol-gel transition of tetraethoxysilane hydrolysis and condensation», *J. Sol-Gel Sci. Technol.*, vol. 88, fasc. 1, pp. 255–262, ott. 2018, doi: 10.1007/s10971-018-4788-6.

[71] I. Yu. Skvortsov, L. A. Varfolomeeva, e V. G. Kulichikhin, «The Effect of Tetraethoxysilane on the Phase State, Rheological Properties, and Coagulation Features of

Polyacrylonitrile Solutions», *Colloid J.*, vol. 81, fasc. 2, pp. 165–175, mar. 2019, doi: 10.1134/S1061933X19020145.
[72] S. V. Nitta, A. Jain, P. C. Wayner Jr., W. N. Gill, e J. L. Plawsky, «Effect of sol rheology on the uniformity of spin-on silica xerogel films», *J. Appl. Phys.*, vol. 86, fasc. 10, pp. 5870–5878, nov. 1999, doi: 10.1063/1.371605.
[73] C. A. Fyfe e P. P. Aroca, «A Kinetic Analysis of the Initial Stages of the Sol−Gel Reactions of Methyltriethoxysilane (MTES) and a Mixed MTES/Tetraethoxysilane System by High-Resolution 29Si NMR Spectroscopy», *J. Phys. Chem. B*, vol. 101, fasc. 46, pp. 9504–9509, nov. 1997, doi: 10.1021/jp971559x.
[74] «The Sol-Gel Process for Non-Metallic Inorganic Materials | SpringerLink». Consultato: 23 agosto 2024. [Online]. Disponibile su: https://link.springer.com/chapter/10.1007/978-3-642-93313-4_6
[75] V. Aquilanti, K. C. Mundim, M. Elango, S. Kleijn, e T. Kasai, «Temperature dependence of chemical and biophysical rate processes: Phenomenological approach to deviations from Arrhenius law», *Chem. Phys. Lett.*, vol. 498, fasc. 1, pp. 209–213, set. 2010, doi: 10.1016/j.cplett.2010.08.035.
[76] J. C. Echeverría *et al.*, «Kinetics of the acid-catalyzed hydrolysis of tetraethoxysilane (TEOS) by 29Si NMR spectroscopy and mathematical modeling», *J. Sol-Gel Sci. Technol.*, vol. 86, fasc. 2, pp. 316–328, mag. 2018, doi: 10.1007/s10971-018-4637-7.
[77] J. Geltmeyer, «Electrospinning and functionalization of silicon oxide nanofibers via sol-gel technology», PhD Thesis, Ghent University, 2017. Consultato: 26 agosto 2024. [Online]. Disponibile su: https://biblio.ugent.be/publication/8518328/file/8518329